



National Library
of Canada

Bibliothèque nationale
du Canada

Canadian Theses Service

Service des thèses canadiennes

Ottawa, Canada
K1A 0N4

NOTICE

The quality of this microform is heavily dependent upon the quality of the original thesis submitted for microfilming. Every effort has been made to ensure the highest quality of reproduction possible.

If pages are missing, contact the university which granted the degree.

Some pages may have indistinct print especially if the original pages were typed with a poor typewriter ribbon or if the university sent us an inferior photocopy.

Reproduction in full or in part of this microform is governed by the Canadian Copyright Act, R.S.C. 1970, c. C-30, and subsequent amendments.

AVIS

La qualité de cette microforme dépend grandement de la qualité de la thèse soumise au microfilmage. Nous avons tout fait pour assurer une qualité supérieure de reproduction.

S'il manque des pages, veuillez communiquer avec l'université qui a conféré le grade.

La qualité d'impression de certaines pages peut laisser à désirer, surtout si les pages originales ont été dactylographiées à l'aide d'un ruban usé ou si l'université nous a fait parvenir une photocopie de qualité inférieure.

La reproduction, même partielle, de cette microforme est soumise à la Loi canadienne sur le droit d'auteur, SRC 1970, c. C-30, et ses amendements subséquents.



National Library
of Canada

Bibliothèque nationale
du Canada

Canadian Theses Service Service des thèses canadiennes

Ottawa, Canada
K1A 0N4

The author has granted an irrevocable non-exclusive licence allowing the National Library of Canada to reproduce, loan, distribute or sell copies of his/her thesis by any means and in any form or format, making this thesis available to interested persons.

The author retains ownership of the copyright in his/her thesis. Neither the thesis nor substantial extracts from it may be printed or otherwise reproduced without his/her permission.

L'auteur a accordé une licence irrévocable et non exclusive permettant à la Bibliothèque nationale du Canada de reproduire, prêter, distribuer ou vendre des copies de sa thèse de quelque manière et sous quelque forme que ce soit pour mettre des exemplaires de cette thèse à la disposition des personnes intéressées.

L'auteur conserve la propriété du droit d'auteur qui protège sa thèse. Ni la thèse ni des extraits substantiels de celle-ci ne doivent être imprimés ou autrement reproduits sans son autorisation.

ISBN 0-315-59192-7

**Characteristics of Separated Flows Including
Cavitation Effects**

R. Balachandar

**A Thesis
in
The Faculty
of
Engineering**

**Presented in Partial Fulfillment of the Requirements
for the Degree of Doctor of Philosophy at
Concordia University
Montreal, Quebec, Canada**

March 1990

© R. Balachandar, 1990

ABSTRACT**Characteristics of Separated Flows Including Cavitation Effects**

Ramaswami Balachandar, Ph.D.
Concordia University, 1990

A program of study has been carried out to obtain the characteristics of two-dimensional separated flows including cavitation effects. The effects of wall interference and cavitation on the characteristics of flow past bluff bodies and backward facing steps were examined. Separated flows so generated can be a major source of flow induced vibration and noise.

For non-cavitating flow past sharp-edged bluff bodies, a simplified procedure is developed to determine the effects of wall interference on the drag coefficient. The characteristics related to inception, choking, cavity geometry and cavity pressure field were determined on the basis of experimental results for cavitating flow past bluff bodies. In this context, models based on theoretical considerations were also developed to determine the inception and choking cavitation characteristics. For sharp-edged bluff bodies, the length of vortex formation region was determined, recognising it as a significant parameter which precedes the zone where cavitation damage is most probable. Visual observations of the length of formation region supported the view that cavitation stabilises the vortex against its break-up.

The effects of wall interference and cavitation on the frequency of vortex shedding behind bluff bodies were also determined. The absence of the Karman vortex street was noted for flow past bluff bodies which were subject to very severe wall interference effects.

At very large Reynolds numbers, the reattachment of two-dimensional separated shear layers downstream of backward facing steps were investigated. Two backward facing steps were used to study the influence of expansion ratio on incipient cavitation indices at various Reynolds numbers. The frequency of vortex shedding and pressure distribution downstream of separation were obtained for both cavitating and non-cavitating flow conditions.

ACKNOWLEDGEMENT

The author wishes to express his appreciation to Dr. A. S. Ramamurthy for his guidance in the course of this investigation. Thanks are due to the technical staff of the Department of Civil Engineering and the members of the machine shop for their assistance. Special thanks are due to Mr. Diep Ngoc Vo for his assistance in the design of Water Tunnel -II used in this study.

TABLE OF CONTENTS

		PAGE
NOTATIONS.....		x
LIST OF FIGURES.....		xiii
LIST OF TABLES		xvii
CHAPTER I	INTRODUCTION.....	1
	1.1 General Remarks	1
	1.1.1 Separated Flow Regions	1
	1.1.2 Cavitation	2
	1.2 Scale Effects	3
	1.2.1 Blockage Effects	4
	1.2.2 Miscellaneous Scale Effects	5
	1.3 Scope of the Present Investigation	6
CHAPTER II	EXPERIMENTAL SET-UP AND	
	PROCEDURES.....	7
	2.1 Description of Water Tunnels	7
	2.2 Test Models	8
	2.3 Instrumentation and Procedure	9
	2.3.1 Pressure Pulsation Measurements	9
	2.3.2 Velocity Measurements	10
	2.3.3 Cavitation Nuclei Measurements	11

2.3.4	Other Measurements	11
2.3.5	Cavitation Inception Detection	12
2.3.6	Geometrical Characteristics	12
2.3.7	Detection of Choking Cavitation Conditions	13
2.4	Tunnel Qualification	13
2.5	Non-Dimensional Test Variables	14
CHAPTER III	NON-CAVITATING FLOW PAST BLUFF	
	BODIES.....	17
3.1	Previous Studies	17
3.2	Theoretical Considerations to Evaluate C_d	18
3.3	Analysis of Results	21
CHAPTER IV	INCEPTION CHARACTERISTICS OF	
	CONFINED SHARP EDGED BLUFF BODIES	23
4.1	Previous Studies	23
4.2	Theoretical Considerations to Determine σ_i	24
4.3	Analysis of Results	28
CHAPTER V	WAKE CHARACTERISTICS OF CONFINED BLUFF	
	BODIES	32
5.1	Previous Studies	33
5.2	Analysis of Results	35
5.2.1	Reynolds Number effects	35

5.2.2	Geometric Characteristics	36
5.2.3	Cavity Pressure Pulsations	37
5.2.4	Wake Static Pressure Distribution for 0° Wedges	39
5.2.5	Cavity Pressure Field Characteristics	40
5.2.6	Wake Static Pressure Distribution for Circular Cylinders	41
5.2.7	Length of Vortex Formation Region	42
5.2.8	Flow Past Over-sized Bluff Bodies	45
CHAPTER VI	CHOKED FLOW PAST BLUFF BODIES.....	47
6.1	Previous Studies	47
6.2	Theoretical Considerations to Determine σ_{ch}	48
6.3	Analysis of Results	50
CHAPTER VII	FLOW PAST BACKWARD FACING STEPS	52
7.1	Previous Studies	52
7.1.1	Non-Cavitating Flows	52
7.1.2	Cavitating Flows	54
7.2	Analysis of Results	55
7.2.1	Velocity Measurements and Reattachment Lengths	55
7.2.2	Pressure Distribution Behind Backward Facing Steps	56
7.2.3	Frequency of Pressure Pulsations	58
7.2.4	Cavitation Inception Measurements	59

CHAPTER VIII	CONCLUSIONS AND SCOPE FOR FURTHER STUDY.....	60
8.1	Conclusions	60
8.2	Scope for Further Study	62
APPENDIX I	REFERENCES.....	63
APPENDIX II	FIGURES.....	70
APPENDIX III	TABLES.....	146
APPENDIX IV	EXPERIMENTAL UNCERTAINTY.....	171

NOMENCLATURE

B	=	test section width
b	=	width of bluff body
b/B	=	blockage ratio (Constraint)
C_c	=	contraction coefficient
C_d	=	drag coefficient
C_{pb}	=	back pressure coefficient
C_{pf}	=	forebody pressure coefficient
C_{pj}	=	jet pressure coefficient
C_{pr}	=	rear pressure coefficient
C_{ps}	=	separating pressure coefficient
C_{px}	=	centre line wake pressure coefficient
D	=	drag force
f	=	frequency of pressure pulsations
h	=	Height of Step
K_j	=	U_j/U (jet velocity / free stream velocity)
K_s	=	U_s/U (separating speed / free stream velocity)
L	=	length of cavity
L_f	=	length of vortex formation region
P	=	free stream pressure
P_b	=	back pressure
P_j	=	contracting jet pressure
P_s	=	separating pressure

P_v	=	vapor pressure
P_w	=	wake pressure
P_x	=	pressure along wake axis
P_∞	=	free stream pressure
R	=	constant (Eq.(3.3))
Re	=	Reynolds number ($= Ub/v$)
r_c	=	radius of vortex
S	=	Strouhal number
S_s	=	modified Strouhal number based on U_s
S_L^*	=	modified Strouhal number based on L
S	=	Strouhal number based on step height
U	=	mean velocity upstream of the body
U_{max}	=	maximum velocity at a particular section
U_j	=	mean velocity at the vena contracta
U_s	=	velocity at separation
U_∞	=	free stream velocity
U_{ref}	=	reference velocity ahead of the step
u'	=	turbulent component in the flow direction
W	=	maximum wake width
x	=	distance along wake axis of bluff body
X	=	distance from step edge along separation bubble
x'	=	lateral distance along front face of bluff body
X'	=	dimensionless lateral distance ($=2 x'/b$)
X_r	=	reattachment length

- y = ordinate measured from the step
 α = fractional circulation
 β = momentum coefficient
 Γ = Circulation
 δ = boundary layer thickness
 δ_1 = displacement thickness
 θ = orientation
 ε = variable (Eq.(3.5))
 ρ = density of fluid
 σ = cavitation number
 σ_{ch} = choking cavitation number
 σ_i = Inception cavitation number
 σ_s = modified cavitation number
 ν = kinematic viscosity
 η = $\int_{-b/2}^{b/2} C_{pf} dx$

LIST OF FIGURES

FIGURE		PAGE
1.1	Classification of separated flows	70
2.1a	Water tunnel - I	71
2.1b	Test section and bluff body	72
2.2	Water tunnel - II	73
2.3a	Blockages tested (Bluff bodies)	74
2.3b	Backward facing step	75
2.4	Instrumentation	76
2.5	Laser doppler velocimeter system	77
2.6a	LDV calibration unit	78
2.6b	Velocity measurements at the exit of a nozzle	79
2.7a	Schematic of PDA system	80
2.7b	Typical cavitation nuclei measurements	81
2.8a	Typical calibration curve for pressure gage	82
2.8b	Typical calibration curve for pressure transducer	82
2.9a	Geometrical characteristics of bluff body wake	83
2.9b	Length of formation region	84
2.10a	Span-wise Velocity distribution - Water Tunnel I	85
2.10b	Span-wise Velocity distribution - Water Tunnel II	86
2.11	Variation of K_s with b/B (Non-cavitating flow)	87
2.12	Variation of S with b/B (Non-cavitating flow)	88
3.1	Definition sketch and Control volume for non-cavitating flow	89

3.2	Variation of C_{ps} with b/B for non - cavitating flow	90
3.3	Variation of K_j and K_s with b/B	91
3.4	Variation of C_d with b/B (Non - cavitating flow)	92
4.1	Forebody pressure distribution in non-cavitating flows ($b/B = 0.072$ and 0.325)	93
4.2	Potential flow velocity distribution on fore-body face ($b/B = 0.325$)	94
4.3	Variation of S and C_{ps} with σ at inception conditions	95
4.4	Power spectra of pressure pulsations at inception conditions	96
4.5	Variation of σ_i with Re for $b/B = 0.243$ and 0.325	97
4.6	Variation of σ_i with b/B	98
5.1a	Variation of C_{pb} Re for a circular source ($b/B = 0.08$)	99
5.1b	Variation of C_{ps} with Re for a 0° wedge ($b/B = 0.097$)	99
5.1c	Variation of C_{pb} and C_{ps} with σ	99
5.2	Variation of L/b with σ for circular sources	100
5.3	Variation of L/b with σ for 0° wedges (Moderate blockages)	101
5.4	Variation of L/b with σ for 0° wedges (Large blockages)	102
5.5	Variation of L/b with σ_s	103
5.6	Variation of W/b with σ_s for 0° wedges	104
5.7	Variation of S vs σ_s (Moderate blockages)	105
5.8	Variation of S vs σ_s (Large blockages)	105
5.9	Power spectra at various σ ($b/B = 0.58$)	106
5.10	Power spectra at various σ ($b/B = 0.82$)	107
5.11	Variation of S_s vs σ_s	108
5.12	Variation of S_L^* vs σ_s	109

5.13a	Wake static pressure distribution ($b/B = 0.325$)	110
5.13b	Wake static pressure distribution ($b/B = 0.243$)	111
5.14a	Variation of $-C_{ps}$ with σ ($b/B = 0.325$)	112
5.14b	Wake pressure distribution for non-cavitating normal plates (Sullerey 1975)	112
5.15a	Wake static pressure distribution ($b/B = 0.58$)	113
5.15b	Wake static pressure distribution ($b/B = 0.66$)	114
5.15c	Wake static pressure distribution ($b/B = 0.82$)	115
5.16	Probability density function ($b/B = 0.243$)	116
5.17	Probability density function ($b/B = 0.82$)	117
5.18	Wake static pressure distribution for circular cylinder ($b/B = 0.33$)	118
5.19	Variation of $-C_{pb}$ with σ for circular cylinder ($b/B = 0.33$)	119
5.20	Wake static pressure distribution for circular cylinder ($b/B = 0.08$)	120
5.21	Variation of L_f/b with σ	121
5.22	Variation of L_f/b with σ_s	122
5.23	Variation of S_s with b/B (Non-cavitating conditions)	123
5.24	Variation of $-C_{ps}$ with σ for a 0° wedge, Normal flat plate and Gate ($b/B = 0.932$)	124
5.25	Variation of S_s with σ_s for a 0° wedge, Normal flat plate and Gate ($b/B = 0.932$)	124
6.1	Control volume for choking conditions	125
6.2	Variation of η with b/B	126
6.3	Variation of σ with velocity ($b/B = 0.325$)	127
6.4	Variation of σ_{ch} with b/B	128

7.1	Flow past a backward facing step	129
7.2	Streamwise mean velocity distribution (ER = 1.07)	130
7.3	Streamwise turbulence distribution (ER = 1.07)	131
7.4	Streamwise mean velocity distribution (ER = 1.14)	132
7.5	Loci of streamwise zero mean velocity (ER = 1.07)	133
7.6	Loci of streamwise zero mean velocity (ER = 1.14)	134
7.7	Variation of X_r with Re	135
7.8	Typical streamline pattern (ER = 1.14)	136
7.9a	Variation of u'/U_{\max} with X/X_r	137
7.9b	Velocity distribution at $X/h = 5.20$ ($2.36 < \sigma < 1.03$)	138
7.10	Separated region static pressure distribution at various Re (ER = 1.07)	139
7.11	Separated region static pressure distribution various Re (ER = 1.14)	139
7.12	Separated region static pressure distribution	140
7.13	Variation of C_p with X/h - Cavitating conditions (ER = 1.14)	141
7.14	Variation of C_p with X/h - Cavitating conditions (ER = 1.07)	142
7.15	Typical spectra of pressure fluctuations downstream of a backward facing step	143
7.16a	Variation of with Re	144
7.16b	Variation of S with σ (ER = 1.07)	144
7.16c	Variation of S with σ (ER = 1.14)	144
7.17	Variation of σ_i with Re	145

LIST OF TABLES

TABLE		PAGE
1	Summary of some related previous studies	146
2	Cavitation inception data ($b/B = 0.243$ and 0.325)	147
3	Inception cavitation indices at various blockages	147
4a	Test results for 0° wedge ($b/B = 0.097$)	148
4b	Test results for 0° wedge ($b/B = 0.243$)	149
4c	Test results for 0° wedge ($b/B = 0.325$)	150
4d	Test results for 0° wedge ($b/B = 0.575$)	151
4e	Test results for 0° wedge ($b/B = 0.658$)	152
4f	Test results for 0° wedge ($b/B = 0.823$)	153
5a	Wake static pressure distribution ($b/B = 0.243$)	154
5b	Wake static pressure distribution ($b/B = 0.325$)	155
5c	Wake static pressure distribution ($b/B = 0.575$)	156
5d	Wake static pressure distribution ($b/B = 0.658$)	157
5e	Wake static pressure distribution ($b/B = 0.823$)	158
6	Length of formation region data for $b/B = 0.097$	159
7	Length of formation region data ($b/B = 0.243$ and 0.325)	160
8	Test results for circular bluff body ($b/B = 0.08$)	161
9	Wake static pressure distribution for circular bluff body ($b/B = 0.08$)	163
10	Wake static pressure distribution for circular bluff body ($b/B = 0.33$)	164
11	Inception cavitation data for backward facing steps	165

12	Strouhal number data for backward facing steps	165
13	Test results for backward facing steps (ER = 1.07)	166
14	Test results for backward facing steps (ER = 1.14)	167
15	Typical Boundary layer parameters for backward facing steps	168
16	Test data for $b/B = 0.097$ (Tunnel - II)	169
17	Test data for $b/B = 0.243$ (Tunnel - II)	169
18	Test data for $b/B = 0.325$ (Tunnel - II)	170
19	Test data for $b/B = 0.823$ (Tunnel - II)	170

CHAPTER I
INTRODUCTION

CHAPTER I

INTRODUCTION

1.1 GENERAL REMARKS

1.1.1 Separated flows regions

Flow fields containing separated flow regions occur frequently in fluid handling systems. Examples of separated flow regions can be found near the leading edges of airfoils, struts and turbine blades, flow over surface discontinuities such as slots and steps, along the walls of rapidly expanding diffusers and flow past blunt structures. A general classification of separated flows is shown in Fig 1.1. Flow separation can cause significant energy losses and the optimum performance of fluid machinery can be predicted by a better understanding of the characteristics of flow separation. Further, flow separation occurs just prior to or at maximum loading conditions [Chang 1970]. The complex turbulent flow field generated due to separation can significantly change the local pressure field besides exhibiting unsteady low frequency behaviour. Separated flows can thus be a major source of flow induced vibration, noise and cavitation.

Several simple geometries like backward facing steps, forward facing steps, bluff circular cylinders, sharp edged bluff bodies, fences and trips have been used to study separated flow regions. Flow past backward facing steps and sharp edged bluff bodies are good model shapes for investigation, as the separation points are fixed and the complications involved with moving separation points can be avoided to a good extent. A bluff or a non-streamlined obstacle refers to a body where the major contribution of the drag force is due to pressure forces arising from flow separation. Table 1 gives a summary of some of the existing results related to cavitation in separated flow regions.

1.1.2 Cavitation

In liquid flow systems, when the pressure reaches a value close to the vapor pressure of the liquid, vapor or gas and vapor filled bubbles are formed. Cavitation signifies the phenomenon of formation, growth and subsequent collapse of such bubbles. Because of its detrimental effects on flow systems, cavitation has been recognised as an important design parameter for a broad variety of devices handling liquids. Since 1950, several investigators have made significant contributions towards understanding the mechanisms of cavitation and cavitation damage. Despite a great deal of research work, many aspects of the phenomenon remain unresolved. Attempts to obtain an analytical solution to the problem of cavitation have not been very successful. Emphasis has, by necessity, been concentrated on laboratory experiments to explore the physics of the problem and develop empirical relationships among the different contributing parameters for predicting the various levels of cavitation (Tullis 1989). Increased drag of marine vehicles, limitations on the thrust produced by various propulsion systems and decreased power output and efficiency of turbines can be partly traced to the effects of cavitation. Typical examples illustrating the disastrous effects of cavitation in hydraulic structures include the collapse of tunnel number 2 of the Tarbela project in Northern Pakistan (Arndt 1983, Kenn and Garrod 1981) and the large scale cavitation damage of Arizona spillway tunnel of Hoover dam (Falvey 1983). Cavitating flows are commonly described by the cavitation number σ , given by,

$$\sigma = \frac{P - P_v}{\frac{1}{2} \rho U^2} \quad (1.1)$$

where, P and U are the reference pressure and velocity respectively, P_v is the vapor

pressure and ρ is the mass density of the liquid. The "non cavitating flow" regime occurs at sufficiently large values of σ associated with the absence of cavitation bubbles. On the other hand, "cavitating flow" regime occurs at sufficiently small values of σ characterised by the presence of a large number of cavitation bubbles. Between these two regimes, lie the regime of "limited cavitation" where a very small number of cavitation bubbles are present. Limited cavitation may be attained by first establishing cavitating flow and then increasing σ until cavitation just disappears. This state is referred to as "desinent cavitation". Limited cavitation may also be attained by approaching from the non cavitating flow regime by decreasing σ . This state is referred to as "incipient cavitation". Some differences between the incipient and desinent states of cavitation have been reported [Holl 1966] and the term "cavitation hysteresis" is used to denote such a difference. As one decreases the cavitation number of a flow system from a developed state, a stage is reached when it is not possible to decrease σ any further. This state is referred to as "choking cavitation".

1.2 SCALE EFFECTS

It is generally difficult or almost impossible to make direct observations of cavitation when it occurs in prototype hydraulic systems. The difficulties associated with testing or observing in operation a full scale prototype has led to the extensive use of model testing to determine the various effects of cavitation. To predict full scale behaviour from model tests, an adequate knowledge of the scaling parameters is required. From the point of view of the present study, scale effects are broadly classified into two types. These are: (i) Blockage effects and (ii) Miscellaneous scale effects. The latter include the effects of roughness, Reynolds number and cavitation nuclei.

1.2.1 Blockage effects:

In fluid dynamic tests, it is desirable to use a smaller size model to avoid the wall interference effects of the test section on the measurements made. However, the need to use a model relatively large, compared to the test section dimensions, occurs in model simulation due to certain imposed physical limitations. Some of these may be related to the sensitivity of the instrumentation, which requires a threshold value of the physical variable to be present for effective recording (higher signal-to-noise ratio). Physical limits of machining may also require the use of larger models. When the model is large, considerable details can be incorporated in it. From a purely practical view point, most of the model testings are done in flows bounded by side walls while the prototype applications are generally in unlimited flows. Further, the need to maintain flow similarity necessitates the use of larger models to achieve high enough Reynolds numbers. These requirements cause the test conditions to deviate from prototype performance, as the rigid boundaries of the test section prevent the lateral displacement of streamlines. In wind tunnel and water tunnel tests, the side walls of the test section can alter the hydrodynamic force coefficients and the vortex shedding frequency of the model. Further, there are several fluid-structure interaction situations where streamlines are laterally restrained. These factors indicate that wall interference data are needed in practical applications. The ratio of the model area to the test section area is denoted as blockage and it determines the influence of the side walls on the flow characteristics. In two-dimensional flows, the ratio b/B denotes blockage. Here, b is the height of the body and B is the height of the test section. Although the results obtained would be immediately applicable only to two-dimensional flows, the scope of application is less restrictive than it would appear. The bulk characteristics of certain free-streamline flows have been found to be essentially the same for two-dimensional and axi-symmetric patterns [Sarpkaya 1961, Rouse 1950, Plesset and Shaffer 1948].

1.2.2 Miscellaneous scale effects:

The presence of imperfections or weak spots in liquids, commonly denoted as 'cavitation nuclei' influence the scaling laws. The weak spots prevent the liquid from supporting higher tensions. Studies indicate that two forms of cavitation nuclei, namely, stream nuclei and surface nuclei influence the cavitation process. Stream nuclei exist in such forms as solid particulates and microbubbles. Surface nuclei originate from cracks and crevices in the boundary. Qualitative relationships between cavitation inception and nuclei have been developed by Holl [1970] and Gates et al. [1979]. As rightly pointed out by Blake [1986], beyond a rather notional relationship between nucleus population and cavitation, there is no rigorous theory in hydrodynamic cavitation that satisfactorily explains or accounts for the influence of nuclei in a quantitative sense. In the present series of tests, the type and size of bluff bodies chosen are such that the inception cavitation index (σ_i) values are reasonably high. Consequently, it is expected that nuclei characteristics and dissolved gas effects of the water used may not have a very significant effect on the results related to inception characteristics [Arakeri 1981].

In several of the previous investigations related to blockage effects on flow past bluff objects, circular cylinders were used as the test model. Under these conditions, Reynolds number is a dominant flow parameter and the location of the flow separation point varies with Reynolds number, especially when the test conditions span the critical Reynolds number of the test source. In order to reduce or avoid the dependence of the test results on the flow Reynolds number, the use of bluff bodies with fixed separation points have been suggested [Ramamurthy 1973]. More detailed discussions of the effects of Reynolds number in cavitating flows are provided in a latter section.

1.3 SCOPE OF THE PRESENT INVESTIGATION:

In the present study, separated flow characteristics are studied in conjunction with wall interference and cavitation effects. In tests related to bluff bodies, a large blockage range ($0.097 < b/B < 0.93$) is covered. In studies related to backward facing steps, two expansion ratios of 1.07 and 1.14 are used. Attention is focussed on the following specific aspects:

A. The effect of wall interference on:

- i). Steady drag of non-cavitating sharp edged bluff bodies.
- ii). Cavitation inception characteristics of sharp edged bluff bodies.
- iii). Wake characteristics of sharp edged bluff bodies including the wake pressure distributions, length of vortex formation region, frequency of wake pressure pulsations, geometry of the cavity formed behind the bluff sources and the effects of Reynolds number.
- iv). Choking cavitation characteristics of sharp edged bluff bodies

B. Flow past backward facing steps:

- i). The effect of Reynolds number and expansion ratio on the frequency of vortex shedding in non-cavitating flows.
- ii). The effect of Reynolds number and expansion ratio on the cavitation numbers related to inception conditions.
- iii). The effect of cavitation on the frequency of vortex shedding and separation bubble pressure characteristics.

CHAPTER II
EXPERIMENTAL SET-UP AND PROCEDURES

CHAPTER II

EXPERIMENTAL SET-UP AND PROCEDURES

In this chapter, a general description of the two water tunnels used and the associated instrumentation are presented. The various non-dimensional parameters pertinent to the study are identified.

2.1 DESCRIPTION OF WATER TUNNELS

For purposes of identification, the two water tunnels are denoted as "Tunnel - I" and "Tunnel - II" respectively. The tunnels were located at about 6 m above the water level in the sump to ensure that low enough pressures could be obtained in the test section. This arrangement permitted the occurrence of cavitation in the presence of a model in the test section. Since cavitation increases the free gas content in closed circuit tunnels, the created bubbles should have sufficient time to redissolve or reach a free surface where they get expelled. To ensure a long enough residence time, a large sump (160 m³) was used. Further, the exit line of the water tunnel was always completely immersed and placed close to the floor of the sump far from the entrance to the pump.

Tunnel I :

Tunnel I is essentially a Venturi type water tunnel (Fig. 2.1a) found suitable for cavitation flow studies [Knapp 1970]. The turbulence level in the test section was considerably reduced by adopting a large rectangular settling chamber which was followed by a smooth contraction leading to a rectangular test section 154.0 mm high and 4.76 mm wide. A ten fold increase in velocity was achieved at the test section by means of the contractions provided (Fig. 2.1a). The test section was 508 mm long and was equipped with a plexiglas window to facilitate visual observation. The whole arrangement beginning with the settling chamber to the end of the test section was fabricated in a single continuous

machined plate of steel to avoid flow separation and local cavitation at surface discontinuities that might otherwise be present. A fine measuring grid of 3 mm squares drawn on the plexiglas window enabled the measurements of the wake geometry and the length of the vortex formation region. Several pressure taps located along MN (Fig. 2.1b) in the test section walls enabled the measurement of the mean static pressure distribution along the wake centre line by means of calibrated pressure gages.

In the absence of a bluff source, the test section wall pressure fluctuations were found to be of the order of 0.5% of the dynamic pressure. An accelerometer was rigidly mounted to the test section window and the accelerometer signals in the absence of the test body indicated a dominant frequency at 238.75 Hz for a wide range of velocities. This indicated that the resulting frequency was a characteristic of the tunnel and piping system. The range of vortex shedding frequencies encountered in the present series of tests were well below 238.75 Hz.

Tunnel II:

A schematic of Tunnel II is shown in Fig. 2.2. A 10 to 1 contraction is provided to obtain a uniform flow at the test section. The test section was 101.6 mm high, 50.8 mm wide and 508 mm long. Wall static pressures were measured with 0.5 mm diameter pressure taps located along the tunnel centerline, typically spaced 12.7 mm apart throughout the length of the test section. The test section was provided with plexiglas windows to facilitate visual observation. A 60 h.p. pump was used to circulate the water through the test section.

2.2 TEST MODELS

Bluff bodies :

Polished, circular and equilateral prisms made of brass formed the basic bluff body models. Fig. 2.3a indicates the different blockages tested. In Fig. 2.1b; B, b, b/B denote the height of the test section, the height of the body and blockage respectively. In the case

of equiangular prisms (Fig.2.1b), 0.6 mm diameter pressure taps were located both at the centre of the front face and at the tip of the afterbody of the prisms to measure the stagnation pressure and the back pressure (P_b) respectively. The two separating pressures (P_s) were measured by means of pressure taps close to the separation points located on the rear of the body. The prisms were always mounted such that the front face was normal to the flow. This orientation was designated as 0° (Fig. 2.1b). The circular source had two pressure taps, one at A ($\theta = 0^\circ$ - Fig.2.3a) to measure the stagnation pressure and the other at B ($\theta = 180^\circ$ - Fig.2.3a) to measure the back pressure. The sources were mounted as struts across the test section spanning its entire width.

At a large blockage of 93%, limited studies related to the cavitation characteristics of a gate and a normal flat plate were also carried out. The former denoted a wall mounted model and the later a denoted a centrally mounted body which had no significant afterbody.

Backward facing steps:

The backward facing step models used in the present study are indicated in Fig. 2.3b. Machined steps of heights 6.35 mm and 12.7 mm resulting in expansion ratios (ER) of 1.07 and 1.14 were used. Several pressure taps were provided along PQ (Fig. 2.3b) to obtain the wall pressures in the separated bubble region.

2.3 INSTRUMENTATION AND PROCEDURE

2.3.1 Pressure pulsation measurements:

The data reduction system and the associated instrumentation are shown in Fig. 2.4. The frequency of pressure pulsations in the cavity were obtained with the help of pressure transducers [Validyne, DP15] located close to the edge of free shear layer (Fig. 2.1b). Transducers were also placed at other locations along the wake to record the pressure pulsations. The output signal from the transducer demodulator [Validyne, CD15] was fed to a Fast Fourier Transform Analyser [Wavetek, 5830-A] to carry out the spectral analysis. Standardised probability density functions were also obtained by operating the analyser in

the histogram mode. The data was sometimes recorded on to a four channel frequency modulated tape recorder [Hewlett-Packard, 3960-A] for later analysis. A stroboscope [Brueel and Kjaer, Type 4912] and a battery of powerful lights were used to aid visual observation.

2.3.2 Velocity measurements:

Use was made of a TSI Laser Doppler Velocimeter (LDV) system in the forward scatter mode to obtain the velocity distributions in the test section. Fig. 2.5 shows a simple schematic of the LDV system. The system includes a 15mW He-Ne laser having a wave length of 632.8 nm, transmitting optics (collimator, beam splitter, beam expander, 40 MHz bragg cell and transmitting lens) to focus the light beams into the measuring region, receiving optics (receiving assembly and lens) to collect the light scattered by the particles in the flow, a photodetector to convert the light signals into electrical signals and a signal processor interfaced to a personal computer. To measure the reverse velocities in the separated regions behind the backward facing steps, a standard frequency downshift of 2 MHz was used. The LDV system and the data analysis software were calibrated using a specially fabricated nozzle unit (Fig.2.6a). In order to cover a wide range of flow, three nozzles with different orifice diameters (3.175, 6.35 and 12.70 mm) were adopted. The nozzles had very high contractions to reduce the turbulence levels. The velocities at the exit of the nozzles (Fig.2.6b) were measured using the LDV system in the forward scatter mode and compared to the velocities obtained through direct discharge measurements. The discharge through the nozzle unit were measured using an in-situ weighing scale. Long enough time samples were adopted during the weighing process. The velocities in the potential core of the nozzle mouth measured by the LDV system compared very favourably with those obtained through the discharge measurements.

2.3.3 Cavitation Nuclei measurements:

The cavitation nuclei measurements were made with a Laser Particle Dynamics Analyser (PDA). The PDA system (DANTEC Inc.) is essentially an extension of the LDV system. The transmitting optics essentially resembles that of the LDV system with the 40 MHz bragg cell being an essential part of the optic train (Fig. 2.7a) The receiving optics includes a system of 3 photomultiplier tubes (PM tubes) located at different scattering angles. The signals received at the PM tubes have a phase difference which is linearly dependent on the particle diameter. The system of 3 PM tubes assist in data validation checks and aid in discrimination of spherical particles from other particulates. In the present study, test data indicated that the mean diameter of the spherical particles range from 14 to 20 micrometers and did not vary over a range of velocities (Fig. 2.7b).

2.3.4 Other measurements:

During each test, the water temperature was noted to the nearest 0.25°C. Due to the large sump capacity, the temperature rise during a test was negligible. The dissolved air content ranged from 11 to 17 ppm and was estimated by obtaining the dissolved oxygen content using a YSI-57 D.O. meter [Morgan 1972]. During any specific run, the change in air content was negligibly small. The rate of flow was measured with the help of a calibrated venturimeter or a V-notch. The depth of flow over the notch was measured to the nearest 0.1 mm. The accuracy of discharge measurement is estimated to be 3%. Using calibrated pressure gages, the positive pressures were measured to the nearest 0.25 kPa, while the negative pressures were measured to the nearest 6.35 mm of mercury. The positive pressure gages were calibrated using dead weight testers. The negative pressure gages and pressure transducers were calibrated using a vacuum pump in the presence of an accurate U - tube mercury manometer. Typical calibration curves are shown in Figs. 2.8a and 2.8b. The range of test cavitation numbers spanned the non-cavitating, partially

cavitating and near choking conditions. The error ranges of the observed or computed data presented in the forthcoming sections are given in Appendix IV.

2.3.5 Cavitation Inception detection:

Cavitation inception was detected visually by noting the occurrence of a few minute bubbles. Since desinent cavitation number has been shown to be more repeatable in several studies [Holl 1960], the desinent cavitation number is adopted to denote the limited cavitation index. In the present study no significant cavitation hysteresis was distinguishable and as such the desinent and incipient indices are essentially the same. The incipient condition was obtained at each velocity by reducing the free stream pressure until cavitation began to occur in the wake and then increasing the pressure until cavitation just disappeared or occurred intermittently. This state of cavitation was generally accompanied by the intermittent presence of a sharp crackling noise. A stethoscope placed on the plexiglas window close to the free shear layer further aided this observation.

2.3.6 Geometrical characteristics:

The various geometrical characteristics of the cavity formed behind the bluff body measured during the test series are indicated in Fig. 2.9a. In Fig. 2.9a, "L" denotes the total length of the wake measured from the stagnation point to the tip of the cavity. The width (W) of the cavity was recorded at the location of the maximum wake width. The geometrical parameters were obtained several times during a test run and the values plotted in the forthcoming figures are the average values. During tests related to the measurement of the length of vortex formation region L_f (Fig. 2.9b), the internal generator of the strobe was manually set at the vortex shedding frequency "f" obtained from the spectral measurements. The values of L_f were determined visually under periodic illumination of the strobe. The presence of cavitation in the core of the vortices aided the flow visualization process. Several measurements were made during a given run and the values presented are

the average values of L_f .

The location of reattachment behind the backward facing steps were determined by extrapolating the loci of the streamwise zero mean velocity ($U=0$) to the wall. Details regarding the measurement of X_r (Fig. 7.1) are provided in Chapter 7.

2.3.7 Detection of Choking cavitation conditions:

The choking cavitation state was attained by increasing the velocity of flow and thereby decreasing the cavitation number until no significant change in cavitation index was obtained. This is the least possible cavitation number obtainable at a given blockage. Under these conditions, the spectra did not indicate the existence of a dominant frequency. This fact served as an indicator for the approach of choking conditions.

2.4 TUNNEL QUALIFICATION

Preliminary experiments were conducted to check the quality of flow in the unobstructed test section of both the water tunnels. The following tests were carried out to obtain the flow quality:

(i) A span-wise uniformity check of the axial velocity distribution at a section 50 mm downstream of the inlet in a horizontal plane perpendicular to the flow was carried out. Figs. 2.10a and 2.10b show typical span-wise velocity distributions measured using the LDV system in the forward scatter mode for a range of flow rates in the two water tunnels. In these figures, the velocities are normalised by the centre-line velocity U_c . In the test section of Tunnel I, the velocities appear to be uniform to within 3% over the mid 75 percent of the span. Furthermore, the ratio of the average velocity to the centre-line velocity was found to be of the order of 0.90 in Tunnel I and 0.94 in Tunnel II. This is a good indication of the two-dimensionality of the flow in the test sections and compares favourably with standard two-dimensional flow investigations [Lee 1973, Vigander 1965, Kim 1986]. Following Adams and Eaton (1988), a mass balance was carried out over the entire test

section assuming two-dimensionality. The mass flux balanced to within 3.5%. The maximum turbulence level in the test section of the Tunnel I was found to be of the order of 4%. However, during a typical run when non-cavitating conditions prevailed, the turbulence intensity was generally of the order of 2%. The maximum turbulence level in Tunnel II was of the order of 2%.

(ii) Calibration of equipment and validation of test procedures were carried out by the ability to reproduce well established results. Figs. 2.11 and 2.12 show the variation of $K_s=U_s/U$ and $S=fb/U$ with b/B obtained in Tunnel I for non-cavitating flows. Here, K_s is the ratio of the separating streamline velocity to the free stream velocity (Fig. 3.1) and S is Strouhal number. As seen in these figures, the present set of data is in good agreement with several previously established data. As will be shown later, most of the test results obtained in non-cavitating flow past backward facing steps and sharp-edged bluff bodies mounted in Tunnel II compare favourably with those obtained in several previous studies.

2.5 NON-DIMENSIONAL TEST VARIABLES

Based on the vapor pressure P_v , the cavitation number σ is defined as follows,

$$\sigma = \frac{P - P_v}{\frac{1}{2} \rho U^2} \quad (2.1)$$

where, P and U are the free stream pressure and velocity respectively (Fig.2.2) and ρ is the density of water. σ_i and σ_{ch} denote the value of σ at incipient and choking conditions respectively. Based on the pressure P_s and velocity U_s along the separating stream line, the following parameters are defined,

$$C_{ps} = \frac{P_s - P}{\frac{1}{2}\rho U^2} \quad (2.2)$$

$$\sigma_s = \frac{P - P_v}{\frac{1}{2}\rho U_s^2} \quad (2.3)$$

where, C_{ps} is the separating pressure coefficient and σ_s is a modified cavitation number.

From energy considerations, one notes that ,

$$\sigma_s = \frac{\sigma}{1 - C_{ps}} \quad (2.4)$$

The wake pressure coefficient C_{px} at any point x along MN in Fig. 2.1b is defined as,

$$C_{px} = \frac{P_x - P}{\frac{1}{2}\rho U^2} \quad (2.5)$$

The pressure coefficients C_p along the bottom of the separation bubble along PQ in Fig. 2.3b are defined as,

$$C_p = \frac{P_x - P}{\frac{1}{2}\rho U^2} \quad (2.6)$$

The modified pressure coefficient C_p^* is defined as

$$C_p^* = \frac{C_p - C_{p \min}}{1 - C_{p \min}} \quad (2.7)$$

where, $C_{p \min}$ is the minimum pressure coefficient occurring along PQ (Fig. 2.3b). In the case of the bluff body, the Strouhal number and the modified Strouhal numbers based on U_s and L are defined as follows,

$$S = \frac{f b}{U} \quad (2.8)$$

$$S_s = \frac{f b}{U_s} \quad (2.9)$$

$$S_L^* = \frac{f L}{U_s} \quad (2.10)$$

In the case of the backward facing step, the Strouhal number is defined as,

$$S = \frac{f h}{U} \quad (2.11)$$

L/b , W/b , X_r/h , b/B , $ER = B/(B-h)$ and the Reynolds number $Re = Ub/\nu$ or Uh/ν are the other non-dimensional variables significant in this study. Here, W is the maximum wake width (Fig. 2.9a), X_r is the reattachment length (Fig.2.3b), ER is the expansion ratio and ν is the kinematic viscosity of the fluid.

CHAPTER III
NON-CAVITATING FLOW PAST BLUFF BODIES

CHAPTER III

NON - CAVITATING FLOW PAST BLUFF BODIES

To form a precursor for the present study related to wall interference effects on cavitating flow past bluff bodies, the existing data related to the influence of blockage on non-cavitating flows were re-analysed. This chapter deals with the development of semi-empirical relations derived for the variation of the steady drag force of two-dimensional sharp edged bluff bodies due to blockage effects on the basis of the momentum balance approach. These shapes were chosen to eliminate or reduce Reynolds number effects in interpreting the results. The range of blockage corrections include very low blockages ($b/B \leq 0.15$), where the contracted jet velocity and the separating velocity are recognised to be different and incorporated in the model. In the analysis, to account for the non-uniform velocity distribution in the contracting jet, a secondary correction factor is included. For $b/B \geq 0.30$, an estimate of the drag coefficient C_d is obtained without recourse to empirical relations. Experimental data is used to verify the predicted expression for the estimation of the drag force at various blockages.

3.1 PREVIOUS STUDY

The effect of blockage on non-cavitating flow past bluff bodies have been the subject of many previous investigations. A rigorous discussion is not attempted as much of the work cited here serves principally as a background information for the current study. To account for the interference effects due to the side walls of a test facility, an increment to the flow velocity is often proposed [Glauret 1933, Maskell 1963]. A few models have been developed [Allen and Vincenti 1944, Roshko 1954, Modi 1977] to predict the drag of bluff bodies subject to wall confinement on the basis of hydrodynamic principles. Allen

and Vincenti [1944] carried out an analytical treatment of blockage effects including the effect of compressibility and provided a general correction formula. However, Dalton [1971] in a later study concluded that this correction formula was limited to lower blockages. Based on the concept of a quasi steady wake, Maskell [1963] provided a blockage correction formula. Toebes [1971] questioned Maskell's assumption regarding the wake pressure P_w being equal to the back pressure P_b (Fig. 3.1). It is now well established that even the near wake is dynamic. The variation of the pressure along the wake axis has been reported for both two-dimensional and axisymmetric bluff bodies [Sullerey et al. 1975]. Shaw [1969, 1971] has suggested that the contracted jet velocity U_j (Fig. 3.1) is close to the separation velocity U_s when blockage is relatively high. Consequently, the contraction coefficient C_c is a significant parameter for flow past bluff bodies, since it enables one to estimate the value of U_j . Other earlier studies [Ramamurthy et al. 1973a, 1973b] have shown that the steady drag coefficient for non-cavitating bluff bodies normalised by the contracted jet velocity is independent of wall interference over a large range of blockages.

3.2 THEORETICAL CONSIDERATIONS TO EVALUATE C_d

The following assumptions are made in developing the governing equation:

- (i) For a given blockage, the pressure coefficient C_{ps} at the separating point is independent of the Reynolds number, $Re = Ub/\nu$.
- (ii) The back pressure P_b immediately behind the body is essentially the same as the separation pressure, P_s [Shaw 1969].
- (iii) The boundary friction is negligible along the control surfaces.

As stated earlier, the pressure along the centre line of the wake varies and is different from the separating pressure. In view of this, a control volume denoted by the line enveloping the points E, F, G, H, I, J, K and L is chosen (Fig.3.1). The pressure acting

along the surfaces FG and JK is denoted as P_j . Further, as the separation speed U_s is nearly constant, P_s does not vary very much along HG and IJ. Consequently the pressure all along the control surface GHIJ will be equal to P_s . Considering unit depth of flow and applying a momentum balance for the control volume, one obtains,

$$PB + \rho U^2 B = P_j (B-b) C_c + P_s [B - (B-b) C_c] + \beta \rho U_j^2 (B-b) C_c + \frac{1}{2} C_d \rho U^2 b \quad (3.1)$$

where, C_d is the drag coefficient and C_c , the contraction coefficient of the jet [Shaw 1969] is given by Eq.(3.2),

$$C_c = \frac{\pi}{\pi + R \tan^{-1} \frac{2}{R}} \quad (3.2)$$

with,

$$R = \frac{\left[1 - \left(\left(1 - \frac{b}{B} \right) C_c \right)^2 \right]}{\left(1 - \frac{b}{B} \right) C_c} \quad (3.3)$$

At sections FG and JK (Fig.3.1), the velocity varies from a maximum value of U_s at the separating streamlines to a value of zero at the walls and further U_s is not necessarily equal to U_j for very low blockages. To account for this non-uniform velocity distribution, a momentum correction factor β is proposed. In Eq.(3.1), β is commonly defined as,

$$\beta = 1 + \epsilon^2 \quad (3.4)$$

where, according to Chow [1959],

$$\varepsilon = \frac{\text{Maximum velocity}}{\text{Mean velocity}} = 1.0 \quad (3.5)$$

Hence,

$$\varepsilon = \frac{U_s}{U_j} = 1.0 = \frac{K_s}{K_j} = 1.0 \quad (3.6)$$

In Eq.(3.6) $K_s = U_s/U$ and $K_j = U_j/U$. Using continuity relations,

$$UB = U_j(B-b)C_c \quad (3.7)$$

Hence,

$$\frac{U_j}{U} = K_j = \frac{1.0}{\left[1 - \frac{b}{B}\right] C_c} \quad (3.8)$$

For inviscid flow, Bernoulli's equation along the free streamline (Fig.3.1), relates the separation pressure coefficient C_{ps} with K_s . Thus,

$$C_{ps} = \frac{P_s - P}{\frac{1}{2} \rho U^2} = 1.0 - K_s^2 \quad (3.9)$$

Similarly, from energy considerations including the contracted jet region, one obtains,

$$C_{pj} = 1.0 - K_j^2 \quad (3.10)$$

Substituting Eqs. (3.8), (3.9) and (3.10) in Eq. (3.1), and simplifying,

$$C_d = \frac{B}{b} \left[2.0 - C_{ps} - \frac{1}{K_j} (1.0 - C_{ps} - K_j^2) - 2 \beta K_j \right] \quad (3.11)$$

3.3 ANALYSIS OF RESULTS

Most of the existing studies related to the effect of blockage on the drag coefficient of bluff bodies are based on momentum considerations. The difference between the various approaches [Roshko 1954, Maskell 1963] can be traced to the assumptions made in the development of the model. The assumptions made in the present model are very appropriate for flow past flat plates. However, assumption (ii) of Section 3.2 is only approximately true for bluff shapes which have after bodies (equiangular prism with orientation $\theta = 0^\circ$ - Fig 2.1b, Insert). For such shapes, the back pressure is non-uniform [Ramamurthy 1973b].

Fig.3.2 shows the variation of C_{ps} with b/B when blockage is low ($0.0 \leq b/B \leq 0.15$) and moderate ($0.15 \leq b/B \leq 0.50$). Using this data, an empirical relation between C_{ps} and b/B can be obtained . Thus ,

$$C_{ps} = -1.06 - 1.80 \left(\frac{b}{B}\right) - 24.35 \left(\frac{b}{B}\right)^2 \quad (3.12)$$

For two-dimensional sharp-edged bluff bodies, Fig.3.3 shows the theoretical variation of K_j with b/B (Eq.(3.8)) and the experimental variation of K_s with b/B . For vanishingly small values of blockages, test results indicate that there is a minimum value of U_s and hence K_s . For any blockage, the theoretical value of C_c for flat plates can be computed using Eqs.(3.2) and (3.3). Consequently, one can estimate the values of K_j for all

blockages (Eq.(3.8)). It can be seen from Fig.3.3 that the values of K_j will be equal to the experimental values of K_s , only when the blockage is relatively higher ($b/B > 0.3$). When blockage is not high, $K_s \neq K_j$, since the value of U_s will always be greater than a threshold value of $1.47U$. Using Eqs.(3.4), (3.8) and (3.12) in Eq.(3.11), one can estimate the values of C_d for $b/B < 0.30$.

For higher blockages, $\beta = 1.0$ (Eq.(3.4)) and K_j can replace K_s in Eq. (3.11). Accordingly, Eq.(3.11) can be rewritten as,

$$C_d = \frac{B}{b} (K_j - 1)^2 \quad 0.3 < \frac{b}{B} < 0.7 \quad (3.13)$$

For $b/B \geq 0.30$, the value of C_c is known. Hence, K_j and C_d can be evaluated using Eq.(3.13) without recourse to any experimental data. Fig. 3.4 shows the variation of the drag coefficient C_d with blockage in the wide range $0.025 < b/B < 0.7$. A reasonably good agreement is found between the experimental values and Eq. (3.11). At extremely low blockages, minor discrepancies seem to occur between the test data and Eq.(3.11). Part of the discrepancy can be attributed to the fact that the theoretical estimate of the momentum components in Eq.(3.1) based on C_c are only approximate, since the contraction is ill defined and the "outer layers of the contracting jet quickly diffuse after separation" [Shaw 1969]. At larger blockages, the experimental values for prisms ($\theta=0^\circ$, Insert - Fig.3.3) appear to be higher than the predicted values. This discrepancy can be traced partly to the presence of the after body of the prisms, where the back pressure is non-uniform. In fact, at the apex of the afterbody, the pressure drops below the value of the pressure at the separating point [Ramamurthy 1973b]. Consequently, the experimental value of the drag coefficient is expected to be higher.

CHAPTER IV
INCEPTION CHARACTERISTICS OF CONFINED
SHARP-EDGED BLUFF BODIES

CHAPTER IV
INCEPTION CHARACTERISTICS OF CONFINED SHARP - EDGED
BLUFF BODIES

It is of interest to the design engineer to determine the inception cavitation index σ_i of liquid handling devices like hydraulic pumps, turbines and valves. As indicated earlier, σ_i denotes the first occurrence of cavitation in the flow system and is defined as,

$$\sigma_i = \frac{P - P_v}{\frac{1}{2} \rho U^2} \quad (4.1)$$

This chapter deals with the procedure to determine σ_i in the wake of confined, sharp edged two-dimensional bluff bodies such as flat plates and wedges.

4.1 PREVIOUS STUDIES

Several investigators have studied the cavitation inception characteristics of bluff bodies having large separated flow regions. For instance, in studies related to cavitating flow behind sharp edged disks, Kermeen et al. (1957) and Arndt (1978) found that inception occurred in the free shear layer downstream of the separating points and that σ_i increases with Reynolds number. Arakeri (1979) and Katz (1981) respectively studied cavitating flow past axi-symmetric downstream facing step and blunt circular cylinders and observed that σ_i increases with Reynolds number.

Kermeen et al. [1957] developed a theoretical model to predict the cavitation inception index in the near wake of axi-symmetric disks. Arndt [1976] suitably extended the analysis of Kermeen and Parkin [1957] related to the correlation between Reynolds

number and σ_i and validated his predictions with experimental data. He also suggested that the boundary layer developed on the face of the disk of diameter d should be laminar for $Re = Ud/\nu < 2 \times 10^5$. It is appropriate to note that the wake characteristics of axi-symmetric disks are not quite similar to that of sharp-edged two dimensional bluff bodies. As one would expect, the wake pattern of the latter is characterised by alternate vortex shedding and the formation of the well known Karman street.

In the present study, attention is focussed on the inception characteristics of two-dimensional, constrained sharp edged bluff bodies. A procedure to predict σ_i for flat plates and wedges with the front face normal to the flow is provided over a range of Reynolds numbers at various blockages. The advantage of studying the inception characteristics of a bluff source lies in the fact that the body acts only as a vortex generator and no cavitation occurs on the body itself. Thus, some of the complications introduced by cavitating solid boundaries could be avoided to a certain extent. The present semi-empirical model includes the effects of blockage, boundary layer growth on the fore-body face, the entrainment of the fluid into the vortex and the loss of circulation in the region where the free shear layer develops into the discrete vortex. The proposed model is verified using experimental data.

4.2 THEORETICAL CONSIDERATIONS TO DETERMINE σ_i :

As indicated earlier, the flow pattern in the wake of a two-dimensional bluff body is dominated by the presence of alternate vortex formation on either side of the body. In the near wake flow field, the minimum pressure occurs in the core of the vortex formed by the rolling up of the shear layer. Cavitation first begins to occur when the pressure in the core of the rolled up vortex is equal to the vapor pressure P_v . A Rankine vortex model is used to describe the pressure variation in the discrete vortex shed from a bluff body. Let

P_0 be the pressure at the centre of the vortex formed behind the bluff source. Then,

$$P_0 = \Pi - \frac{k^2 \rho}{a^2} \quad (4.2)$$

where k is the strength of the vortex, a is the radius of the vortex and Π is the pressure corresponding to $a \rightarrow \infty$ [Robertson 1965]. Noting that circulation $\Gamma = 2\pi k$ and the pressure at the outer edge of the vortex is P_s , one can re-write Eq.(4.2) as,

$$\frac{P_s - P_0}{\frac{1}{2} \rho U^2} = 2 \left[\frac{\Gamma}{2 \pi U a} \right]^2 \quad (4.3)$$

Since inception occurs when the pressure in the core of the vortex is equal to P_v , an expression for σ_i can be written as follows,

$$\sigma_i = -C_{ps} + 2 \left[\frac{\Gamma}{2 \pi r_c U} \right]^2 \quad (4.4)$$

In Eq.(4.4), C_{ps} is the separating pressure coefficient at inception conditions and r_c is the radius of the vortex, where the core pressure is equal to P_v . In non-cavitating flows, the value of C_{ps} for any blockage is well documented in literature. As will be shown in a subsequent section, the value of C_{ps} in the presence of incipient cavitation in the wake is essentially the same as that obtained in non-cavitating flows. The problem now essentially consists of evaluating the values of Γ and r_c at a given free stream velocity to determine σ_i .

The wake structures and vortex shedding characteristics of non-cavitating two-dimensional bluff bodies have been subjected to extensive reviews [Marris 1964, Sarpkaya 1979 and Bearman 1984]. Gerrard [1966] has given an extremely useful physical description of the mechanics of vortex formation. As he points out, the key factor in the formation of the vortex street is the mutual interaction between the two separating shear layers. The vortex continues to grow, fed by circulation from the connecting shear layer, until it is strong enough to draw the opposing shear layer across the near wake. As the vortices rotating in opposite directions approach each other, there is a tendency to cut off further supply of circulation to the growing vortex. Consequently, the strength of the individual wake vortex will be less than the total circulation shed from one side of the bluff body. Further, a certain amount of vorticity dissipation is to be expected following the vortex shedding process. Davies [1976] expressed the fractional circulation remaining in the discrete vortex as,

$$\alpha = \frac{2 S \Gamma}{U b (1.0 - C_{ps})} \quad (4.5)$$

where, S is the Strouhal number. From experimental observations, Fage and Johansen [1927] found that α varied from 0.50 to 0.60. Based on computational experiments, Sarpakaya [1975] and Clements [1973] found that the strength of the vortex cluster varies from 84 to 91% of the vorticity generated in each shear layer. More recently, Perry [1987] found a maximum value of 0.67 for α . Abernathy and Kraneur [1962] evaluated a net vorticity of 62% based on a model dealing with the interaction of two inviscid vortex sheets. Consequently, in this study, an average value of 0.7 is adopted for α to evaluate Γ for any required free stream velocity using Eq.(4.5). This value of α has

been very recently confirmed by Zdravkovich (1989).

As pointed out rightly by Gerrard [1966], entrainment plays a very important role in the vortex formation process. Recent studies by Cantwell [1983], Bearman [1984] and Perry [1987] show that the process of entrainment is quite complex. Using a hot wire and considering a circular vortex, Cantwell [1983] found that the entrainment of the fluid into the vortex occurs at a rate of about 6% of the free stream velocity. Extending the suggestion of McCormick, Arndt [1976] applied a mass balance between the fluid in the vortex and that contained in the boundary layer on the fore-body face. Adopting a similar procedure and including the effects of entrainment of the fluid into the vortex and assuming that entrainment occurs at 6% of the free stream velocity during the vortex formation cycle, one can obtain the following expression for r_c ,

$$\pi r_c^2 f = 2 \pi r_c (0.06 U) + \int_0^{\delta} u dy \quad (4.6)$$

where, the first term on the right hand side represents the average mass entrained. In Eq.(4.6), δ is the terminal thickness of the boundary layer on the forebody prior to separation. Eq.(4.6) can be simplified to yield,

$$r_c^2 = \frac{b}{\pi S} \left[K \delta \left\{ 1.0 - \frac{\delta_1}{\delta} \right\} + 0.12 \pi r_c \right] \quad (4.7)$$

where, $K = U_g/U$ and δ_1 is the terminal boundary layer displacement thickness prior to separation. As seen earlier, from energy considerations along the separating streamline, $K^2 = (1.0 - C_{ps})$. Both S and C_{ps} are nearly constant for a given blockage in the range of

interest ($2.0 \leq Re \times 10^{-5} \leq 4.0$). This fact has been reported earlier in non-cavitating flow past bluff bodies [Ramamurthy 1973] and is confirmed by the present test data which is presented subsequently. To evaluate r_c from Eq.(4.7), one should know the boundary layer characteristics on the fore-body face. Using Eq.(4.5) in Eq.(4.4) and simplifying, one can evaluate σ_i . Thus,

$$\sigma_i = 6.206 \times 10^{-3} \left[\frac{K^2 b}{r_c S} \right]^2 - C_{ps} \quad (4.8)$$

From Eq.(4.8), it can be observed that for a bluff body σ_i is a function of r_c when the blockage is fixed. The value of r_c can be easily computed knowing the values of δ and δ_1 for any given Re using Eq.(4.7).

4.3 ANALYSIS OF RESULTS :

In the present study, it is assumed that the boundary layer developed on the fore-body face is laminar for the range of Re ($2.0 \leq Re \times 10^{-5} \leq 4.0$) tested. Based on the fore-body pressure distribution data, δ at separation can be computed using the well known method of Thwaites [Round and Garg 1986]. This in turn enables one to determine r_c and hence σ_i . The forebody pressure distribution of two-dimensional bluff bodies have been obtained by several investigators [Ramamurthy 1973, Modi 1977] at various blockages under non-cavitating conditions. Under these conditions, it has been found that the forebody pressure distribution does not vary over a range of Re. Reanalysing the data presented by Ramamurthy [1977] it was noticed that the forebody pressure distribution at any given blockage is not significantly effected by the presence of partial or full cavitation in the wake. Consequently, one can assume the forebody

pressure distribution at inception to be the same as in non-cavitating flows.

Previous wind tunnel studies [Ramamurthy 1973, Shaw 1971 and Modi 1977], have presented the fore-body pressure distributions for bluff bodies at various blockages. Typical fore-body pressure distributions are shown in Fig 4.1. Using the notations shown in Fig 4.1, $X' = 0.0$ refers to the stagnation point s' (Inset - Fig.4.1) and $X' = 1.0$ refers to the separating edge s of the body. The potential flow velocity distribution just outside the boundary layer is obtained from these pressure distributions (Fig 4.2). Third degree polynomial fits are obtained for the resulting velocities as a function of the distance from the stagnation point. Using such fits, the boundary layer thickness at separation is obtained by adopting the procedure outlined by Thwaites [Round and Garg 1986]. Typical relations are shown below :

$$\left[\frac{\delta}{b} \right]^2 = \frac{0.645}{Re} \quad \text{for } b/B = 0.243 \quad (4.9a)$$

and

$$\left[\frac{\delta}{b} \right]^2 = \frac{0.555}{Re} \quad \text{for } b/B = 0.325 \quad (4.9b)$$

Further, it can be shown that, $\delta_1/\delta = 0.224$ at both the above mentioned blockages.

At any given blockage, the values of Strouhal number S and the separation pressure coefficient C_{ps} are well documented under non-cavitating conditions. For the present series of tests at inception conditions, Fig 4.3 shows a typical variation of S and C_{ps} with Re for a blockage of 0.243. The value of S was computed using the dominant frequency obtained from the power spectra of the wake pressure pulsations. Typical power spectra at inception conditions are shown in Fig 4.4. The values of S and C_{ps}

obtained in the present series of tests are in good agreement with those found in non-cavitating flows [Modi 1977, Ramamurthy 1973].

Using the values of S and C_{ps} and expressions such as Eq.(4.9), one can determine r_c and hence σ_i at any given Reynolds number. Fig 4.5 shows a the theoretical variation of σ_i with Re for $b/B = 0.243$ and 0.325 . For the range of Re tested, the theoretical increase in σ_i is of the order of just 1%. This is not surprising in view of the fact that the other hydrodynamic characteristics like drag coefficient and Strouhal number are almost independent of Re , in the range of Re considered. Also plotted in Fig 4.5 are the experimental values of σ_i observed in the present series of tests. These values are found to be in fair agreement with the predicted values {Eq.(4.8)}. As observed from Fig 4.5, viscous effects do not seem to have a dominant influence on the inception characteristics. However, the influence of blockage is distinctly seen in Fig 4.5. The scatter seen in the data are partially due to the error resulting from difficulties associated with visual observation. There is a certain amount of uncertainty associated with the acoustic methods due to background noise. Furthermore, as pointed out by Katz [1986], the major component of the scatter is due to the fact that cavitation inception requires the simultaneous occurrence of two events, low enough pressures and microscopic free stream cavitation nucleus of such a size that it becomes unstable at the local pressure.

The model developed to determine the value of the inception cavitation index can be extended to a wider range of blockages using the data related to the fore-body pressure distribution for non-cavitating flows from existing literature. Fig 4.6 shows the variation of σ_i with b/B obtained from Eq.(4.8) at a typical Re of 2.0×10^5 . Also plotted in Fig 4.6 are the experimental values of σ_i obtained for 0° wedges in the present study and those of a gate [Narayan 1984], and a normal flat plate [Chu 1967]. The model seems to

predict the σ_i values fairly accurately over the range of blockage tested.

It should be noted from Fig. 4.6, that both the proposed model and the experimental data indicate that as $b/B \rightarrow 0.0$, σ_i does not vanish but attains a value of about 3.1. In the right hand side of Eq.(4.8), the first term is a product of positive values and the second term $-C_{ps}$ is also a positive value and hence σ_i should be expected to have a positive value even for vanishingly small values of b/B . Further, one may recall that for non-cavitating flow past bluff bodies at vanishingly small values of blockage, K ($= (1.0 - C_{ps})^{0.5}$) attains a constant value of about 1.47 (Fig.3.3). Since, C_{ps} tends to maintain a threshold value at very small blockages, Eq. (4.8) indicates that σ_i should also maintain a non-zero value as $b/B \rightarrow 0.0$.

CHAPTER V
WAKE CHARACTERISTICS OF CONFINED BLUFF BODIES

CHAPTER V

WAKE CHARACTERISTICS OF CONSTRAINED BLUFF BODIES

It has been recognised that bluff, unstreamlined bodies are subject to flow induced vibration when air or water flows past them. The near wake flow field of such flows exhibit a dominant periodicity and the body is acted upon by both steady and unsteady forces. If the structure is flexible or lightly damped, resonant oscillations can be excited. A predominant cause of resonant oscillations is the organised periodic shedding of vortices, as the flow separates from the structure. A study of the wake characteristics of such flows would be very useful in a better understanding of flow induced vibration, erosion and noise.

In this chapter, the wake characteristics of constrained, partially and fully cavitating two-dimensional bluff bodies serving as test models are presented, over a large range of blockages. To distinguish cavitation effects, from viscous effects (commonly referred to as Reynolds number effects), sharp edged bluff bodies with fixed separation points are used. The effect of Reynolds number on the test results are discussed by comparing the characteristics of a circular source with that of prismatic source at a very small blockage. The effect of blockage and cavitation on the geometrical characteristics such as the length and the width of the cavity (Fig. 2.9a) formed behind the bluff body are discussed. The frequency of pressure fluctuations in the wake and the mean static pressure distribution along the wake axis are also presented. The generation of small eddies in the shear layers followed by a reduction or elimination of Karman vortex street at very large blockages are discussed.

In the present study, for purposes of identification, the range of blockage in which a distinct Karman vortex street is discernible is denoted as 'moderate' ($0.15 < b/B < 0.50$).

The range of blockage, where the size of the body is comparable to the size of the test section and wall interference effects are severe, is denoted as 'large' ($b/B \geq 0.50$). The separating pressures and vortex shedding characteristics of a wedge at 0° to flow (Fig. 2.3a), a normal flat plate and a wall mounted plate (gate) at a very large blockage ($\approx 93\%$) are compared. At any given blockage, the variations in the wake pressure histograms with gradual reduction in cavitation numbers were noted. Using periodic strobe illumination to freeze the wake region, the effect of cavitation on the length of the vortex formation region (Fig. 2.9b) behind the bluff bodies were obtained. The location of the region of vortex formation precedes the region of erosion due to cavitation. As such, locating the zone of vortex formation assists in interpreting cavitation erosion results. The stability of the vortex against break up in the presence of cavitation was visually observed. Efforts were also made to obtain proper length and velocity scales to form the Cavitation and Strouhal numbers to absorb blockage effects.

5.1 PREVIOUS STUDIES

Several studies have been reported on the characteristics of flow past cavitating bluff bodies mounted in water tunnels [Waid 1957, Varga 1966, Young and Holl 1966, Palanichamy 1974, Ramamurthy 1977, Hammitt 1980, Oba et al. 1980 and Arndt 1981]. A few studies have also been conducted to determine the effects of blockage and cavitation on the hydrodynamic characteristics of flow past bluff bodies [Birkhoff 1950, Cohen and Di Prima 1958, Wu 1969, Syamala Rao 1975 and Bhaskaran 1977]. In some of the earlier investigations, two-dimensional bluff circular cylinders were used as the cavitating source [Shalnev 1965, 1977, Varga 1966, Oba et al. 1981 and Syamala Rao 1975]. As pointed out earlier, in these studies, the test conditions generally spanned the critical Reynolds number of the cylindrical cavitating source. Hence, the results of these tests are expected to be highly Reynolds number dependent. The use of bluff bodies with fixed separation

points like two-dimensional normal plates and wedges are suggested to reduce or eliminate Reynolds number effects [Ramamurthy 1973a]. For constrained non-cavitating flow past bluff bodies, it is shown that the jet contraction velocity U_j (Fig. 3.1) and the gap velocity U_1 are the proper velocity scales to normalize the drag coefficient and the Strouhal number [Ramamurthy et al. 1973]. However, one should note that the width of the cavity itself changes in cavitating flows. As such, for constrained cavitating flow past bluff bodies, the contracted jet velocity is expected to depend on the cavitation number too. Consequently, the contracted jet velocity obtained through the use of the contraction coefficient (Eq.3.8) cannot be expected to normalize the drag coefficient and the Strouhal number to absorb blockage effects, especially at lower cavitation numbers. Very limited studies related to the effect of blockage on flow past severely constrained bluff bodies ($b/B > 50\%$) are available in literature. These include the studies of Chen (1967) for 90° wedges and that of Tozkas (1965) for a normal plate at a blockage of 74% in non-cavitating flow.

Young and Holl (1966) measured the vortex shedding frequency behind symmetric wedges using stroboscopic light techniques and high speed movies. Following this, the frequency of vortex shedding behind cavitating circular and prismatic sources at low and moderate blockages are reported by Ramamurthy (1977). Rao et. al (1975) note that the frequency of vortex shedding increases abruptly to very large values as the cavitation number of the flow is reduced and choking conditions prevail. However, the results of Young (1966) and Bhaskaran (1977) indicate that the Strouhal number tends to zero as choking conditions are approached. Since, Rao et. al (1975) used circular bluff bodies as the cavitating sources, their results are expected to be highly dependent on the flow Reynolds number. In studies related to generation of vortices from surfaces of separation, Appel (1961) states that cavitation may tend to stabilize the vortices formed against further break up. Vigander [1965] supports this hypothesis of vortex stabilizing mechanism due to the presence of a vapor core.

Waid (1957), Varga (1966), Chandrashekara (1973), Syamala Rao (1975) and Oba et al. (1980) have studied the influence of cavitation number on the length of cavity formed behind bluff circular cylinders. For non-cavitating flow past a circular cylinder at an extremely low blockage (5%), Oba et al. (1980) determined the sub-critical Reynolds number range in which viscous effects were not dominant. Using this information, they conducted cavitation experiments to determine the geometrical characteristics of the wake. Even at a fixed Reynolds number, their data indicate that the position of the separating points shift, especially at very low cavitation numbers. Consequently, one can expect the wake geometry to be influenced by the value of σ due to shift in the position of the separating points.

5.2 ANALYSIS OF RESULTS

5.2.1 Reynolds number effects:

A circular cylinder and a triangular prism were chosen to identify the effects of Reynolds number (Re) on the test results. The blockages chosen are very small to keep the influence of wall interference to a minimum. Fig. 5.1a shows the variation of the pressure coefficient C_{pb} with Re for the circular source ($b/B = .08$). The values of C_{pb} are not single valued in certain ranges of Re . As indicated in Fig. 5.1a, in the range $1.2 \leq Re \times 10^{-5} \leq 1.6$, the values of C_{pb} seem to be very highly dependent on Re . Fig. 5.1b shows the variation of C_{ps} with Re for a prismatic source ($b/B = .097$). The effect of Re on the separating pressure coefficient appears not to be very significant when compared to that of a circular cylinder. The same set of data are re-plotted as a function of the cavitation number σ in Fig. 5.1c. It is clear from Figs. 5.1a-c that it is not possible to distinguish the effects of Re from the effects of σ on the separation pressure coefficient in the case of bluff circular cylinders. Further, for nearly identical blockages, the length of cavity formed behind two circular sources obtained from two separate studies, appear to follow two distinct

trends (Fig. 5.3). These factors indicate that Reynolds number is a very significant parameter for flow past cavitating bluff circular cylinders. In order to reduce or eliminate the effects of Re in interpreting test results, bodies with fixed separation points are chosen to study the influence of cavitation on the wake parameters.

5.2.2 Geometric Characteristics:

For 0° wedges, Figs. 5.3 and 5.4 show the variation of the normalised length (L/b) of the cavity with σ at moderate blockages $\{b/B = 0.24, 0.33\}$ and high blockages $\{b/B = 0.58, 0.66 \text{ and } 0.82\}$ respectively. With a decrease in σ , the length of cavity increases monotonically and this increase is considerable as choking conditions are approached ($\sigma \rightarrow \sigma_{ch}$). Some remarks regarding the measurement of L are in order. At moderate blockages, it was visually observed that lateral oscillations of the cavity tip occur at moderate values of σ . This is a consequence of the alternate vortex shedding mechanism. When σ is reduced further, axial oscillations of the cavity tip become more prominent. The scatter in the data (Fig. 5.3) is possibly a consequence of the oscillations of the cavity tip. An attempt was made to absorb blockage effects by choosing a proper velocity scale to suitably normalise the cavitation number. Since, a change in the cavity dimension has a direct effect on P_s , the separating velocity U_s (Fig.3.1) was used to obtain a modified cavitation number σ_s [Eq.(2.3)]. Fig. 5.5 shows the variation of L/b with σ_s . One notes that for $b/B < 0.50$ (Fig. 5.5a), the data appear to be fairly well clustered around a single curve (Curve A). However, for larger blockages ($b/B = 0.58, 0.66 \text{ and } 0.82$), the data maintain separate trends (Fig. 5.5b). At moderate blockages, visual observations of the cavity with a stroboscope indicate the existence of large scale vortices formed in the wake by the interaction of the shear layers which give rise to a regular alternate shedding mechanism and the well known Karman street. On the other hand, at larger blockages ($b/B > 0.50$), a regular Karman vortex street was not discernible. Instead, small discrete vortices

appeared to develop along the shear layers. As such, at large blockages the dominant frequency of pressure pulsations in the wake is not expected to follow the trend of the vortex shedding frequency found at moderate blockages which are characterised by the Karman vortex street. This fact will be presented subsequently.

Similar to the variation of L/b with σ_s , Fig. 5.6 shows the variation of the dimensionless width of the cavity (W/b) with cavitation number σ_s . At moderate blockages, the width of the cavity increases gradually with a decrease in σ_s . The increase is considerable at very low values of σ_s . The data presented for large blockages include the lowest cavitation numbers achieved. At higher blockages, it may be added that, the data in Fig.5.6 indicate a very minor variation in W/b with σ_s . The data also indicate that U_s is the proper velocity scale to normalise the cavitation number at moderate blockages (Fig.5.6). The cavity width data at larger blockages do not merge with this curve. This is not surprising, in view of the fact that the flow pattern is different at higher blockages. The widths of cavity can also be computed on the basis of the contraction coefficient obtained from the well known classical hydrodynamics approach [Shaw 1969]. However, the computed cavity widths appear to agree with the measured values only at very low values of cavitation numbers ($\sigma \rightarrow \sigma_{ch}$).

5.2.3 Cavity pressure pulsations:

Figs.5.7 and 5.8 show the variation of the Strouhal number S (Eq.(2.6)) based on the dominant frequency of pressure pulsations " f " in the cavity with σ_s for 0° wedges at both moderate and large blockages. The values of f were obtained from the power spectra of the measured wake pressure signals. The pressure records and the corresponding spectra were obtained at several points in the wake. The dominant frequency and the general shape of the spectra always remained the same at any particular cavitation number for all locations of the transducers. At lower blockages, a decrease in σ_s from

non-cavitating conditions results in little or no change in the value of S until a certain cavitation number is reached. A similar observation was noticed by Young and Holl (1966) behind symmetric wedges. They found that S was essentially constant from the inception state down to as low as half the incipient cavitation number. With further decrease in cavitation number, S increases reaching a maximum and decreases further as choking conditions are reached. As σ approaches σ_{ch} , the vortex shedding becomes intermittent and finally ceases. At larger blockages, though visual observations indicate the absence of large scale vortex shedding, the flow is characterised by pressure pulsations in the wake. These pulsations are generally associated with a dominant frequency. Insert b in Fig. 5.9 shows a typical pressure record obtained at $b/B = 0.58$ while Fig. 5.9 shows the power spectra obtained at various cavitation numbers for the same blockage. In Fig. 5.9, a decrease in cavitation number, appears to result in an increase in the dominant frequency. At very low cavitation numbers, the spectra does not seem to indicate a clear dominant frequency. A similar observation can be noticed in Fig. 5.10 at $b/B = 0.823$.

An attempt was made to choose the proper velocity and length scales to suitably normalise the Strouhal numbers to absorb blockage effects. In this regard, U_s was used in place of U to obtain a modified Strouhal number $S_s = fb/U_s$. Fig. 5.11 shows the variation of S_s with σ_s for 0° wedges. This attempt failed to group the data for various blockages. For cavitating venturi throats it has been suggested by Hunsaker (1935) that the Strouhal number $S_j = f l/U$ is a constant. Here, 'l' is the length of the venturi cavity. In view of this, an attempt was also made in the present study to normalise the Strouhal number based on the separating velocity and the length L of the cavity (Fig.2.9a). Fig. 5.12 shows the variation of S_L^* with σ_s , where, $S_L^* = f L/U_s$ {Eq.(2.8)}. With the exception of the largest blockage, the data seem to cluster around a single curve.

5.2.4 Wake Static Pressure Distribution for 0° wedges :

Moderate blockages:

Knowledge of wake pressures assist in providing the interpretation of the pattern and degree of material damage in the wake. Figs. 5.13a and 5.13b show the wake static pressure distribution for $b/B = 0.33$ and 0.24 respectively. These figures include the pressure P_s measured at separation ($x/b = 0.0$) and the back pressure P_b measured at $x/b = 0.866$. Fig. 5.14a, indicates the variation of C_{ps} with σ for $b/B = 0.33$ while Fig. 5.14b shows the static pressure distribution in the near wake of non-cavitating normal plates obtained by Sullerey et al. (1975). Their data show that the wake pressures decrease, reach a minimum and thereafter increase with increasing distance from the body along the wake axis. Comparing curve A of Fig. 5.13a at a large value of σ and Fig. 5.14b, one notices that there is a distinct difference in the wake flow pattern in the two cases. With increase in x/b from the separating point, the pressures drop rather rapidly till $x/b = 0.866$. Between $x/b = 0.866$ and 1.0 , the wake pressures increase. With a further increase in x/b , the pressure distributions follow a pattern similar to that of normal plates. The latter is characterised by a single dip in the wake pressure distribution. The tip of the afterbody of the wedge generally lowers the pressure to a value which is much less than P_s . At the same blockage and other values of σ , the wake pressure distributions indicate a pattern similar to that found in curve A of Fig. 5.13a. However, the large pressure gradients occurring in the range $0.866 < x/b < 1.0$ diminish rapidly as the σ values are lowered. In view of Fig. 5.14a, one can conclude that a decrease in σ may be viewed as an increase in C_{ps} . As a result of this, curve E (Fig. 5.13a) representing the wake pressure at $\sigma = 4.24$ is higher than that found at $\sigma = 5.0$ (Curve C). Further, there is a lower limit for the value of P_s attainable which is very close to the vapor pressure of water. As $\sigma \rightarrow \sigma_{ch}$, the cavity gets filled with water vapor and the intense vortical action present at larger values of σ are diminished. Consequently, the pressures are more or less uniform in the

near wake (Fig. 5.13a, curve E).

Large blockages:

Figs. 5.15 a, b and c show the static pressure distribution in the wake of 0° wedges at large blockages of 0.58, 0.66 and 0.82 respectively. At higher blockages, the pressure distributions for wedges appear to be somewhat similar to that of normal plates [Fig.5.14b]. The secondary dip found at $x/b = 0.866$ in the wake of moderate blockages (0° wedges) is absent. It may be recalled that the flow is also characterised by the absence of the Karman vortex street at larger blockages. Included in Fig. 5.15c is an insert showing the variation of $-C_{ps}$ with σ . As at moderate blockages, the $-C_{ps}$ values approach σ as choking conditions are reached and the wake pressures are more or less uniform. It may be added that for lower σ values, the pressures measured at $x/b = 0.866$ are slightly higher than that measured at separation. A similar rise in wake pressure has been noticed in the wake of cavitating axi-symmetric disks by Kermeen et al (1957).

5.2.5 Cavity Pressure Field Characteristics:

In view of the above observations, the pressure histograms at a given blockage were obtained in the form of standardised probability density functions (denoted as pdf) with decreasing σ . Fig. 5.16 shows a typical set of pdf with decreasing σ for $b/B = 0.24$. To begin with, at $\sigma=13.41$ (non-cavitating flow) the resulting curve resembles a standardised pdf of a sine wave in random noise [Bendat and Piersol 1980]. With decreasing σ and the onset of cavitation, the pdf resembles that of a random noise, with the pdf becoming narrower with decreasing σ . The extent to which cavitation affects the characteristics of the pressure records is reflected in Fig. 5.16. At $\sigma = 13.41$, a distinct large scale vortex shedding is noticeable with a clear periodic character resulting from the vortex street mechanism. As σ is lowered, the periodic component loses its dominance. Further, it should be noted that at any given blockage the general shape of the spectral density curves

remain more or less the same at all cavitating conditions except at choking where the cavity is filled with vapor and the resulting pdf resembles that of a typical random noise which is characteristic of turbulence present in the flow.

For larger blockages, Fig. 5.17 shows the pdf obtained at $b/B = 0.82$. Comparing the curves in Fig. 5.16 and Fig. 5.17 at very large values of σ , one notes that the typical sine wave in random noise type of pdf is absent at larger b/B . With lowering σ , the pdf resembles that of a random noise.

5.2.6 Wake Static Pressure Distribution for Circular Cylinders :

Fig. 5.18 shows the typical pressure distribution in the wake of a circular cylinder at a moderate blockage of 0.33. Compared to 0° wedges, the afterbody effects of a circular cylinder are generally small and several investigators have observed that the values of the separation pressure coefficient C_{ps} are not very different from the back pressure coefficient C_{pb} , in both non-cavitating and cavitating flows [Roshko 1954, Ramamurthy 1973]. Consequently, in the present study, the wake pressures were measured starting with the back pressure at $x/b = 1.0$. The curves in Fig. 5.18 have been numbered sequentially from 1 to 6 with decreasing σ . Referring to curve 1, it can be observed that the variation of the wake pressures with increasing distances from the body follow a distribution similar to that found in non-cavitating flow past circular cylinders [Sullerey et al. 1975]. Decreasing σ from 6.39 to 4.17, results in a general decrease in the wake pressure coefficient C_{px} values (curves 1 to 3). Further reductions in σ are associated with an increase in C_{px} values (curves 3 to 6). Simultaneously, at any value of σ , the location at which the minimum pressure occurs along the wake axis, denoted as M , appears to move towards the cylinder with a decrease in σ (curves 1 to 3) followed by a movement of M away from the body with a further decrease in σ (curves 3 to 6). A plausible explanation for this behavior is given below. Fig. 5.19 indicates the variation of C_{pb} with σ observed

in the present study. As the velocity is held constant and the pressure is reduced to lower σ , the flow separation points start moving upstream. Gradually, the area enveloped by the cavity spans a bigger segment of the after body and eventually the flow separation points reach the crown of the cylinder where the separation velocity is larger resulting in lower C_{pb} values. As a result, the values of C_{px} at any x/b in the wake is lower for curve 3 when compared to curve 1 (Fig.5.18). With further reduction of pressure and hence σ , the separation points move farther upstream beyond the crown of the cylinder since the pressure at separation has a lower bound which is close to the vapor pressure of water. For values of σ to the left of B in Fig. 5.19, $-C_{pb}$ decreases. Consequently, at lower σ values ($\sigma < 4.17$), the curves representing the wake pressure translate upwards (Curves 3 to 6) with increasing values of C_{pb} . A similar behavior is found to occur at a lower b/B of 0.08 as indicated in Fig. 5.20.

5.2.7 Length of vortex formation region:

With the strobe generator being set at the frequency of vortex shedding, the vortex appeared to be frozen. This enabled the measurement of the length of formation L_f (Fig. 2.9b). Fig. 5.21 shows the variation of L_f with σ for three typical blockages of 0.097, 0.243 and 0.325. At a given blockage, as the value of σ is reduced, L_f increases. Following Sarpkaya's [1979] model regarding the formation of vortex behind bluff bodies, one notes that the shear layer joining the separation point to one of the vortices begins to develop instabilities and is drawn across the wake in response to the reduction in the base pressure due to the vortex growth across the wake. This nearly corresponds to a time when the sheet drawn in has the least circulation or is most permeable. The stretching, diffusion and dissipation of vorticity tends to break up the deforming shear layer. This causes the shedding of the first vortex. The shedding of the other vortex across the wake does not commence until circulation in its feeding sheet reduces to a minimum making the

sheet most susceptible to diffusion. Observations also indicate that a decrease in cavitation number tends to make the wake more quiescent and the region immediately behind the body is far less turbulent when compared with conditions related to non-cavitating or incipiently cavitating flows. The reduced wake turbulence causes the diffusion of the separating sheet to be delayed, providing more time for the vortex to travel further downstream in its natural course and this consequently increases L_f .

Some remarks regarding the measurement of L_f are also in order. As mentioned earlier, several measurements were made during a given run and the values presented are the average values of L_f . A typical average value of L_f being 32.0 mm at $\sigma = 2.89$ for $b/B = 0.097$. At very large values of σ (non-cavitating conditions), visual observations were not possible and hence the value of L_f could not be determined. At values of σ slightly below incipient conditions, the cavitation bubbles formed in the core of the vortices assisted flow visualization. At these values of σ , all the cavitation bubbles were observed only in the vortex cores and not in the region immediately behind the body. The cavitation bubbles collapsed immediately on reaching the high pressure regions. The vortices were visible only for a few body widths downstream. As the value of σ is reduced to reach partially cavitating conditions (range CD of Inset, Fig. 5.21), the presence of a vapor core in the vortices formed facilitated excellent visual observations. Since the ambient wake pressures are now lower, the collapse of the cavitation bubbles did not occur immediately and the Karman vortex street was distinctly visible several body widths downstream of the cavitating source. Furthermore, under these conditions, the oscillations of the cavity tip were predominantly in the lateral direction. The vortices appeared to be very stable and confirmed the observations of Appel [1961] that cavitation stabilizes the vortex and prevents its further break up. In the range CD (Inset, Fig 5.21), as σ is reduced, both the lateral and longitudinal vortex spacing were reduced. A similar observation was made earlier by Young and Holl [1966]. However, as the value of σ is reduced beyond the point D, large

axial oscillations of the cavity tip were observed. Under these conditions, the errors associated with the measurements of L_f are expected to be large. With the approach of choking conditions, the longitudinal spacing between the two row of vortices is reduced considerably. Under these conditions, the vortices did not appear to be stable. Further, the rolling up of the shear layers appear to be less distinct. At the same time, vortex shedding also becomes more or less intermittent and random. The cavity as a whole appeared to be filled with vapor with the onset of choking conditions.

In studies related to non-cavitating flows, it has been reported by Davies (1976) and several others that the vortices formed distort and are generally non-circular. As they move downstream, vorticity diffuses and further dissipation is enhanced by turbulence. Vortices are also subjected to strain fields imposed by neighboring vortices [Sarpakaya 1979]. These factors generally contribute to the break up of the vortex. As indicated earlier, in the partially cavitating regime of flow (region CD- Inset Fig. 5.21), the wake tends to become more and more quiescent and attains a reduced level of turbulence compared to the non-cavitating flow conditions. Further, the presence of vapor in the vortex core tends to reduce diffusion and keep the vortex circular. Consequently, cavitation tends to keep the vortex from fragmenting and this aids stabilization. Incidentally, as one reduces the value of σ , the maximum radius of the visible portion of the vortex appeared to shrink with increasing L_f .

At very large values of σ , since the vortex is formed very close to the afterbody edge of the prism, it is expected that L_f would be influenced by the afterbody of the prism. At these values of σ , the afterbody of the prism severely influences the wake pressure distributions. However, it should be noted that the values of the Strouhal numbers obtained in non-cavitating flows match fairly well with those obtained in wind tunnel tests behind normal flat plates with no significant after bodies at comparable blockages [Abernathy 1962, Ramamurthy 1973]. Furthermore, as σ is reduced to very low values,

the wake pressures are expected to be more or less constant as the general wake region is filled with vapor. Consequently, the values of L_f are not expected to be influenced by the afterbody of the prism at lower values of σ as the vortices are now being formed further downstream.

The effect of blockage on L_f is clearly discernible from Fig. 5.21. An attempt was made to reduce blockage effects by using a modified cavitation number σ_s obtained through the use of the separating velocity U_s defined earlier. Fig. 5.22 shows the variation of L_f with σ_s . The data seem to be fairly well clustered around a single curve for the range of blockage tested. This indicates that U_s is the proper velocity scale to reduce or eliminate wall interference effects for the range of blockage indicated in Fig. 5.22. As noted earlier, the higher uncertainties in the estimation of L_f at very low σ values contribute to the increased scatter of the plotted points at lower cavitation numbers (Fig. 5.22).

5.2.8 Flow past over-sized bluff bodies:

With the observation of the suppression of the Karman vortex street at larger blockages and in view of the wake static pressure distributions being different at larger blockages, it was thought desirable to compare the characteristics of a wedge having a significant after body with those of a normal flat plate and a gate. This will enable one to study the influence of the separating shear layers on each other at these large blockages. Fig. 5.23 shows the variation of S_s with b/B obtained in a recent study (Ramamurthy 1990) in non-cavitating flows. The figure indicates that for $0.0 \leq b/B \leq 0.25$, S_s remains constant. However, with further increase in blockage ($b/B > 0.25$), S_s increases upto a b/B of 0.60 beyond which S_s rapidly decreases. As noted earlier, the rapid decrease in S_s was essentially a result of the difference in the nature of vortex shedding at larger blockages.

Fig. 5.24 shows the variation of $-C_{ps}$ with σ for $b/B = 0.93$ for a wedge a normal

flat plate and a gate. The behavior is very similar to that noticed at other lower blockages. The values of $-C_{ps}$ decrease with decreasing σ and at very low values of cavitation numbers, $-C_{ps} \rightarrow \sigma$. However, the values of $-C_{ps}$ for a wedge are lower than that of a normal flat plate and a gate. It is expected that the significant after body of the wedge acts like a splitter plate thereby increasing the base pressures. This results in lower values of $-C_{ps}$ and consequently lower values of the drag force.

For the three shapes tested, Fig. 5.25 shows that S_s remains almost constant for the range of σ_s studied. However, at very low values of cavitation numbers ($\sigma_s < 1.1$), no distinct dominant frequency was obtainable from the power spectra of pressure pulsations. One notes that in the case of a wall mounted gate there is the presence of only one shear layer which rolls up into discrete vortices. Further, the relation between S_s and σ_s is similar for both a flat plate and a gate, which seems to confirm the observation noted earlier that the two separating shear layers may not interact in the case of severely constrained bluff bodies. Visual observations also indicated that the shear layers individually roll up into discrete vortices.

CHAPTER VI
CHOKED FLOW PAST BLUFF BODIES

CHAPTER VI

CHOKED FLOW PAST BLUFF BODIES

Not all cavitating flow conditions can be modelled in a water tunnel as the ability of a water tunnel to operate at very small cavitation numbers may be hindered by choking effects. The importance of choking has been recently pointed out by Tullis (1989). As he notes, care must be taken to avoid choking, since the worst condition to operate a valve, orifice or a pump which form a part of the pipeline and piping system, is near the onset of choking. Further, erosion, noise and vibration are generally a maximum under these conditions. In this chapter, an approach is developed to predict the choking cavitation number for sharp edged bluff bodies subject to wall interference effects.

6.1 PREVIOUS STUDIES

The interference effect of the boundaries of a water tunnel on the cavity dimensions formed behind bluff bodies are significant. As the cavitation number of the flow is reduced, the cavity elongates. According to existing theories, this elongation effect caused by the tunnel boundary may become so extreme that the cavity is expected to become infinitely long at a cavitation number σ greater than zero [Streeter 1961, Cohen 1958]. Under these conditions, the water tunnel or the piping system is said to be choked and further efforts to increase the flow velocity are impossible since σ cannot be reduced further. This choking effect is of considerable importance, since it limits the ability of a water tunnel to operate at small cavitation numbers. Consequently, not all cavitating flow conditions can be modelled in a water tunnel. Theoretical and experimental evidence indicate that a larger degree of confinement is associated with a higher value of choking cavitation number. As indicated earlier, attention is focussed on sharp-edged bluff bodies with fixed separating edges to reduce or eliminate Reynolds number effects. Following

Birkhoff (1950), a momentum balance approach is used to develop a model to predict choking cavitation numbers at various blockages. The model is verified using experimental results from present and previous studies.

6.2 THEORETICAL CONSIDERATIONS TO DETERMINE σ_{ch} :

The following assumptions are made in the development of the model:

- (i). The density of the fluid in the cavity is negligible and the near wake pressure is constant. Hence, the pressure along the slip stream line is nearly constant. Further, at choking conditions, the cavity pressure is essentially equal to the vapor pressure.
- (ii). The maximum wake width W of the cavity behind a cavitating source [Fig.6.1] approaches the value of the wake width predicted by potential flow solutions. Referring to Fig. 6.1, the jet width B_j is given by,

$$B_j = \frac{1}{2}(B - b) C_c \quad (6.1)$$

In Eq.(6.1), C_c is the jet contraction coefficient obtained from potential flow studies [Shaw 1969].

- (iii). The boundary friction is negligible along the control surfaces (Fig. 6.1).

In the previous chapter, it was observed that the centre line wake pressure distribution was almost a constant as choking conditions are approached (Figs. 5.13a and 5.13b). Consequently, the near wake pressure can be taken to be equal to the separating pressure P_s . Further, it was also observed that at very low values of σ , the separating pressure is essentially equal to the vapor pressure (Fig. 5.14a). Choosing the control volume EFGHIJ of unit width (Fig. 6.1) and applying the momentum balance, one obtains

$$PB + \rho U^2 B = P_j(B-b)C_c + \rho U^2(B-b)C_c + P_s(B-(B-b)C_c) + \frac{1}{2}\rho U^2 b C_d \quad (6.2)$$

where, P = free stream pressure in the approaching flow, U = free stream velocity, P_j = jet pressure in sections FG and HI, C_d = drag coefficient and ρ = density of fluid. Using assumptions (i) and (ii) and simplifying Eq. (6.2), one gets,

$$\sigma_{ch} = \frac{2}{(1 - \frac{b}{B}) C_c} + C_d \frac{b}{B} - 2.0 \quad (6.3)$$

where, the cavitation number σ_{ch} at choking is given by,

$$\sigma_{ch} = \frac{P - P_v}{\frac{1}{2} \rho U^2} \quad (6.4)$$

Eq.(6.5) below defines C_d in terms of the fore and rear body pressure coefficients C_{pf} and C_{pr} ,

$$C_d = \int_{-b/2}^{b/2} C_{pf} dx' - \int_{-b/2}^{b/2} C_{pr} dx' \quad (6.5)$$

Here, x' is the lateral distance along the forebody. Re-analysing the data presented in an earlier study [Ramamurthy 1977], one can conclude that the forebody pressure distribution in the presence of cavitation in the wake, essentially resembles the forebody pressure distribution obtained in non-cavitating flows. Using this argument, one can evaluate the

value of the first term on the right hand side of Eq.(6.5) from existing non-cavitating flow data at any given blockage. Consequently, at choking conditions,

$$C_d = C_d\{\sigma_{ch}, b/B\} = \eta - \int_0^1 C_{ps} dX' = \eta + \sigma_{ch} \quad (6.6)$$

where, $\eta\{b/B\} = \int_0^1 C_{pf} dX'$. Using Eq.(6.6) in Eq.(6.3), one obtains,

$$\sigma_{ch} = \frac{1}{(1 - \frac{b}{B})} \left[\frac{2}{(1 - \frac{b}{B}) C_c} + \eta \frac{b}{B} - 2.0 \right] \quad (6.7)$$

In Eq.(6.7), C_c is a function of b/B . Further, based on existing non-cavitating flow test data related to the dependence of η on b/B , σ_{ch} can be evaluated for two-dimensional sharp edged bluff bodies such as flat plates and wedges, without recourse to new experimentation.

ANALYSIS OF RESULTS

The forebody pressure distributions for two-dimensional flat plates [Shaw 1971, Modi 1977] and wedges [Lee 1973] at various blockages were obtained from previously published non-cavitating flow data. Inset of Fig. 6.2 {Fig. 4.1} shows the pressure distribution for two typical blockages. Using these sketches, the value of η at any particular blockage for sharp-edged bluff bodies can be evaluated by integrating the forebody pressure distribution. Fig. 6.2 shows the variation of η with b/B . A straight line fit was obtained for η in the range $0 \leq b/B < 0.5$. The straight line fit is denoted as,

$$\eta = 0.805 - 1.450 (b/B) \quad ; \quad 0 \leq b/B \leq 0.5 \quad (6.8)$$

It should be noted that as $b/B \rightarrow 1.0$, $\eta \rightarrow 0.0$ (Shaw, 1969). Using Eq. (6.8) in Eq. (6.7), σ_{ch} can be evaluated at any blockage, since C_c can be evaluated theoretically at any required blockage [Shaw 1969].

When σ is reduced to very low values, the value of S drops rapidly and a stage is reached when S approaches zero for $\sigma > 0$ (Fig.5.7). Under these conditions, the unsteady pressure records indicate that vortex shedding becomes highly intermittent and finally ceases. The corresponding spectra do not indicate a dominant frequency. The cavitation number of the flow at this stage is denoted as σ_{ch} . Fig 6.3 shows the variation of cavitation number σ with increasing velocities for a typical blockage of 0.325. With increasing velocities, a stage is reached, where further acceleration of the flow does not result in a decrease in the value of σ . At choking conditions, inset A of Fig. 6.3 indicates that the pressure distribution in the wake region is almost constant and is nearly equal to the vapor pressure (Inset B, Fig 6.3).

Fig 6.4 shows the variation of σ_{ch} with b/B obtained from Eq.(6.7). The proposed method of obtaining σ_{ch} requires only the data related to the distribution of pressure around the sharp-edged bluff body under non-cavitating conditions and the theoretical contraction coefficient C_c . The former data is quite abundant for common sharp-edged bluff bodies and the techniques for obtaining the theoretical values of C_c are well known. In other words, the suggested procedure can be used to determine σ_{ch} without recourse to experimentation. Fig 6.4 also indicates that the experimental values of σ_{ch} agree well with the predicted values of σ_{ch} for a large range of blockages.

CHAPTER VII
FLOW PAST BACKWARD FACING STEPS

CHAPTER VII

FLOW PAST BACKWARD FACING STEPS

Separated flows associated with boundary discontinuities result in highly turbulent, recirculating flows and are of considerable interest in many branches of engineering. Flow past backward facing steps exhibit well defined regions of flow separation and reattachment. The resulting complex turbulent flow field can significantly change the local wall pressure field. An understanding of the flow parameters and geometrical constraints governing the scaling of the wall pressure field is therefore essential. Further, the separating and reattaching flows often exhibit an unsteady low frequency behaviour. A study of the turbulence characteristics in such flows can be obscured by the unsteadiness. Interpretation of the turbulence characteristics will be less difficult when one can remove the unsteady flow behaviour. The intense vortical action present may lead to inception of cavitation. Hence, the flow field generated can be a major source of flow induced vibration, noise and cavitation.

7.1 PREVIOUS STUDIES

7.1.1 Non-cavitating flows:

Numerous studies dealing with non-cavitating flow past backward facing steps have been reported. Extensive reviews like those of Eaton and Johnston [1981], Bradshaw and Wong [1972] and Simpson [1989] are available in literature. With the advent of the Laser Doppler Velocimeter (LDV) system, the problems associated with measurements in the reversed flow region have been effectively overcome. This has resulted in the availability of some new experimental information related to the behaviour of separated flows [Adams 1988b, Durst and Tropea 1982, Etheridge and Kemp 1978, Isomoto and Honami 1989, Stevenson 1984].

Moss [1977], Narayanan [1974], Tani [1961], Westphal [1984] and Kim [1980] have presented the pressure distribution downstream of a backward facing step. Adams [1988] studied the effect of the separating shear layer thickness on the structure of the flow in the reattachment region downstream of a backward facing step. They found that the wall pressure profiles were insensitive to the nature of the boundary layer and depended only on the parameter δ/h , where δ is the boundary layer thickness ahead of separation and h is the height of the step. Based on δ/h , Bradshaw and Wong [1972] have suggested a "strength of perturbation" criterion for classifying flows with separated regions. They also report that the recovery of the shape parameters of the reattached layer (Fig.7.1) to those of a flat-plate boundary layer was not completed even at distance of fifty two step heights downstream of the step.

Driver [1987], Eaton [1982], Farabee [1984], Greshilov [1969], Katz [1982] and Rockwell [1979] studied the effects of the flow past backward facing steps on the downstream wall pressure fluctuations. Eaton [1982] reports that Tani [1961] did not observe low frequency motions in flow past backward facing steps. Rockwell [1979] has suggested that the low frequency motions may be a result of the oscillations of the shear layer induced by a feed back of disturbance from the impingement point to the separation point. Driver [1987] observed a global flapping of the shear layer which appeared not to contribute much to the fluctuating energy. They also observed a second type of fluctuating vortical motion and found that a majority of the energy in the flow resides in the frequencies characteristic of roll-up and pairing of vortical structure. For an expansion ratio of 1.13 and a single Reynolds number $Re = Uh/\nu = 37000$, Driver [1987] obtained a Strouhal number $S=fh/U$ of 0.098. Eaton and Johnston [1982] recorded a value of 0.065 for S at an expansion ratio of 1.67. Mabey [1972] formed a modified Strouhal number based on the length of the separation bubble and the free stream velocity, which appeared to display an almost universal trend.

Several methods have been used to obtain the reattachment lengths X_r (Fig. 7.1) behind backward facing steps. Narayanan [1974] used a surface-oil flow observation and report that X_r varied from 5.8 - 6.4 step heights for $1.01 < ER < 1.14$. Here, ER is the expansion ratio (Fig.7.1). Based on surface-oil flow visualisation, Baker [1978] reports a value of $X_r/h = 5.8$ at an expansion ratio of 1.1. Westphal [1984], Adams [1988], and Driver [1987] used a thermal tuft probe to determine the near-wall instantaneous flow direction. This device was used to determine X_r based on the assumption that the location of reattachment corresponds to the point where the flow direction is downstream 50% of the time. Using a Laser Doppler anemometer, Durst and Tropea [1982] obtained X_r for a range of expansion ratios by extrapolating the line of zero velocity to the wall. Using a special skin friction probe, Westphal [1984] also determined X_r by finding the position where the skin friction coefficient was zero. These values of X_r compare favourably with the reattachment lengths obtained by the thermal tuft probe and pulsed wire anemometry.

7.1.2 Cavitating flows:

Literature dealing with cavitation in large scale separated flows associated with boundary discontinuities are limited. Vigander [1965] and Appel [1961] observed cavitation along the surface of separation in two-dimensional sudden expansions. Lush [1975] studied the sound generated by cavitating flows past a backward facing step. Arakeri [1981] investigated the inception of cavitation downstream of an axi-symmetric backward facing step having an hemispherical forebody. Katz [1982] studied the cavitation phenomenon behind a similar model and observed that cavitation appeared in the form a ring that surrounded the body. Katz [1982] also obtained the incipient and desinent cavitation indices over a range of Reynolds numbers.

In the present study, two backward facing steps of heights 0.635 and 1.270 cms,

yielding expansion ratios of 1.07 and 1.14 (Fig.2.3b) were used to study the effect of expansion ratio on the incipient cavitation indices at various Reynolds numbers. The effect of cavitation on the frequency of vortex shedding and pressure distribution downstream of separation were also obtained. In these tests, the Reynolds number of the flow was maintained constant at 1.28×10^5 and 0.77×10^5 for $ER = 1.14$ and 1.07 respectively. The corresponding ratio of the boundary layer thickness to the step height was of the order of 0.2 and 0.3 respectively. Typical boundary layer parameters for flow past a backward facing step are given in Table. 15.

7.2 ANALYSIS OF RESULTS:

7.2.1 Velocity measurements and Reattachment lengths:

Fig.7.2 shows the LDV measurements related to the streamwise mean velocity distribution, downstream of the backward facing step at $ER = 1.07$. The Reynolds number $Re = U_{ref}h/\nu$ was 0.61×10^5 . Here, U_{ref} is the free stream velocity measured ahead of the step. In Fig.7.2, at any location, the velocities are normalised by the maximum velocity U_{max} measured at that particular section. The maximum reverse velocities are of the order of $0.2 U_{ref}$. Fig.7.3 shows the streamwise fluctuating components u' measured at $Re = 0.61 \times 10^5$. Fig. 7.4 indicates the streamwise mean velocity distributions for an expansion ratio of 1.14.

The reattachment lengths were obtained by extrapolating the streamwise zero mean velocity line to the wall. Figs. 7.5 and 7.6 were developed using sketches such as Figs. 7.2 and 7.4. Figs. 7.5 and 7.6 show the loci of the streamwise zero mean velocity line. In most of the cases, the value of X_r was also confirmed by obtaining the streamwise velocity measurements in the neighbourhood of the reattachment zone and locating the section where the velocity was almost zero most of the time. To this end, the probability density functions of the velocity measurements were obtained by operating the signal

analyser (IFA 550 - TSI Inc.) in a real time mode.

Fig. 7.7 shows the variation of X_r with Re . One notices from Fig. 7.7 that X_r shows a very minor dependence on Re for the range of Re tested in the present series of tests. Also shown in Fig. 7.7 are the values of X_r obtained from several other previous studies. It should be noted that, in the present study, a much higher range of Re ($0.4 < Re \times 10^{-5} < 1.3$) has been covered. At lower Reynolds numbers ($Re < 0.5 \times 10^5$), parameters such as the shape factor can have a dominant influence on the characteristics of separated flows and hence the value of X_r/h strongly depends on Re . Generally, in field applications, the Reynolds number of the flow will be high and one can hence predict the value of X_r with a higher degree of confidence.

Fig. 7.8 shows a typical plot of the streamlines behind the backward facing step at $ER = 1.14$. Here the stream function Ψ is normalised by $U_{ref}h$. Fig. 7.9a shows relation between the maximum values of u'/U_{max} with X/X_r through the reattachment zone. The maximum values of u' increases with increasing X/h upto reattachment beyond which it decreases. In spite of the varying trends displayed by these relationships ahead of the reattachment, the data seem to collapse downstream of reattachment ($X/X_r > 1.0$) For $ER = 1.07$ and $Re = 0.65 \times 10^5$, Fig. 7.9b shows the velocity distribution obtained at a section $X/h = 5.20$ for different free stream pressures ($2.36 < \sigma < 1.03$). The velocities are normalised by the free stream velocity U_{ref} obtained ahead of the step. The velocity distributions are essentially similar for all the cavitation numbers indicated in Fig. 7.9b. As will be shown later, since inception occurs only around $\sigma = 0.85$, one can conclude that with decreasing σ , the change in X_r is not significant until atleast $\sigma = \sigma_i$.

7.2.2 Pressure distribution behind backward facing steps:

Figs. 7.10 and 7.11 show the static pressure distribution along the floor of the separated flow region. In an attempt to obtain an universal distribution [Roshko and Lau

1965], the abscissa is represented as $X^* = (X-X_r)/X_r$ and the ordinate is represented as C_p^* . As indicated earlier, C_p^* is defined as,

$$C_p^* = \frac{C_p - C_{p \min}}{1 - C_{p \min}} \quad (7.1)$$

where, C_p is the pressure coefficient normalised by the upstream dynamic head and $C_{p \min}$ is the minimum value of C_p occurring along PQ in Fig. 7.1. It is clear from these figures that Re does not appear to have a significant effect on C_p^* especially ahead of reattachment.

Fig. 7.12 shows a similar pressure distribution obtained from several previous studies. It appears that there are distinct trends downstream of reattachment. It should be noted that there are several parameters affecting the flow and as noted by Adams [1988], "the concept of a universal pressure rise curve for the entire region of reattachment is valid only in the limit as $\delta/h \rightarrow 0$ ". Further the data of Adams [1988] also indicate that larger the value of δ/h , the earlier the pressure curve departs from the suggested "universal" curve.

Figs. 7.13 shows the variation of C_p with X/h at $Re = 1.28 \times 10^5$ and different degrees of cavitation. The distribution representing the non-cavitating flow conditions is also shown in Fig. 7.13. In general, the values of C_p obtained under cavitating conditions are lower than those obtained under non-cavitating conditions. From previous studies related to cavitating flow past bluff bodies [Streeter 1961], one notes that as σ is decreased to very low values, the cavity formed by the separating streamlines tend to be longer. Consequently, for step flows, the rate at which the flow expands downstream of the step is expected to be lower, at lower values of σ ($\sigma \ll \sigma_i$). As a result of this, the pressures in the expanding flow will be lower for $\sigma < \sigma_i$ than for the case $\sigma \gg \sigma_i$. The pressure being continuous across the separating streamline, the cavity

pressures are expected to be lower for $\sigma < \sigma_i$ than for the case $\sigma \gg \sigma_i$, which in turn renders the wall pressures to be lower for cavitating flows than for non-cavitating flows. This behavior is also reflected in Fig. 7.14 which shows the pressure distribution at an expansion ratio of 1.14.

7.2.3: Frequency of Pressure Pulsations:

Typical spectra of pressure fluctuations downstream of a backward facing step are shown in Fig. 7.15. Fig. 7.16a shows the variation of $S = fh/U_{ref}$ with Re for the two expansion ratios. The present tests cover a range of Reynolds numbers. S shows a decreasing trend with Re . Figs. 7.16b and 7.16c show the variation of Strouhal number S with σ for the two expansion ratios. With decreasing σ , the value of S decreases. Unlike sharp-edged bluff bodies, S does not remain constant at the non-cavitating value for $\sigma > 0.5 \sigma_i$. In the case of backward facing steps, S begins to decrease slightly ahead of inception. Beyond inception, the value of S drops rapidly. The differences in behaviour between a bluff body and a backward facing step is a consequence of the difference in the nature of vortex shedding. For instance, in the case of bluff bodies, the flow begins to contract immediately after separation. Furthermore, at lower blockages there is a considerable interaction between the two separating shear layers resulting in the formation of an alternate vortex shedding mechanism leading to the well known Karman vortex street which is absent in the case of flow past backward facing steps.

With the onset of cavitation, the presence of vapor in the core of the vortices aided visual observation. These observations indicate that the initial location of the visible portion of the vortices appear to move upstream along the shear layer with decreasing σ . At very low values of σ , cavitation bubbles are visible at the step edge and further decrease in σ results in the separating region presenting a foamy appearance. At this stage there is the absence of any dominant frequency in the pressure records. A similar

trend has also been noticed in flow past sharp-edged bluff bodies.

7.2.4 Cavitation Inception measurements:

Fig.7.17 shows inception cavitation indices σ_i for the backward facing steps obtained at various Reynolds numbers for the two expansion ratios. The values of σ_i appear to be more or less constant for the range of Re tested. As in the case of the bluff bodies, inception of cavitation is accompanied by the presence of a sharp crackling noise. Some remarks regarding inception behind backward facing steps are in order. It should be noted that at inception, span-wise vortex like filaments were visible in the shear layer at about 3 or 4 steps heights downstream of separation. With increasing Re, these vortex like filaments appeared to initialise earlier though the value of σ_i remained the same. Previous visual observations [Durst 1982] with the use of a dye in non-cavitating flow indicate that the shear layer rolled up into vortices and this location of the initial formation of the vortices appeared to move upstream with increasing Re. From the studies of Driver [1987], one notes that the streamwise velocity fluctuations near the wall correlate negatively with the velocity fluctuations in the outer part of the boundary layer. This is clearly a characteristic of clockwise rotating flow. It is conjectured that as the location of the initial formation of the vortices move towards the edge of the step, the vortices rotating in clockwise direction become smaller in diameter and hence are expected to have higher rotational speeds. This in turn causes the vortex core pressure to reach the vapor pressure value at earlier locations along the shear layer and consequently account for the inception of cavitation at more upstream locations with increasing values of Re.

CHAPTER VIII
CONCLUSIONS AND SCOPE FOR FURTHER STUDY

CHAPTER VIII

CONCLUSIONS AND SCOPE FOR FURTHER STUDY

8.1 CONCLUSIONS:

The major conclusions of the present study related to separated flow past bluff bodies and backward facing steps are summarised as follows:

1. Based on theoretical considerations, an expression is obtained for the drag coefficient of bluff bodies such as flat plates and equiangular prisms ($\theta = 0^\circ$) which are subject to blockage effects. In the case of equiangular prisms, the presence of the afterbody results in back pressures which are much lower than the separating pressures and hence the experimental drag coefficient will be larger than the predicted values. Eqs.(3.11) and (3.13) provide good estimates of the drag coefficient for a large range of blockage ratios. Further, Eq.(3.13) can be used to directly estimate C_d for $b/B \geq 0.30$ without recourse to empirical relations. The range of blockage corrections include very low blockages $b/B \leq 0.15$ where the contracted jet velocity and the separating velocity are recognised to be different. Experimental data appear to validate the predicted expression for the estimation of the drag force at various blockages.
2. A semi-empirical analysis is developed on the basis of a Rankine vortex model to predict cavitation inception in the wake of two-dimensional sharp edged flat plates and equiangular prisms ($\theta = 0^\circ$). Suitable corrections are provided for boundary layer growth, vortex dissipation and entrainment effects. A fair correlation is obtained between the theoretical prediction and experimental data for a range of blockages. Both the developed model and the experimental data indicate that Reynolds number effects on cavitation inception characteristics are not dominant. Blockage effects on cavitation inception index are found to be rather severe.
3. At a given blockage, the length of the cavity increases with a decrease in the

cavitation number. For $b/B < 0.5$, a modified cavitation number normalised by the separating velocity aided in eliminating blockage effects on the geometrical characteristics. For $b/B > 0.5$, normalising the cavitation number by the separating velocity does not seem to absorb blockage effects. The wake flow pattern at higher blockages is therefore expected to be different from that found at moderate blockages. Further, at higher blockages the maximum wake widths show a very minor variation with cavitation number.

4. For flow past bluff bodies, visual observations of the cavity at moderate blockages ($b/B < 0.5$) indicate the presence of large scale vortex shedding characterised by the well known Karman vortex street. At moderate blockages, the length of the cavity and the separating velocity are found to be the proper length and velocity scales to normalise the Strouhal numbers to absorb blockage effects. At higher blockages, a distinct Karman vortex street was absent. Small scale vortices were found to develop along the separated shear layers. As such the frequency of vortex shedding pattern at higher b/B is not expected to follow the trend found at lower blockages.

5. For flow past bluff bodies, at moderate blockages, the centre line wake pressure distributions are modified because of the presence of the afterbody of the wedge. At very low cavitation numbers, the intense vortical action found at partially cavitating conditions are absent and the wake pressures are nearly constant. At larger blockages, the afterbody does not appear to have a distinct effect on the wake pressure distributions. In the case of circular cylinders, the location of the separation points change with cavitation number and have a direct influence on the wake pressure distributions.

6. The length of formation region of the vortex behind bluff bodies increases with decreasing cavitation number. The vortex appears to be stable in the partially cavitating regime of flow where only lateral oscillations of the cavity tip caused by the alternate vortex shedding is discernible in the wake. At very low values of σ , large axial oscillations of the cavity tip were also observed. Further, the lateral and longitudinal spacing of the vortex

street tend to decrease with decreasing σ . Visual observations indicate that the vortices appear to be less stable as choking conditions are reached. In tests related to the determination of L_f/b under cavitating conditions, the separation velocity is the proper velocity scale to reduce or eliminate blockage effects.

7. A semi-empirical analysis is developed on the basis of a simple momentum balance approach to predict choking cavitation numbers for sharp edged bluff bodies subject to wall interference effects. The procedure suggested enables one to determine σ_{ch} by using existing information related to non-cavitating flow past bluff bodies. The predicted results are validated by experimental data from both previous studies and present series of tests.

8. At fairly large Reynolds numbers, the reattachment length for the backward facing step is found to be dependent on the expansion ratio and not to be significantly affected by the Reynolds number. Under non-cavitating conditions, the Strouhal number of the flow is found to be dependent on the Reynolds number. Inception cavitation indicies are independent of Re and are found to be strongly dependent on the expansion ratio. Under cavitating conditions, separated region wall static pressure coefficient values are slightly lower than those found at non-cavitating flows. The frequency of vortex shedding is severely influenced by the cavitation number of the flow and at very low values of σ , vortex shedding ceases.

8.2 SCOPE FOR FURTHER STUDY:

The present investigation can be extended to other kinds of separated flows, especially those associated with wall mounted obstacles such as fences, forward facing steps, slots and diffusers. The studies can be conducted when these objects are attached to both plane walls and streamlined bodies. Attempts can also be made to study the influence of the free stream turbulence and boundary layer state on cavitation inception and vortex shedding characteristics.

APPENDIX I
REFERENCES

APPENDIX I REFERENCES

- Abernathy, F. H., "Flow over an inclined flat plate", *Journal of Basic Engineering*, Trans. ASME, Sept. 1962, pp.380-388.
- Adams, E. W., Johnston, J. P and Eaton, J. K, "Experiments on the structure of turbulent reattaching flow", Report MD-43, Thermosciences division, Dept. of Mechanical Engineering, Stanford University, May 1984.
- Adams, E. W., and Johnston, J. P., "Effects of separating shear layer on the reattachment flow structure", Part I: Pressure and turbulence quantities, *Experiments in Fluids*, Vol.6, 1988, pp.400-408.
- Adams, E. W., and Johnston, J. P., "Effects of separating shear layer on the reattachment flow structure", Part II: Reattachment and wall shear stress, *Experiments in Fluids*, Vol.6, 1988, pp. 493-499.
- Adams, E. W., and Eaton, J. K., "An LDA study of Backward facing step flow, including the effects of velocity bias", *J. Fluids Engg.*, Trans. ASME, Vol.110, 1988b, pp.275-282.
- Arakeri, V. H., and Ramarajan, V., "Inception of cavitation from a backward facing step", *Journal of Fluids Engineering*, Trans. ASME, Vol.103, June 1981.
- Arndt, R. E. A., "Semi-empirical analysis of cavitation in the wake of a sharp edged disk", *J. Fluids Engg.*, Trans. ASME, 1976, pp.560-562.
- Arndt, R. E. A., "Cavitation in turbulent shear flows - An overview", Proc. of the conference on Frontiers in Hydraulic Engg., ASCE, August 1983, pp. 412.
- Allen, H. J., and Vincenti, W. G., "Wall interference in a two-dimensional flow wind tunnel, with consideration for the effect of compressibility", NACA Technical Report No. 782, 1944.
- Appel, D.W., "Cavitation along surfaces of separation", ASME paper No. 60-WA-205, 1961.
- Bearman, P. W., "Vortex shedding from oscillating bluff bodies", *Ann. Rev. Fluid Mech.*, Vol.16, 1984, pp.195-222.
- Bendat, J. S., and Piersol, A.G., "Engineering applications of correlation and spectral analysis", John Wiley and sons, New York, 1980.
- Bhaskaran, P., "Characteristics of cavitating flow of past bluff bodies", D.Engg. thesis, Concordia University, Montreal, 1977.

- Birkhoff, G., Plesset, M. and Simmons, N., "Wall effects in cavity flow", Part I, *Quarterly of Applied Mathematics*, Vol.8, No.2, 1950, pp.151-168.
- Blake, W. K., "Flow induced sound and vibration", Vol.1, Academic Press Inc., New York, 1986.
- Bradshaw, P., and Wong, F. Y. F., "The reattachment and relaxation of a turbulent shear layer", *J. Fluid Mechanics*, Vol.52, pt.1, 1972, pp.113-135.
- Cantwell, B., and Coles, D., "An experimental study of entrainment and transport in the turbulent near wake of a circular cylinder". *J. Fluid Mech.*, Vol.136, 1983, pp.321-374.
- Chandra Shekara, D. V., "Studies on characteristics of cavity and cavitation damage behind circular cylinders in water with a venturi", Ph.D. thesis, Indian Institute of Science, Bangalore, 1973.
- Chang, P. K., "Separation of Flow", Mc Graw Hill, New York, 1970.
- Chen Yi Shung, "Effect of confining walls on the periodic wake of 90 degree wedges", M.S., Thesis, Dept. of Mechanics and Hydraulics", University of Iowa, 1967.
- Chu Yen-hsi, "Pressure fluctuations in a cavitating flow past a wall", M.S thesis, Dept. of Mechanics and Hydraulics, University of Iowa, February, 1967.
- Chow, V. T., "Open Channel Hydraulics", Mc Graw Hill Book Co., New York, 1959.
- Cohen, H and Di Prima, R. C., "Wall effects in cavitating flows", 2nd Symposium on Naval Hydrodynamics", August 1958. pp.367-390.
- Clements, R.R., (1973) "An inviscid model of two dimensional vortex shedding", *J. of Fluid Mechanics*, Vol.57, part 2, pp.321-336
- Dalton, C., "Allen and Vincenti blockage corrections in a wind tunnel", *AIAA Journal*, Vol 9, No.9, September 1971, pp.1864-1865.
- Davies, M. E., "Wake structure of a stationary and oscillating bluff body, *J. Fluid Mech.*, Vol.75, 1976, pp.209-231.
- Driver, M. David, Seegmiller, H. L and Marvin, G. J., "Time-dependent behavior of a reattaching shear layer", *AIAA Journal*, July 1987, pp.914-919.
- Durst, F., and Tropea, C., "Flows over two-dimensional backward facing steps", *Structure of Complex Turbulent Shear Flows*, IUTAM symposium, Marseille, 1982, pp.41-52.
- Eaton, J. K., and Johnston, J. P., "Low frequency unsteadiness of a reattaching turbulent shear layer", *Third Intl. Symposium on Turbulent shear flows*, Springer-Verlag, Berlin, 1982, pp.162-170.
- Eaton, J. K., and Johnston, J. P., "A review of research on subsonic turbulent flow reattachment", *AIAA Journal*, 1981, pp.1093-1100.

- Etheridge, D. W., and Kemp, P. H, "Measurements of turbulent flow downstream of rearward facing step", J. Fluid Mechanics, Vol.86, pt.3, 1978, pp.549-566.
- Fage, A., and Johansen, F. C., "The flow of air behind an inclined flat plate of infinite span", Aero. Res. Council R & M. No. 1104, 1927.
- Falvey, H. T., "Prevention of cavitation on chutes and spillways", Proc. of the conference on Frontiers in Hydraulic Engg., ASCE, August 1983, pp. 432.
- Farabee, T. M., and Casarella, M. J., "Effects of surface irregularity on turbulent boundary layer wall pressure fluctuations", J. Vib., Acoustics, Stress and Reliability in design, Trans. ASME, Vol.106, 1984, pp.343-350.
- Gates, E. M., Billet, M. L., Katz, J., and et al., "Cavitation and nuclei distributions, Joint ARL/CIT experiments", Report No. 244.1, California Institute of Technology, September 1979.
- Gerrard, J. H., "The mechanics of the formation region of vortices behind bluff bodies", J. Fluid Mech., Vol.25, 1966, pp.401-413.
- Greshilov, E. M., Evtushenko, A. V and Lyamshev, L. M, "Spectral characteristics of the wall pressure fluctuations associated with boundary layer separation behind a projection on a smooth wall", Soviet Physics - Acoustics, Vol.15, No.1, 1969, pp.29-34.
- Glauret, H., "Wind tunnel interference on wings, bodies and air screws", A.R.C, R & M 1566, 1933.
- Hammit, F. G., "Cavitation and Multiphase flow phenomena, 1980, Mc Graw Hill, New York.
- Holl, J. W and Treaster, A. L., "Cavitation hysteresis", J. of Basic Engineering, Vol.88, Trans. ASME, March 1966, pp. 199-212.
- Holl, J.W., "Nuclei and Cavitation", J. of Basic Engineering, Trans. ASME, Dec 1970, pp.681-688.
- Isomoto, K., and Honami, S., "The effect of inlet turbulence intensity on the reattachment process over a backward facing step", J. Fluids Engg., Vol.111, 1989, pp.87-92.
- Katz, J., and O'Hern, T. J., "Cavitation in large scale shear flows", J. Fluids Engineering, Trans. ASME, Vol.108, September 1986, pp.373-376.
- Katz, J., "Cavitation inception in separated flows", Ph.D. thesis, California Inst. of Tech. 1982.
- Kenn, M. J., and Garrod, A.D., "Cavitation damage and the Tarbela tunnel collapse of 1974", Proc. of Inst. of Civil Engineers, Part 1, February 1981, pp.65-89.
- Kermeen, R. W., and Parkin, B. R., "Incipient cavitation and wake flow behind

- sharp edged disks", C.I.T, Hydrodynamics report, 85-4, 1957.
- Kim, J., Kline, S. J., and Johnston, J. P., "Investigation of a reattaching turbulent shear layer: Flow over a backward facing step", *J. fluid Engg.*, Trans. ASME, Vol.102, 1980, pp.302-3.08.
- Kline, S. J., "The purpose of uncertainty analysis", *J. of Fluids Engineering*, Trans. ASME, Vol. 107, pp. 153 - 160, June 1985.
- Knapp, R. T., Daily, J. W., and Hammitt, F. G., "Cavitation", 1970, Mc Graw Hill, New York.
- Lee, P. M., "Boundary effects on flow past bluff bodies", Ph.D. thesis, Sir George Williams University, Montreal, Canada, 1973.
- Lush, P. A., "Sound generated by cavitating flows in a duct", Department of Mechanical Engg. Report, University of Southampton, 1975.
- Mabey, D. G, "Analysis and correlation of data on pressure fluctuations in separated flow", *J. Aircraft*, Vol.9, No.9, 1972, pp.642-645.
- Marris, A. W., "A review on Vortex streets, Periodic wakes and Induced vibration phenomena", *J. of Basic Engineering*, Trans. ASME, pp.185-196.
- Maskell, E. C., "A theory of blockage effects on bluff bodies and stalled wings in a closed wind tunnel", A.R.C, R&M 3400, 1957.
- Modi, V. J., and El-Shirbiny, S., "A free stream line model for bluff bodies in confined flows", *Journal of Fluids Engineering*, Trans. ASME, Sept. 1977, pp.585-592.
- Morgan, W. B., "Air content and nuclei measurement", Appendix I - Report of Cavitation committee, 13th Intl. Towing Tank Conference, 1972, pp.657-674.
- Moss, W. D., Baker, S. and Bradbury, J., "Measurements of mean velocity and Reynolds stresses in some regions of recirculating flows", First International Symposium on Turbulent shear flows, The Penn. State Univ., April 1977, pp.198-207.
- Narayanan, R., "The role of pressure fluctuations in hydraulic modelling", Symposium on scale effects in modelling hydraulic structures", IAHR, Esslingen am Neckar, Germany, September, 1984.
- Narayanan, M. A. B, Khadgi, Y. N and Vishwanath, P. R, "Similarities in pressure distribution in separated flow behind backward-facing steps", *Aeronautical Qtly.*, 1974, pp.305-312.
- Oba, R., Ikohagi, T., and Yasu, S., "Supercavitating cavity observations by means of Laser velocimeter", *J. Fluids Engg*, Trans. ASME, Vol 102, Dec. 1980, pp.433-440.
- Palanichamy, K., Rao, C. S., and Rao, N.S.L., "Investigations on cavitation inception in a

- venturi with transverse pins", Cavitation, Fluids Machinery Group of the Inst. of Mech. Enggs., 1974, pp.145-152.
- Perry, A. E., and Steiner, T. R., "Large scale vortex structures in turbulent wakes behind bluff bodies-Part 1, Vortex formation process", J. Fluid Mechanics, Vol.174,1987, pp.233-270.
- Plesset, M. S., and Shaffer, P. A., "Cavity drag in three dimensions", Journal of Applied Physics, Vol.19, 1948, pp.932-939.
- Ramamurthy, A. S., Balachandar, R., and Diep Ngoc Vo., "Blockage correction for sharp edged bluff bodies", Journal of Engineering Mechanics Division, Vol.115, ASCE, July 1989.
- Ramamurthy, A. S., and Ng, C.P., " Effect of blockage on steady force coefficients", Journal of Engineering Mechanics Division, Proc. ASCE, Vol 99, No.EM4, August 1973a.
- Ramamurthy, A. S., and Lee, P. M., " Wall effects on flow past bluff bodies", J. of Sound and Vibrations, Vol 31(4), 1973b, pp.443-451.
- Ramamurthy, A. S., and Bhaskaran, P., " Constrained flow past cavitating bluff bodies", J. of Fluids Engineering, Trans. ASME, Vol 99, No.4, 1977, pp.717-726.
- Ramamurthy, A. S., Balachandar, R and Peter Aberg, "Flow past severely constrained bluff bodies", Under review for possible publication in the J. Engg. Mechanics, Trans. ASCE, March, 1990.
- Robertson, J. M., "Hydrodynamics in theory and application", Prentice-Hall Inc., New Jersey, 1955.
- Rockwell, D., and Knisely, C., "The organised nature of flow impingement upon a corner", J. Fluid Mechanics, Vol.93, 1979, pp.413-432.
- Roshko, A., " On the drag and shedding frequency of two dimensional bluff bodies", NACA, TN 3169, 1953.
- Roshko, A., " A new hodograph for free-stream line theory", NACA, , TN 3168,1954.
- Roshko, A., and Lau, J. C., "Some observations on transitions and reattachment of a free shear layer in incompressible flow", Proc. Heat Transfer and Fluid Mech. Inst., Stanford University Press, 1965, pp.157-167.
- Round, G. F., and Garg, V.K., "Applications of Fluid Dynamics", Edward Arnold Ltd., London, 1986.
- Rouse, H., and Abul Fetouh, A. H., "Characteristics of irrotational flow through axially symmetric orifices", Journal of Applied Mechanics, Trans. ASME, Vol.72, 1950,

- pp.421-426.
- Sarpkaya, T., "An inviscid model of two-dimensional vortex shedding", *J. of Fluid Mechanics*, Vol.68, 1975, pp.109-128.
- Sarpkaya, T., "Vortex induced oscillations, A selective review", *J. of Applied Mechanics*, Trans. ASME, Series E, Vol.46, 1979, pp.241-258.
- Sarpkaya, T., "Torque and vibration characteristics of butterfly valves", *J. of Applied Mechanics*, Trans. ASME, Series E, 1961, pp.511-518.
- Shalnev, K. K., "Boundary effect on cavitating flow past a cylinder", *J. of Applied Mech. and Tech. Physics*, No.3 (*Zhurnal Prikladnoi Mechniki i Tekhnicheskoi Fiziki*) 1965, pp. 103-108.
- Shalnev, K. K and Shapoval, I. F., "The growth of cavitation in restricted flow", *Soviet Physics Dokl.*, 22 (12), Dec. 1977.
- Shaw, T. L., " Steady flow past flat plate in channel, *J. of the Hydraulics Division*, ASCE, Vol 95, No.HY6, Proc. Paper No. 6903, 1969, pp 2013-2018.
- Shaw, T. L., " Effect of side walls on flow past bluff bodies", *Journal of the Hydraulics Division*, ASCE, Vol 97, No. HY1, Proc. Paper 1788, Jan 1971, pp. 65-71.
- Simmons, J. E .L., "The relation between the base pressure on a bluff body and the velocity at separation", *Aeronautical Journal*, July 1974, pp. 330-331.
- Simpson, R. L., "Turbulent boundary layer separation", *Annual review of Fluid Mech.*, 21, 1989, pp. 205-234.
- Sullerey, R. K., Gupta, A. K and Moorthy, C. S., " Similarity in the turbulent near wake of bluff bodies", *AIAA Journal*, Vol 13, No.11, Nov. 1975, pp. 1425-1429.
- Stevenson, W. H, Thompson, H. D and Craig, R. R., "Laser velocimeter measurements in highly recirculating flows", *J. Fluids Engg.*, Trans. ASME, Vol.106, 1984, pp.173
- Syamala Rao, B. C., and Chandrashekhara, D.V., "Some characteristics of cavity flow past cylindrical inducers in a venturi", ASME paper No.75-WA/FE-7, 1975.
- Tani, I., Iuchi, M and Komoda, H, "Experimental investigation of flow separation associated with a step or a groove", *Aero. Res. Inst.*, Report No. 364. April 1961
- Toebes, G.H., " The frequency of oscillatory forces acting on bluff cylinders in constricted passages", *Proc.*, 14th Congress of the International Association for Hydraulic Research, Paris, Vol-2, B-7, 1971, pp.51-58.
- Tozkas, A., "Effect of confining walls on the periodic wake of cylinders and plates"., M.S thesis, Dept. of Engg. Mechanics and Hydraulics, University of Iowa, 1965.
- Tropea, C., "Die turbulente Stufenströmung in Flachkanalen und offenen Gerinnen,

- Doctoral Dissertation, Universtat Karlsruhe, 1980.
- Tullis, J. P., "Hydraulics of pipelines: Pumps, Valves, Cavitation and Transients", John Wiley, New York, 1989.
- Varga, J., and Sebestyen, G. Y., "Determination of the frequencies of wakes shedding from circular cylinders", *Acta Technica Academiae Scientiarum Hungaricae*, Vol.53, 1966, pp. 91-108.
- Vigander, S., "An experimental study of wall pressure fluctuations in a cavitating turbulent shear flow", *Studies in Engineering Mechanics*, Report No. 41, University of Kansas, 1965.
- Waid, R. L., "Water tunnel investigations of two-dimensional cavities", *Hydrodynamics Laboratory, Calif. Inst. of Tech.*, No.E73.6, September 1957.
- Westphal, R. V, Johnston, J. P and Eaton, J. K., "Experimental study of flow reattachment in a single sided sudden expansion", *NASA CR 3765*, 1984.
- Wu, T.Y., Whitney, A. K., and Brennen, C., "Cavity flow wall effects and correction rules", *J. of Fluid Mechanics*, Vol.49, 1971, pp.223-256.
- Young, J. O., and Holl, J. W., "Effects of cavitation on periodic wakes behind symmetric wedges", *Journal of Basic Engineering.*, *Trans. ASME*, Mar. 1966, pp.163-176.
- Zdravkovich, M. M., "Comment on the loss of vorticity in the near wake of bluff bodies", *J. of Fluid Engineering*, Vol.114, March, 1989, pp.104-105.

APPENDIX II
FIGURES

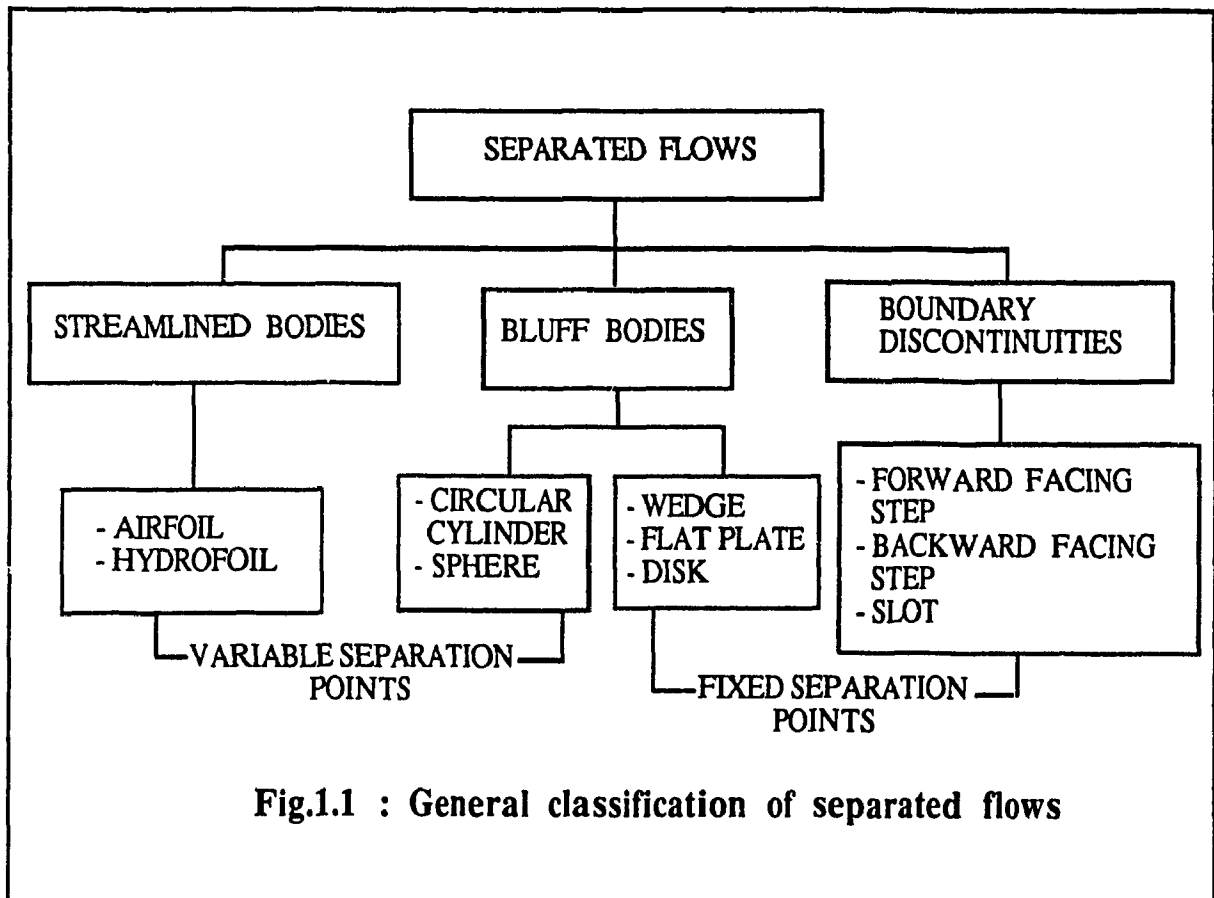
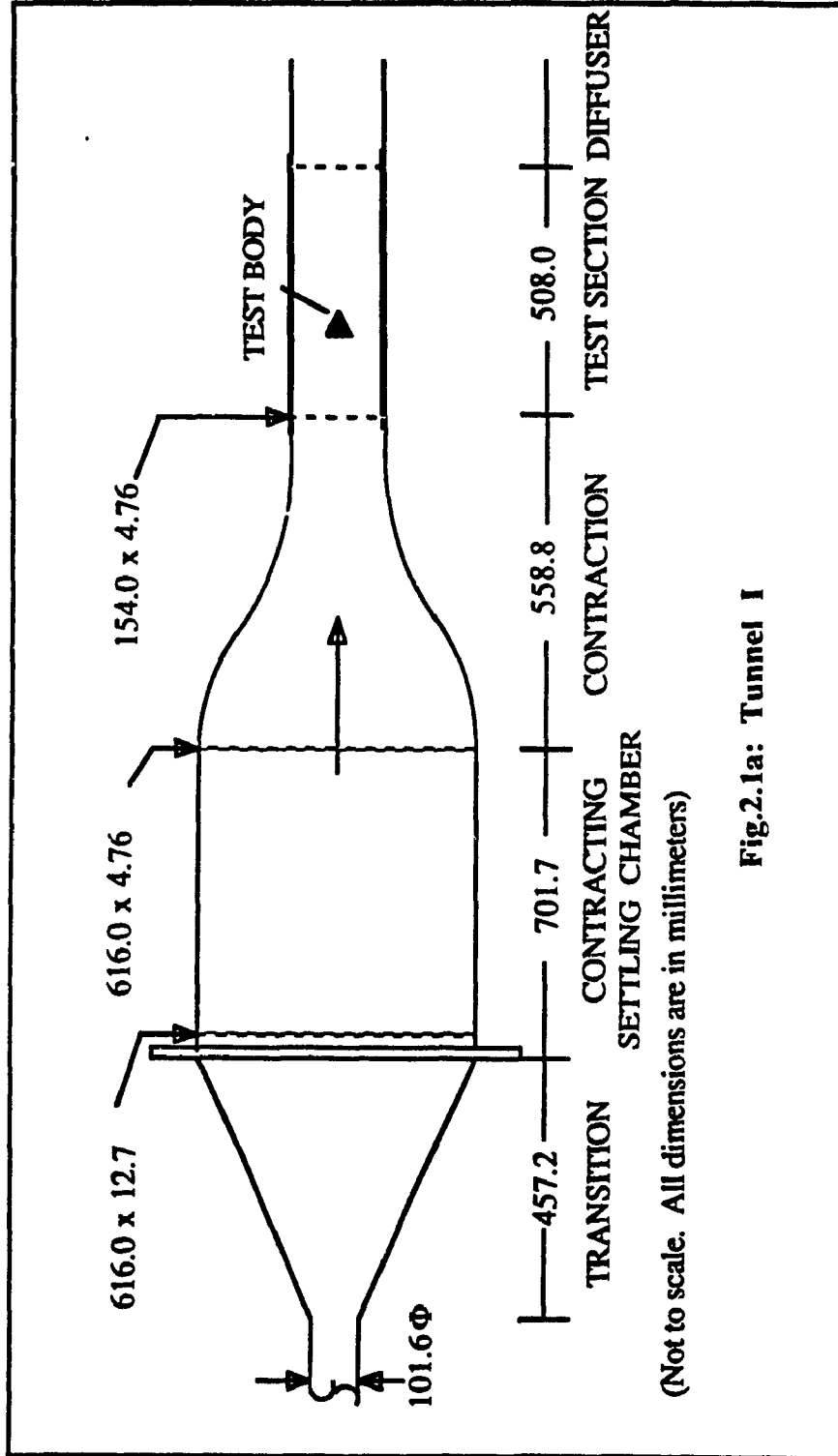


Fig.1.1 : General classification of separated flows



(Not to scale. All dimensions are in millimeters)

Fig.2.1a: Tunnel I

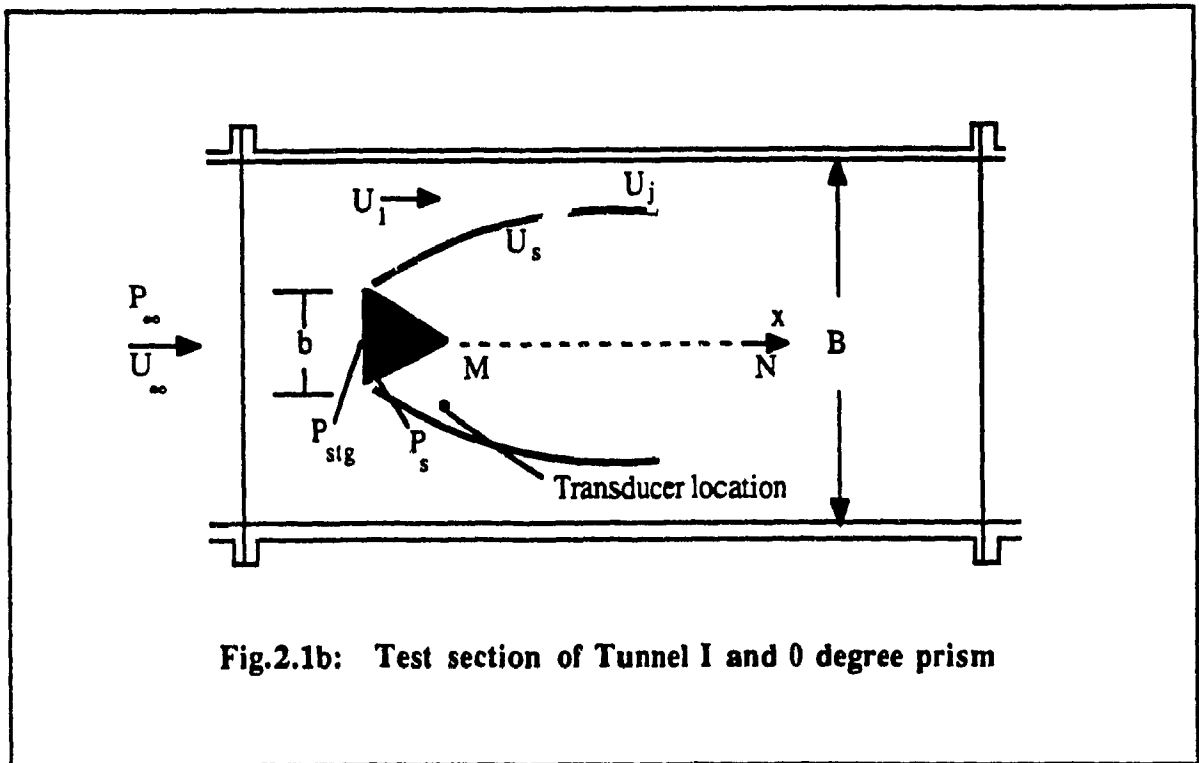


Fig.2.1b: Test section of Tunnel I and 0 degree prism

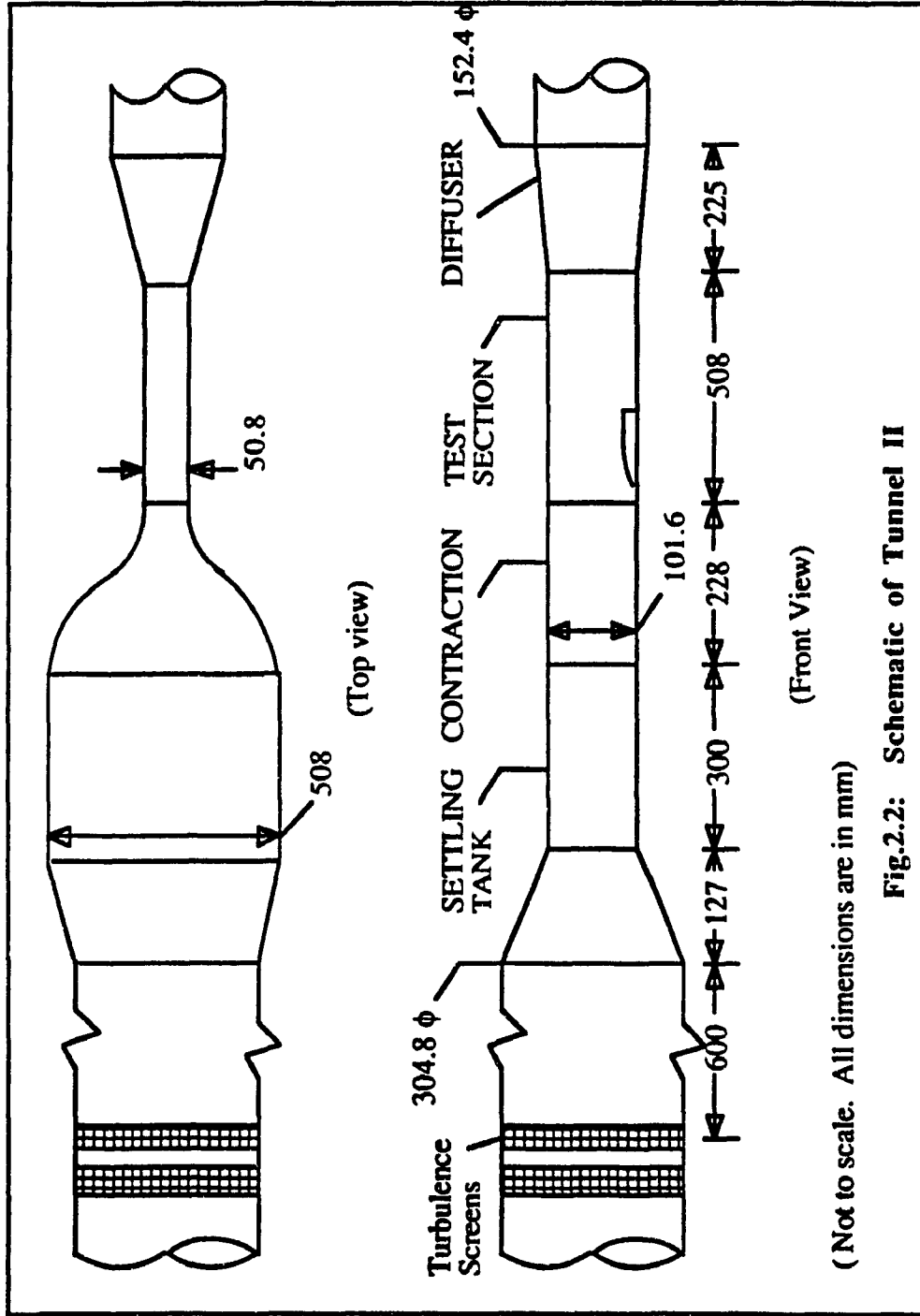


Fig.2.2: Schematic of Tunnel II

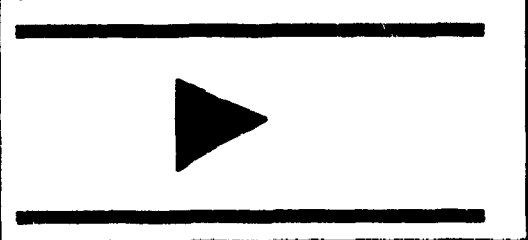
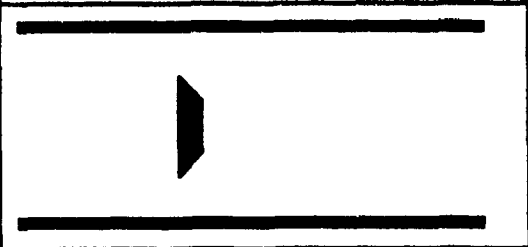
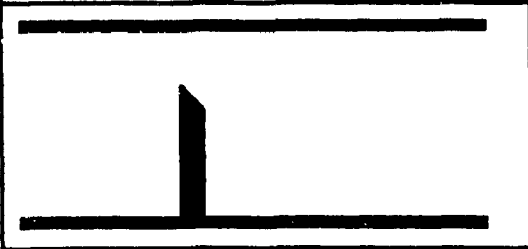
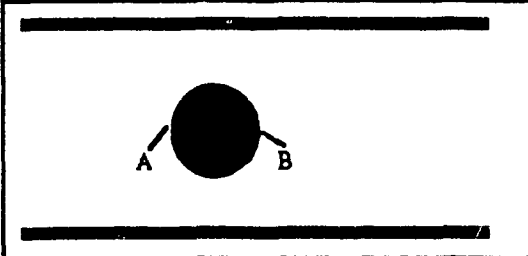
	<p>0 degree wedge $b/B = 0.10, 0.24, 0.33$ $0.58, 0.66, 0.82$ 0.93</p>
	<p>Normal flat plate $b/B = 0.93$</p>
	<p>Wall mounted gate $b/B = 0.93$</p>
	<p>Circular cylinder $b/B = 0.08, 0.33$</p>

Fig. 2.3a : Bluff shapes and blockages tested

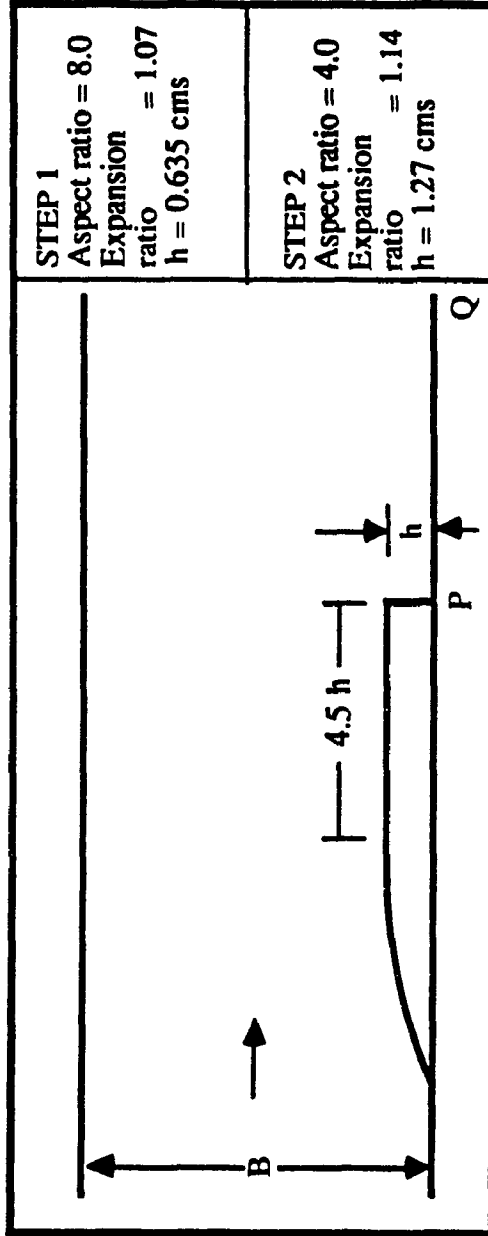
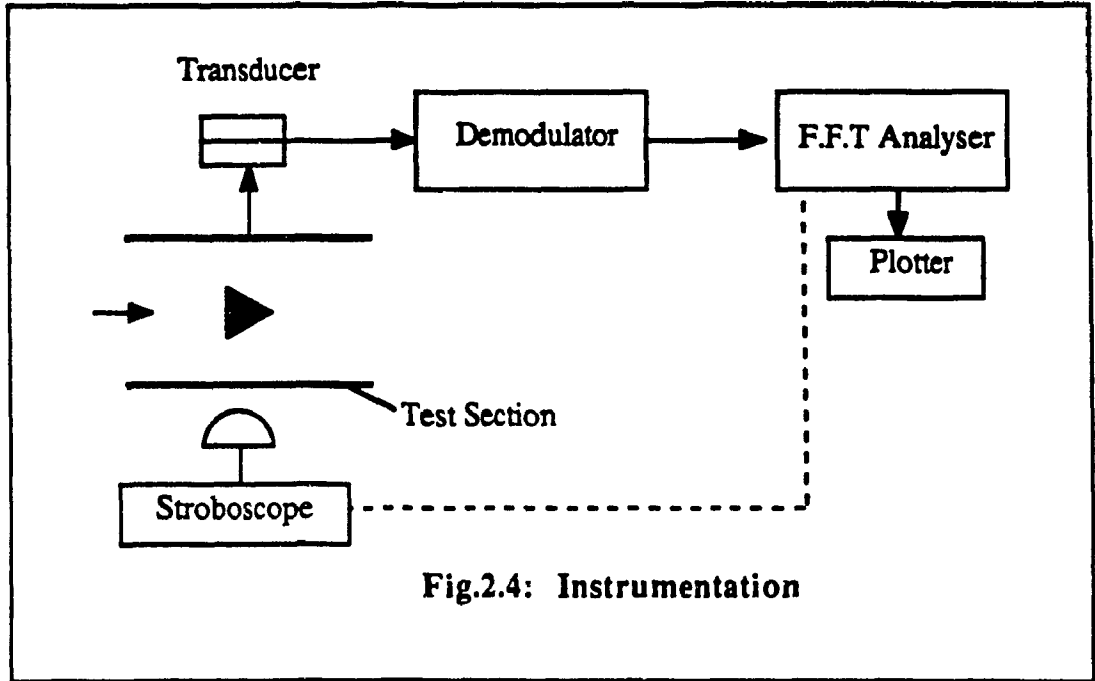


Fig.2.3b: Backward facing step models



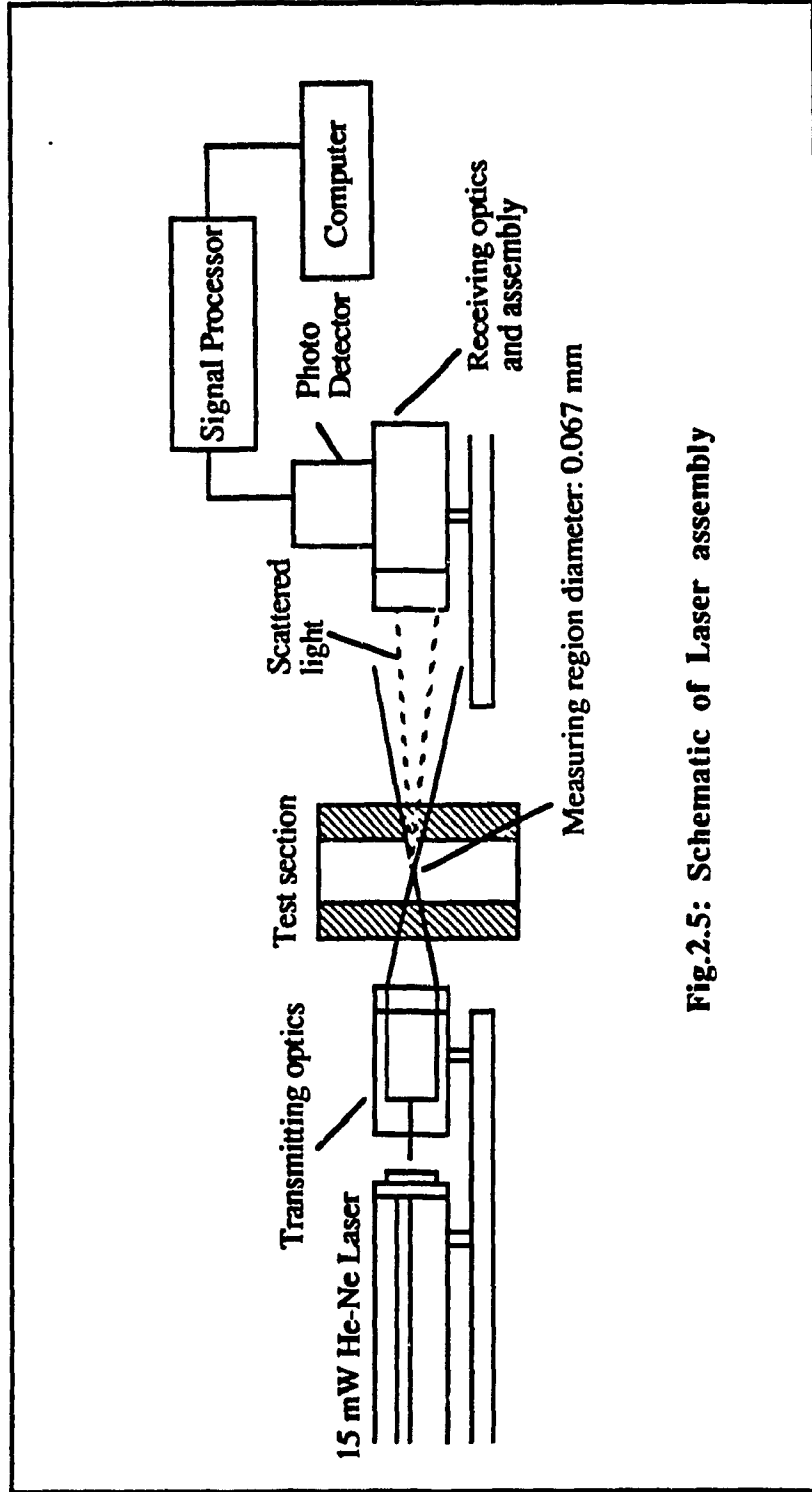


Fig.2.5: Schematic of Laser assembly

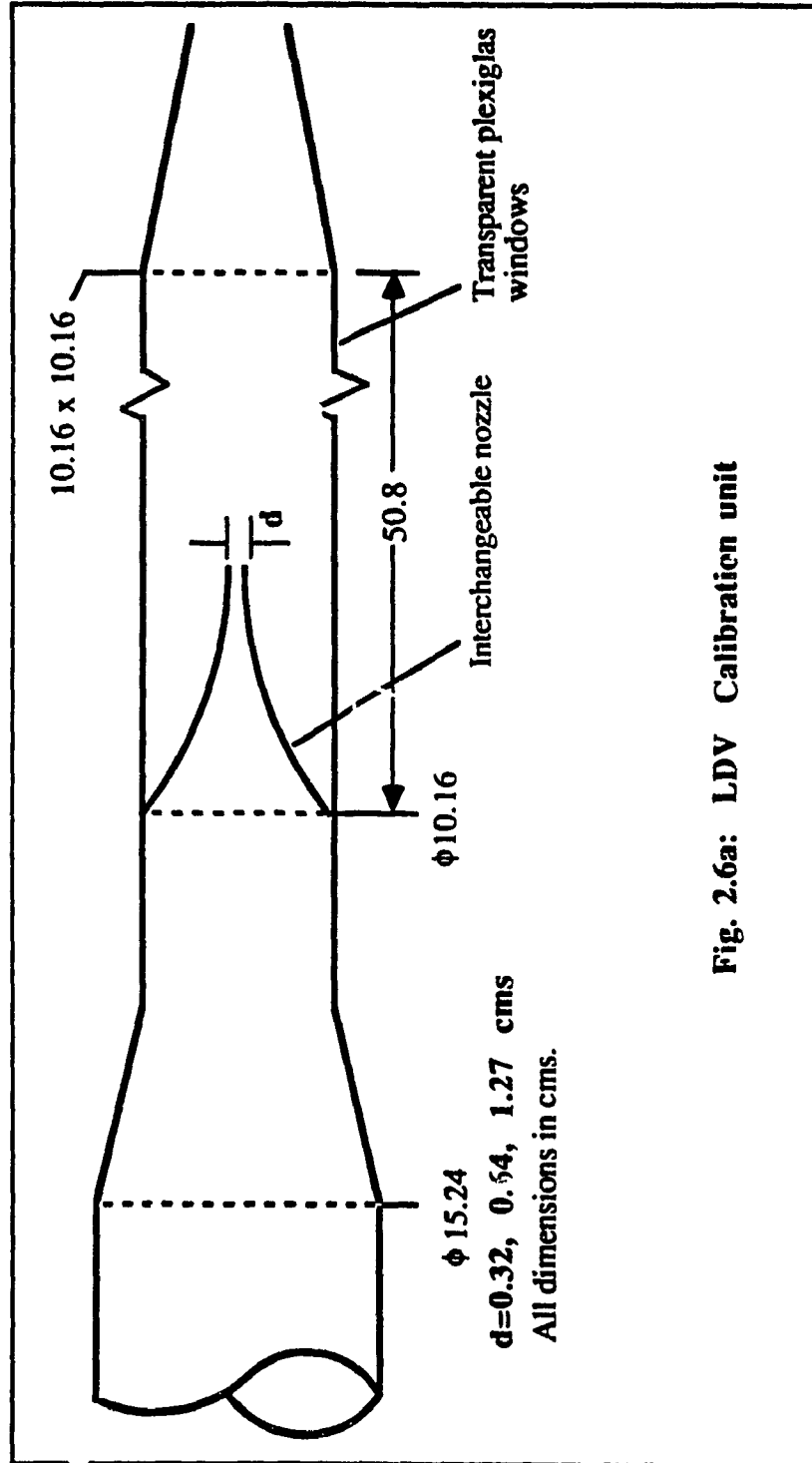


Fig. 2.6a: LDV Calibration unit

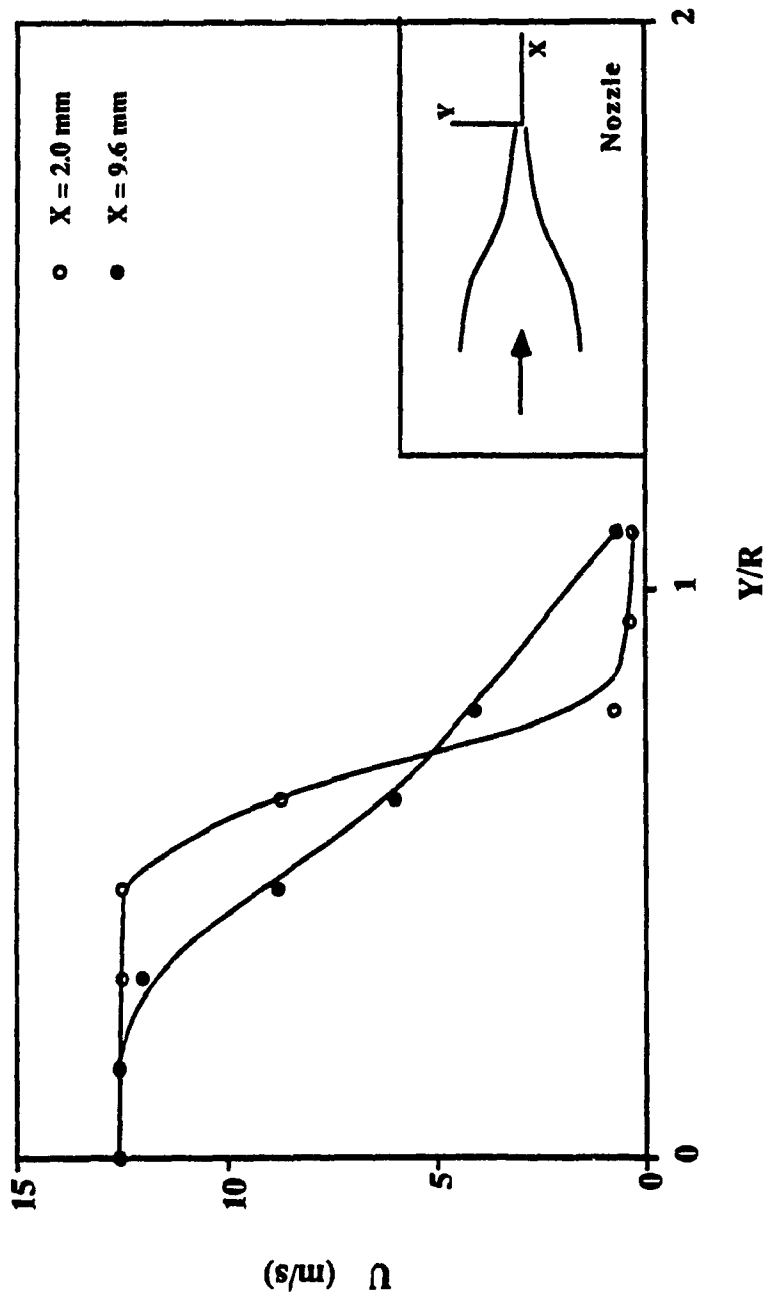


Fig. 2.6b: Velocity distribution at the mouth of the nozzle

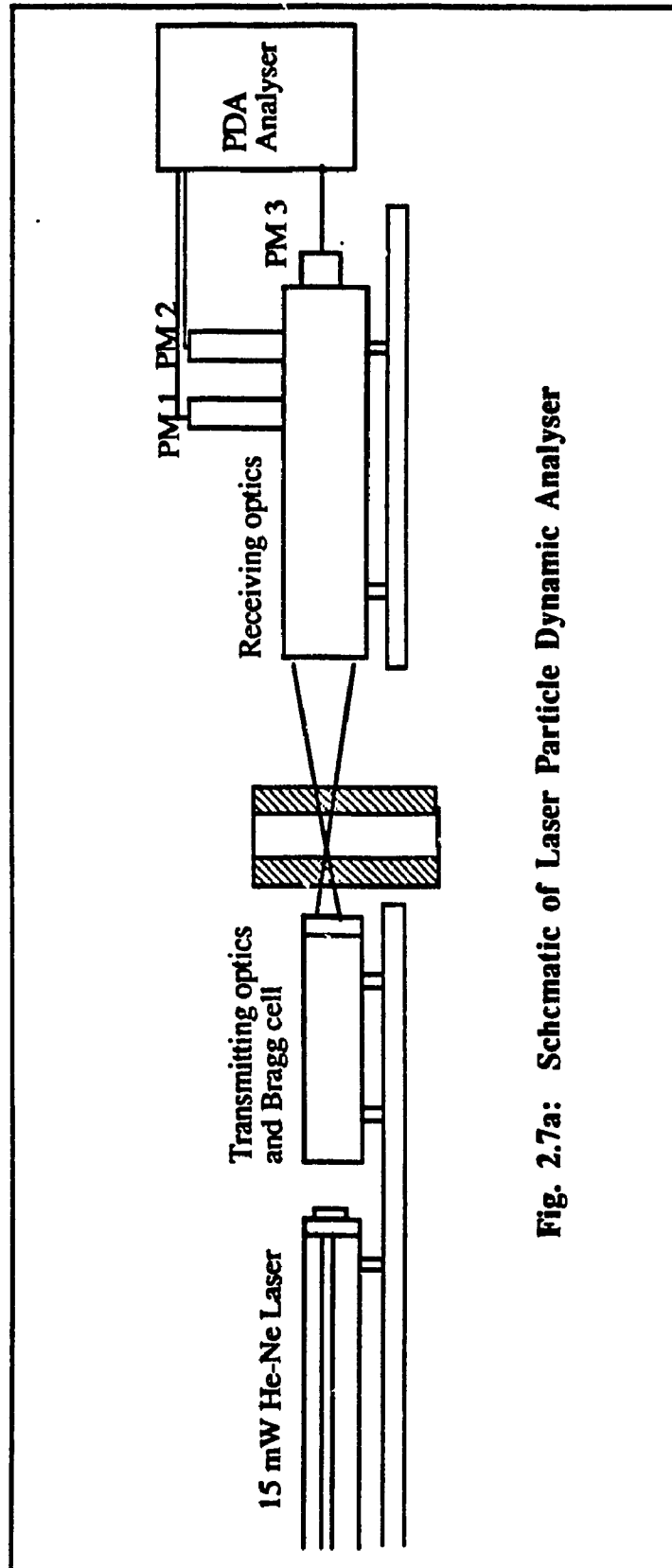


Fig. 2.7a: Schematic of Laser Particle Dynamic Analyser

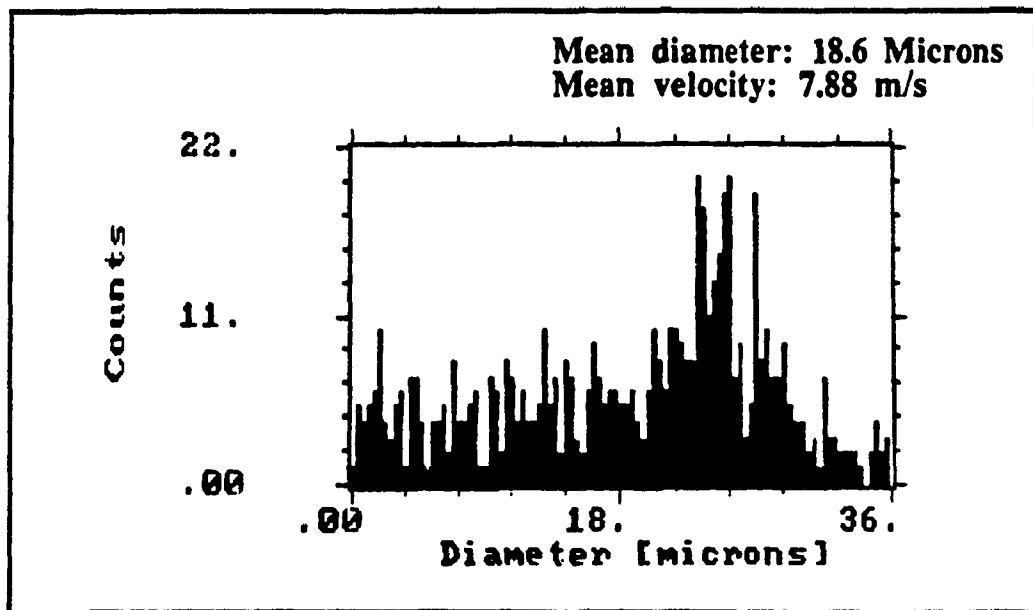
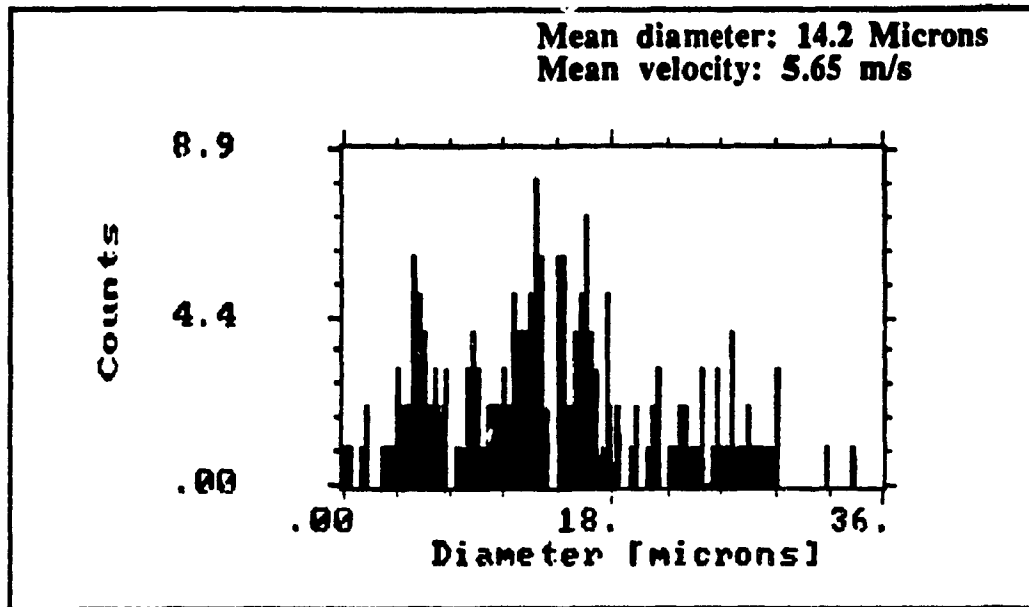


Fig.2.7b: Typical PDA measurement

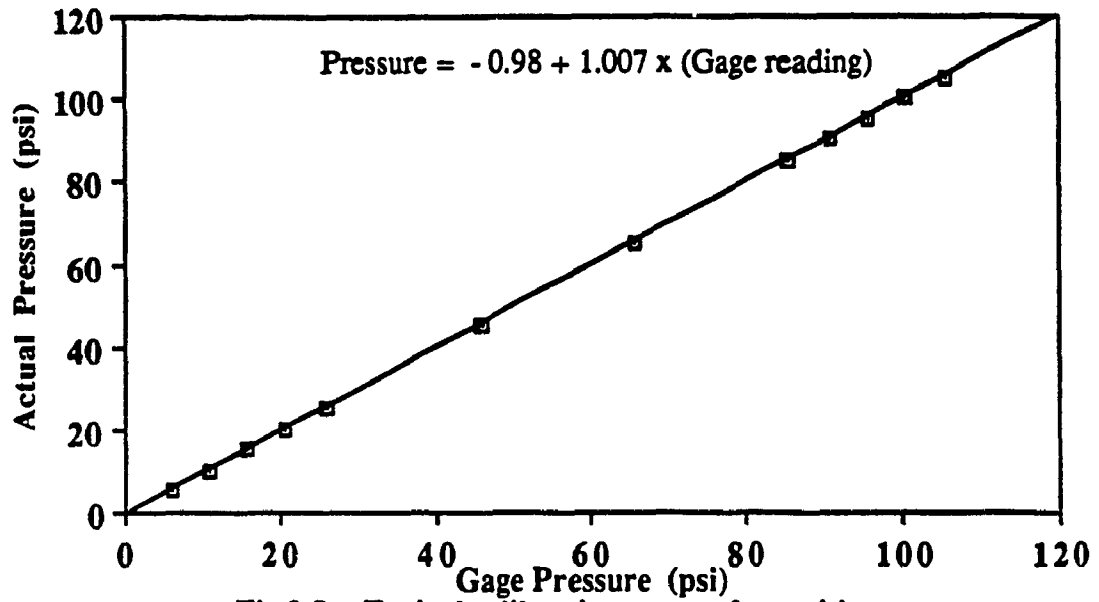


Fig.2.8a: Typical calibration curve of a positive pressure gage

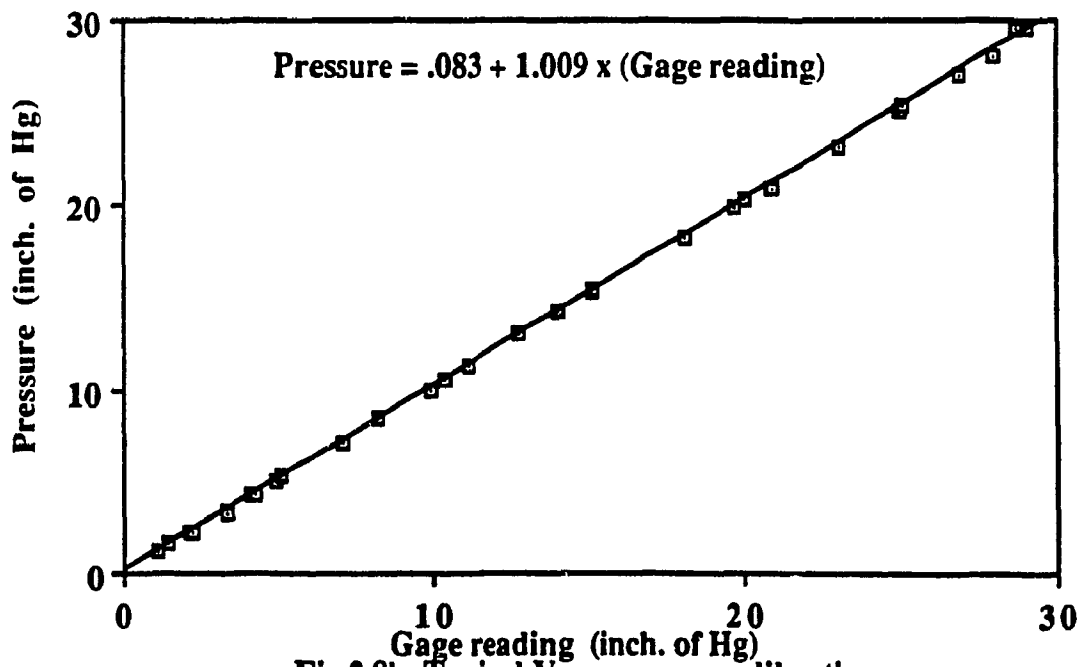


Fig.2.8b: Typical Vacuum gage calibration

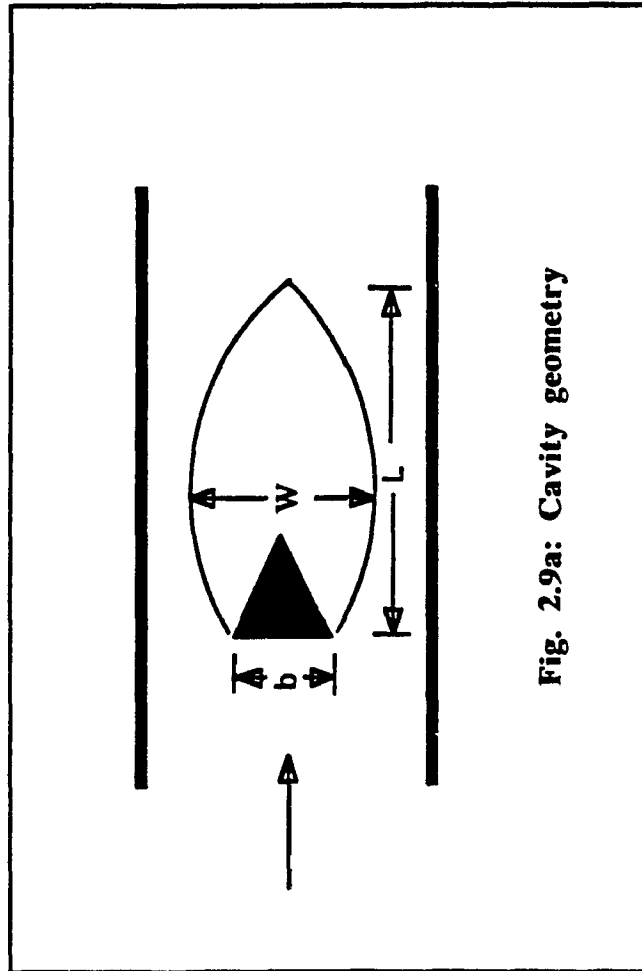


Fig. 2.9a: Cavity geometry

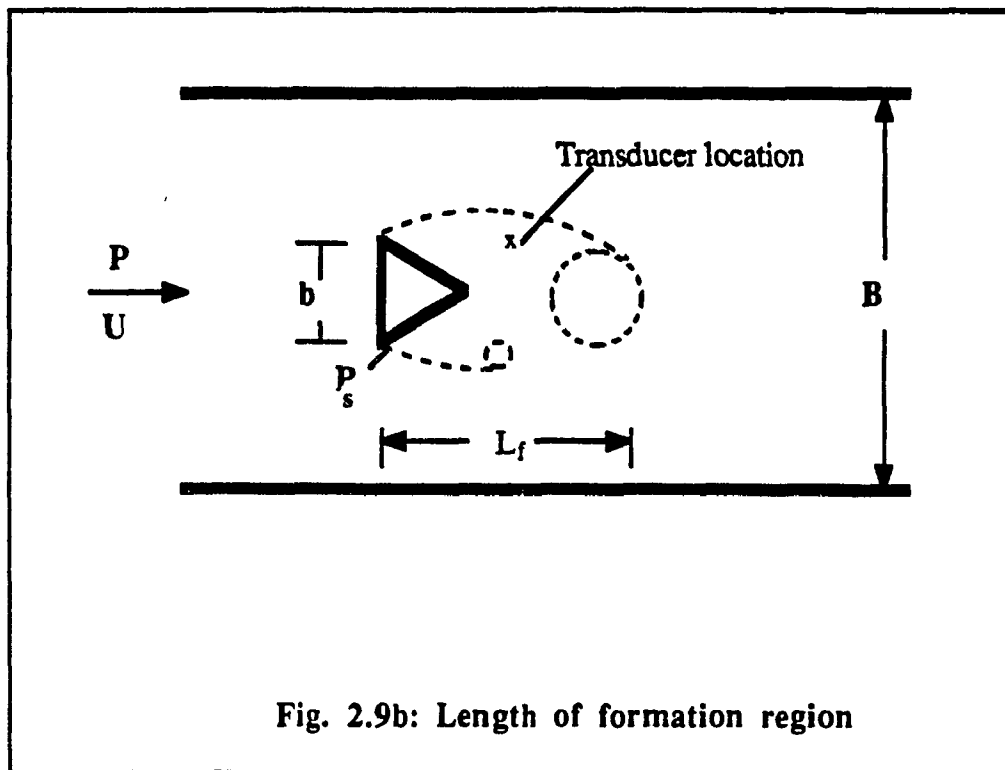


Fig. 2.9b: Length of formation region

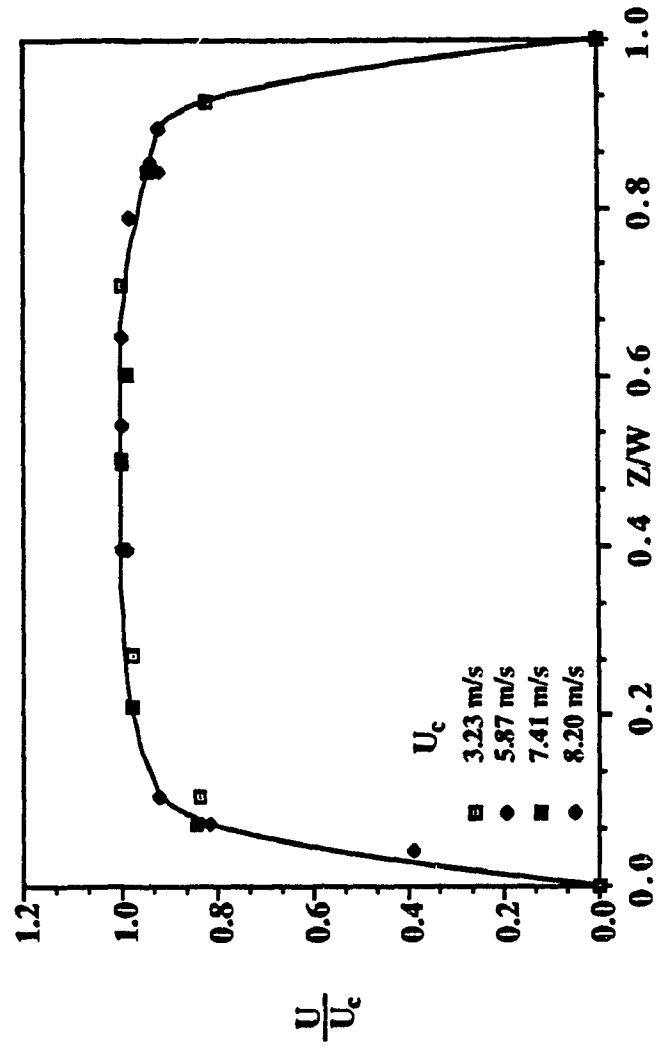


Fig.2.10a: Span-wise velocity distribution (Tunnel D)

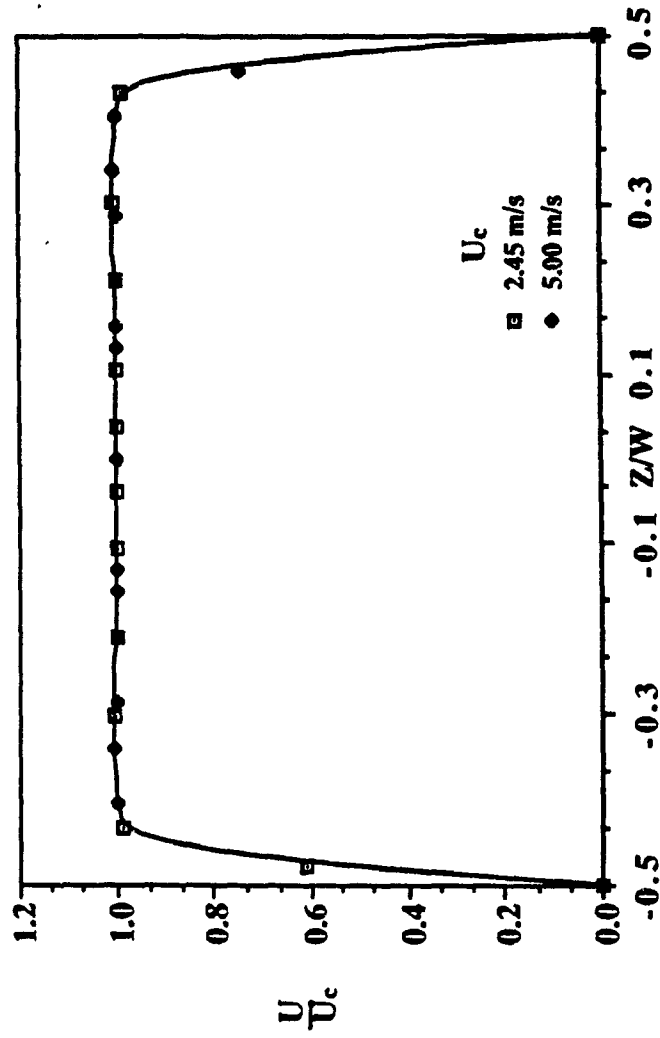


Fig.2.10b: Span-wise velocity distribution in Tunnel - II

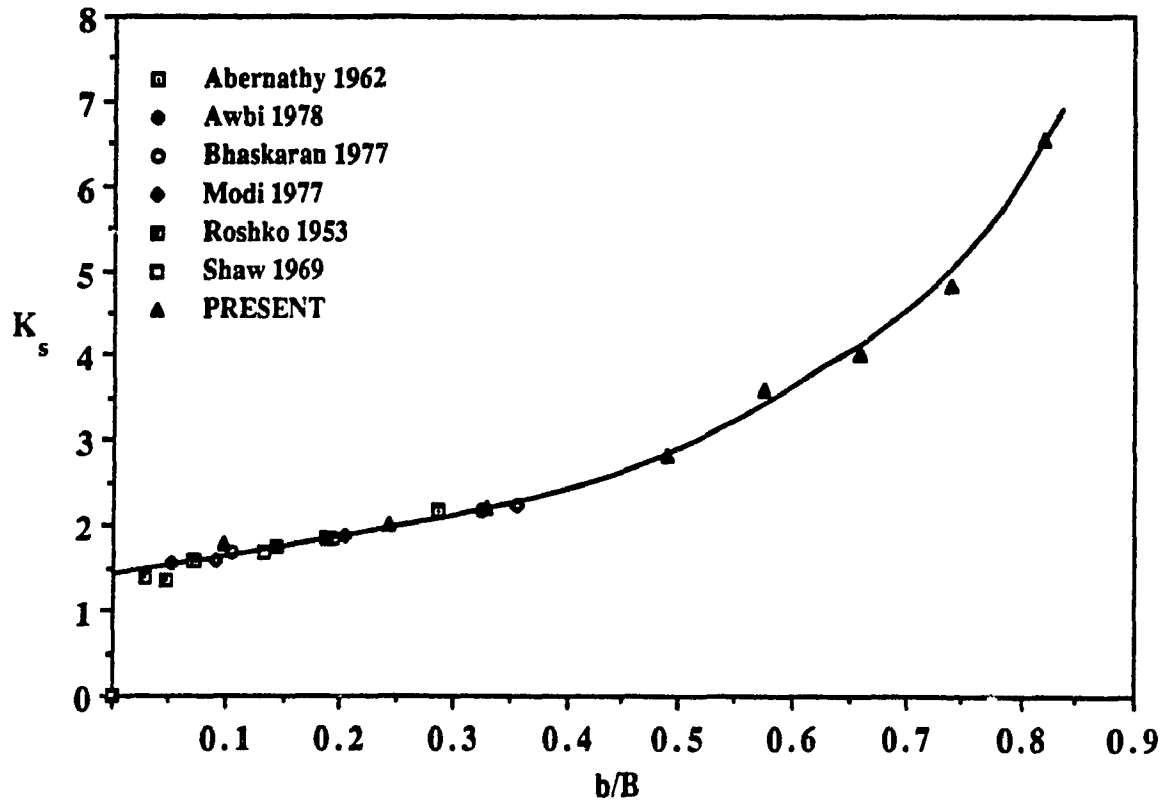


Fig. 2.11: Variation of K_s with b/B (Non-cavitating flow)

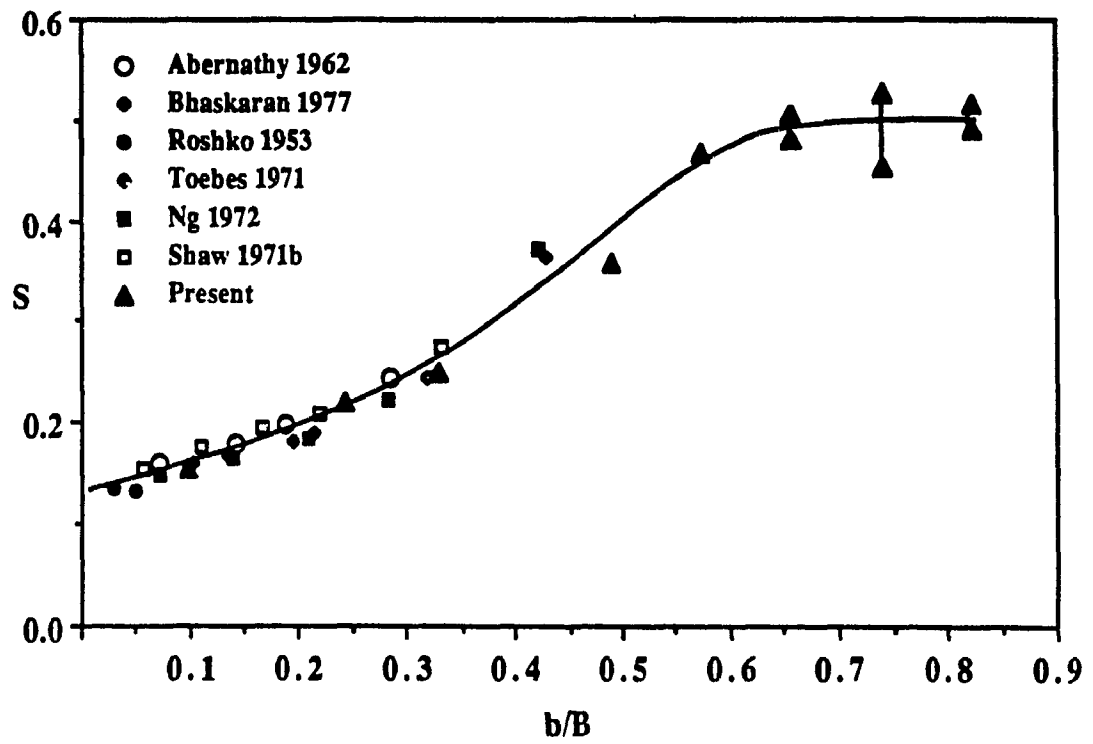


Fig.2.12: Variation of S with b/B (Non-cavitating flow)

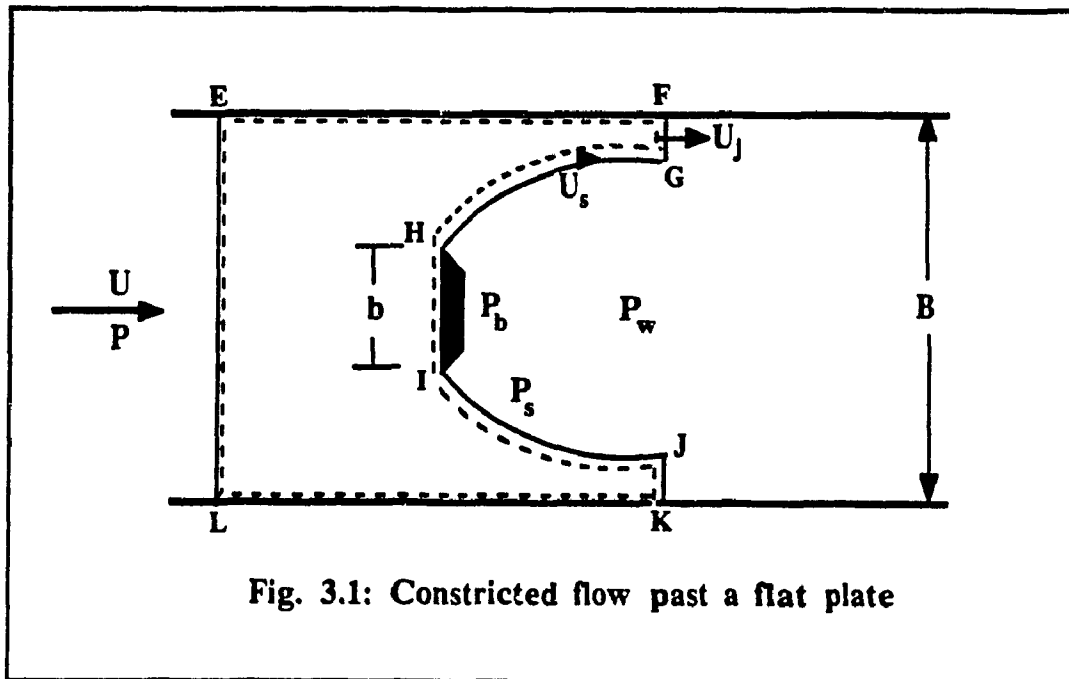


Fig. 3.1: Constricted flow past a flat plate

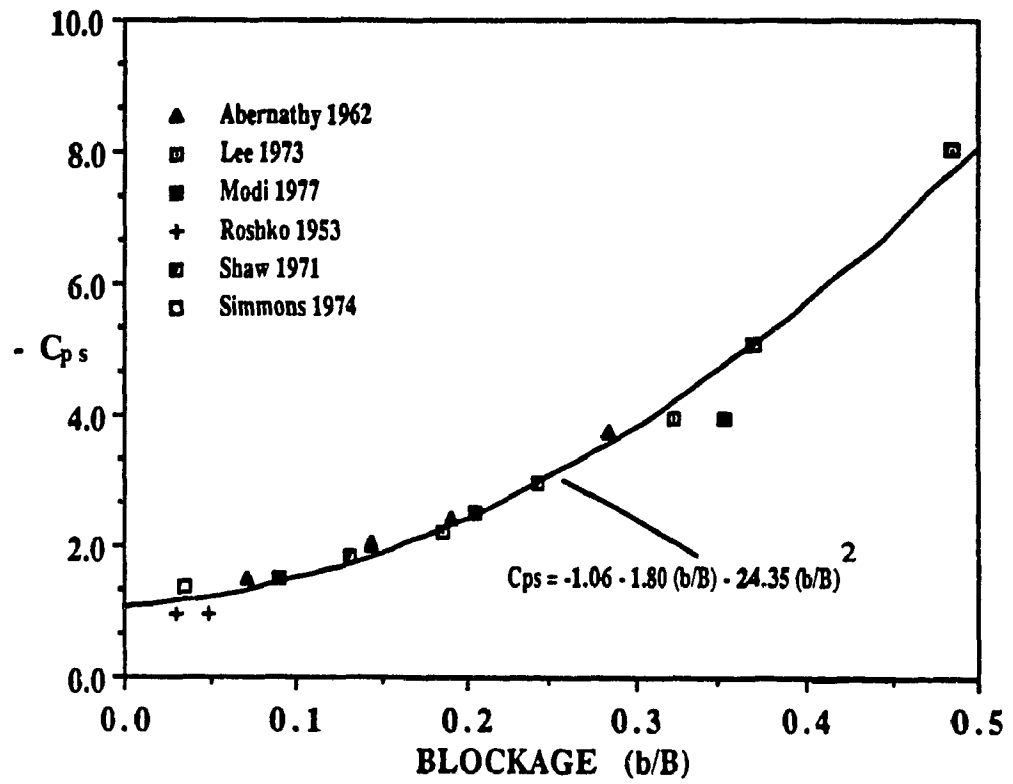


Fig. 3.2: Variation of $-C_{ps}$ with b/B

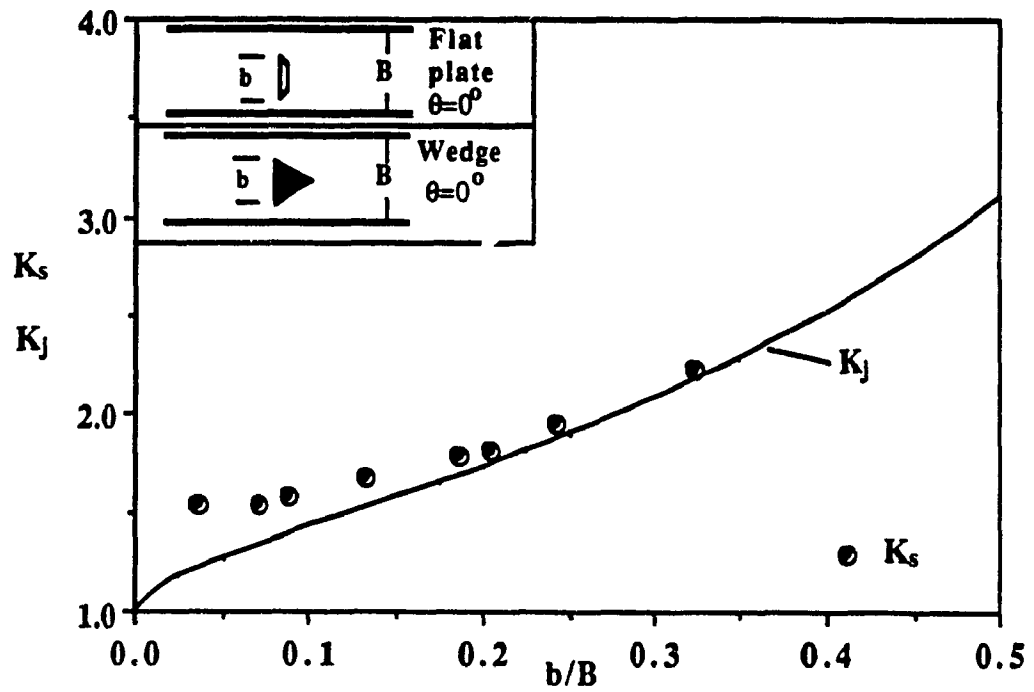


Fig.3.3: Variation of K_s and K_j with blockage

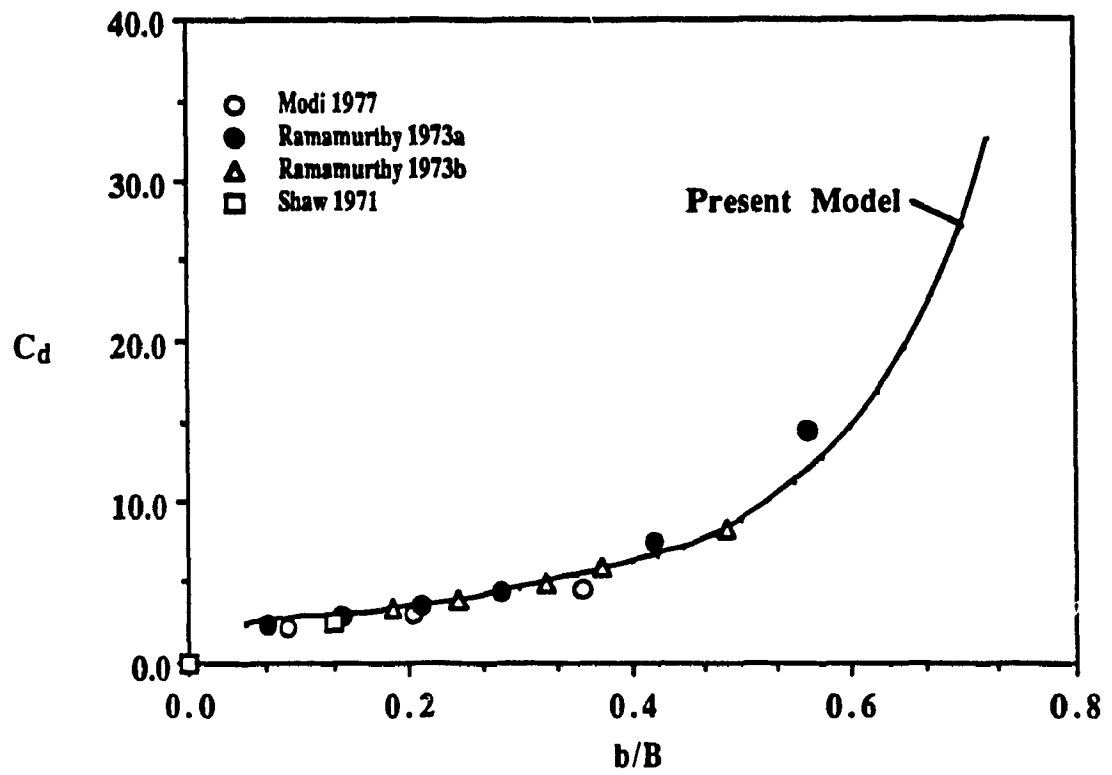


Fig.3.4: Variation of C_d with b/B

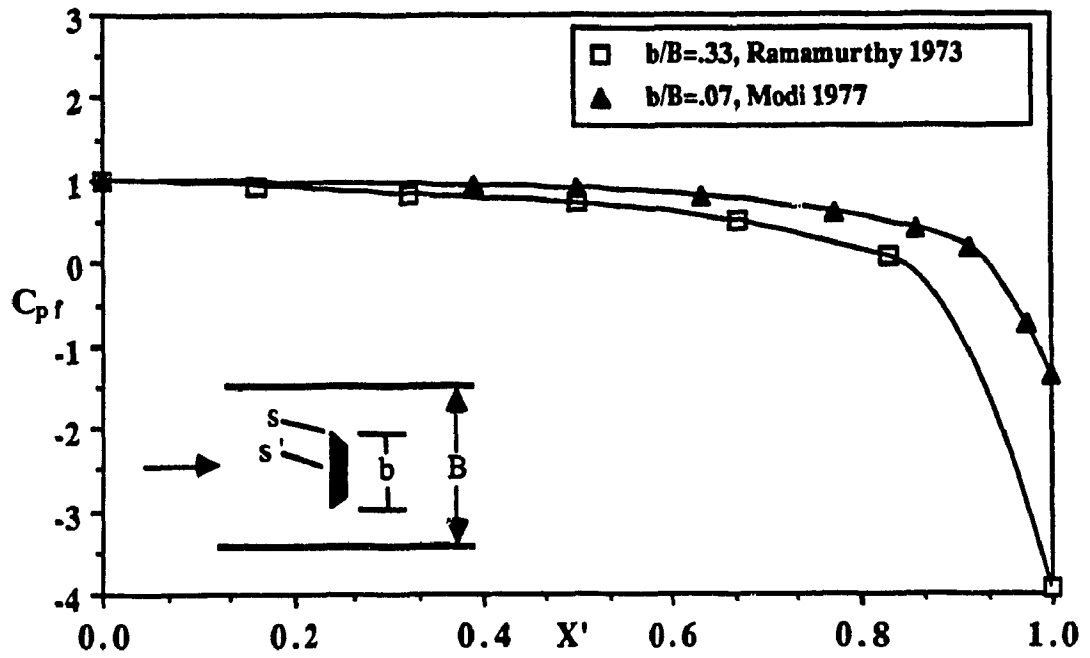


Fig.4.1: Forebody pressure distribution in non-cavitating flows

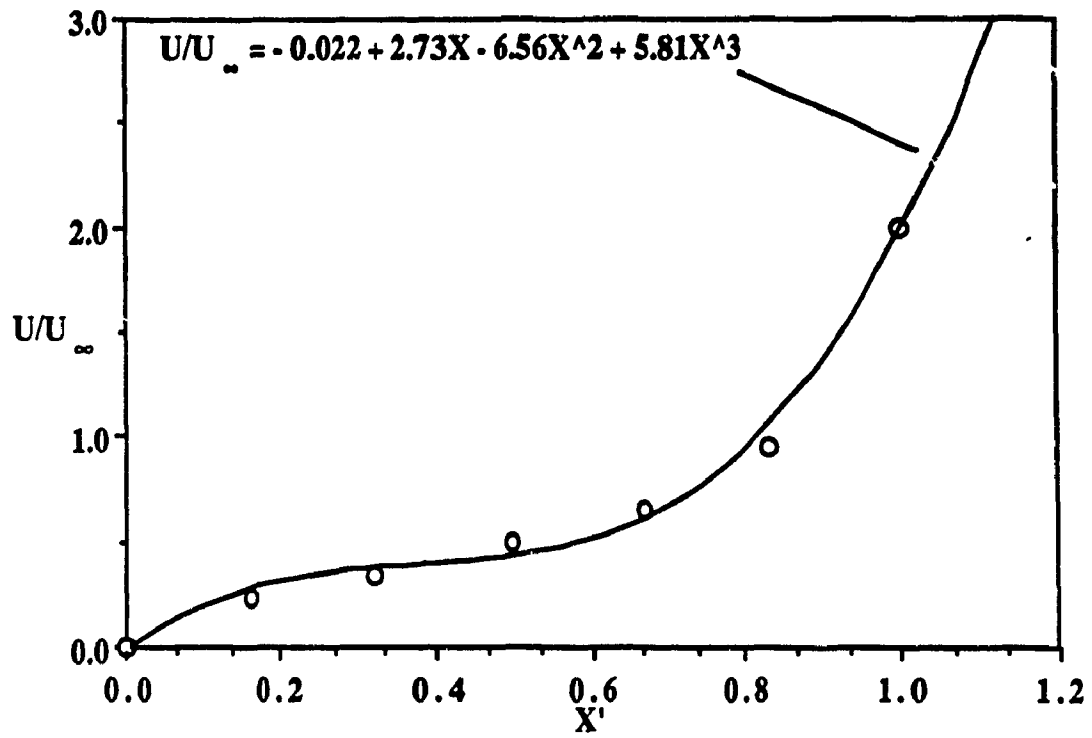


Fig.4.2: Potential flow velocity distribution on forebody face ($b/B = 0.325$)

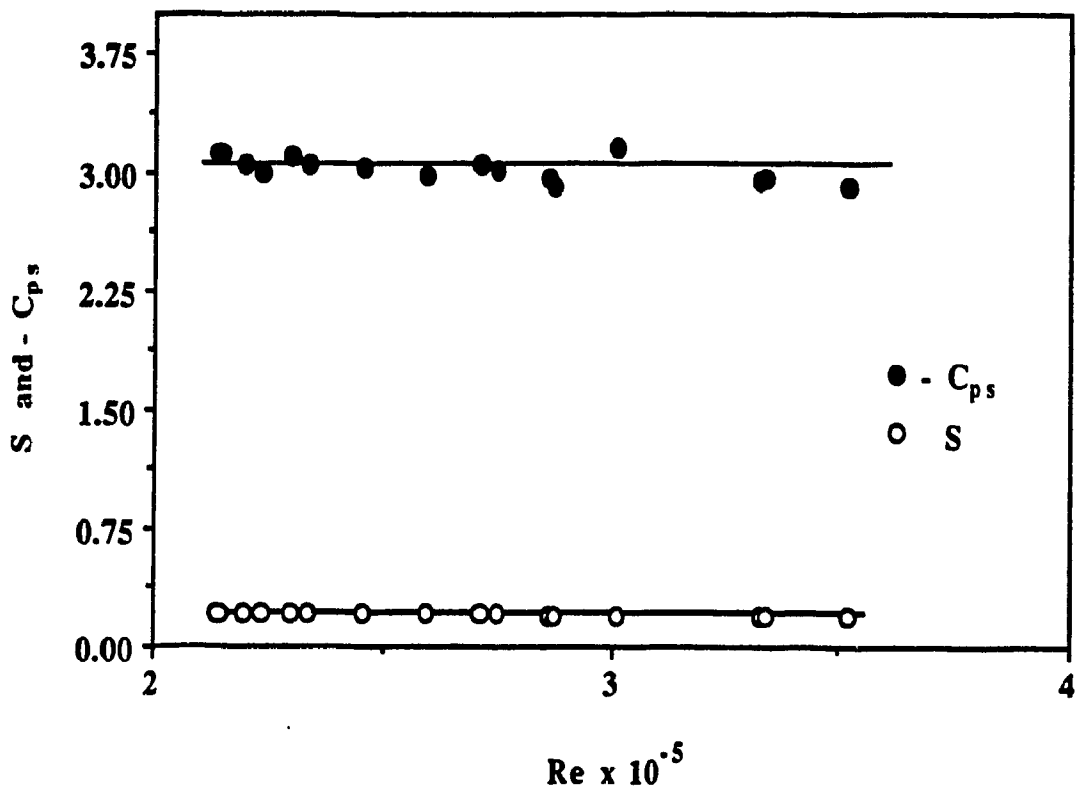


Fig.4.3: Variation of S and - C_{ps} with Reynolds number (Inception conditions)

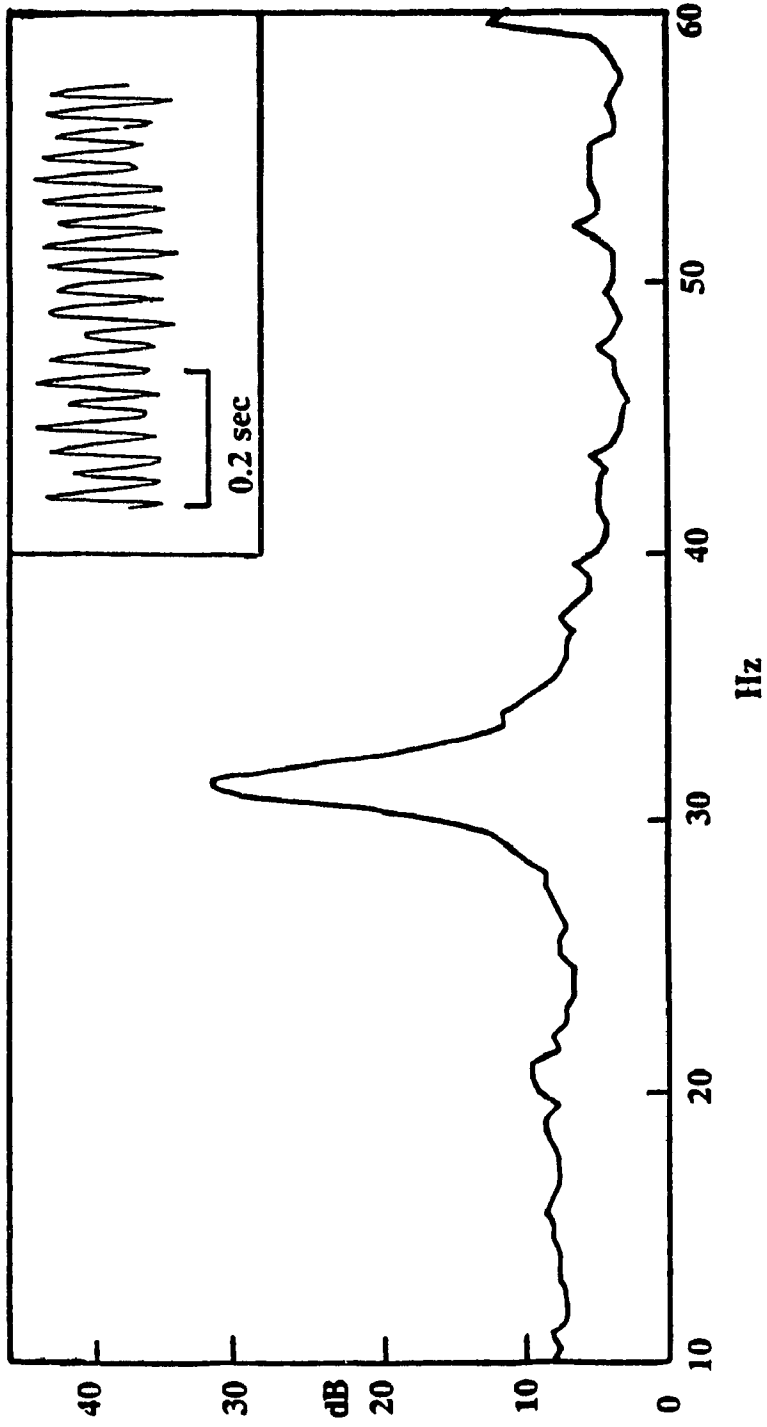


Fig.4.4 : Power spectra of Pressure Pulsations at Inception Conditions

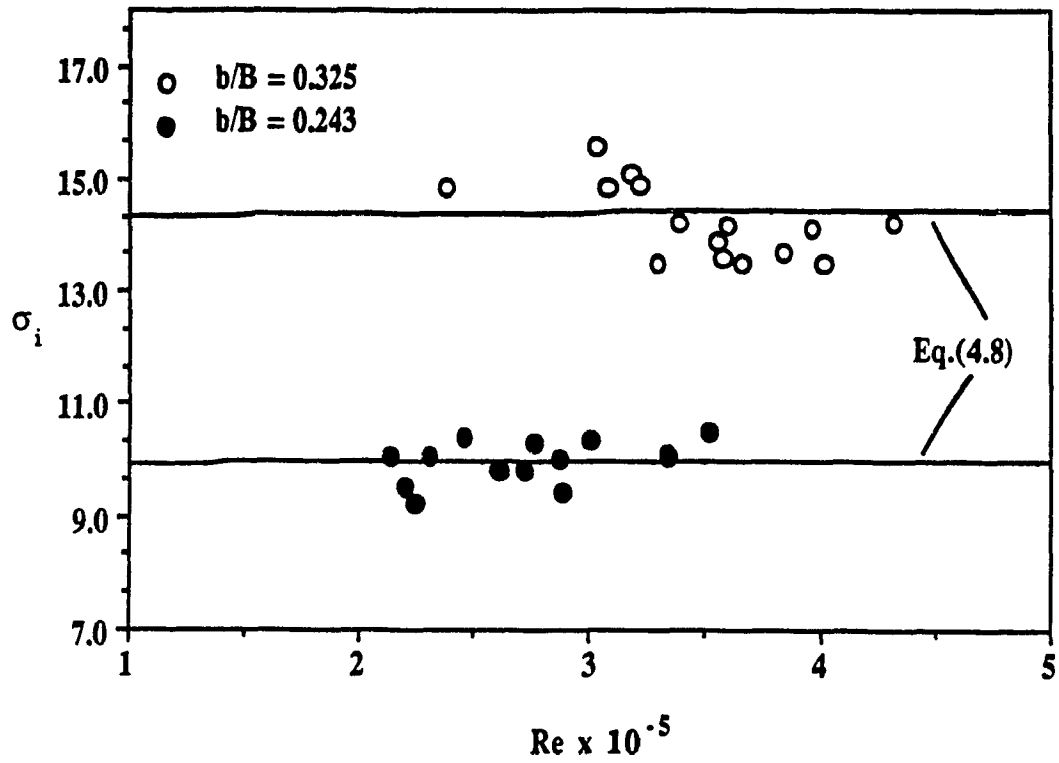


Fig. 4.5: Variation of inception cavitation number with Re ($b/B = .243$ and $.325$)

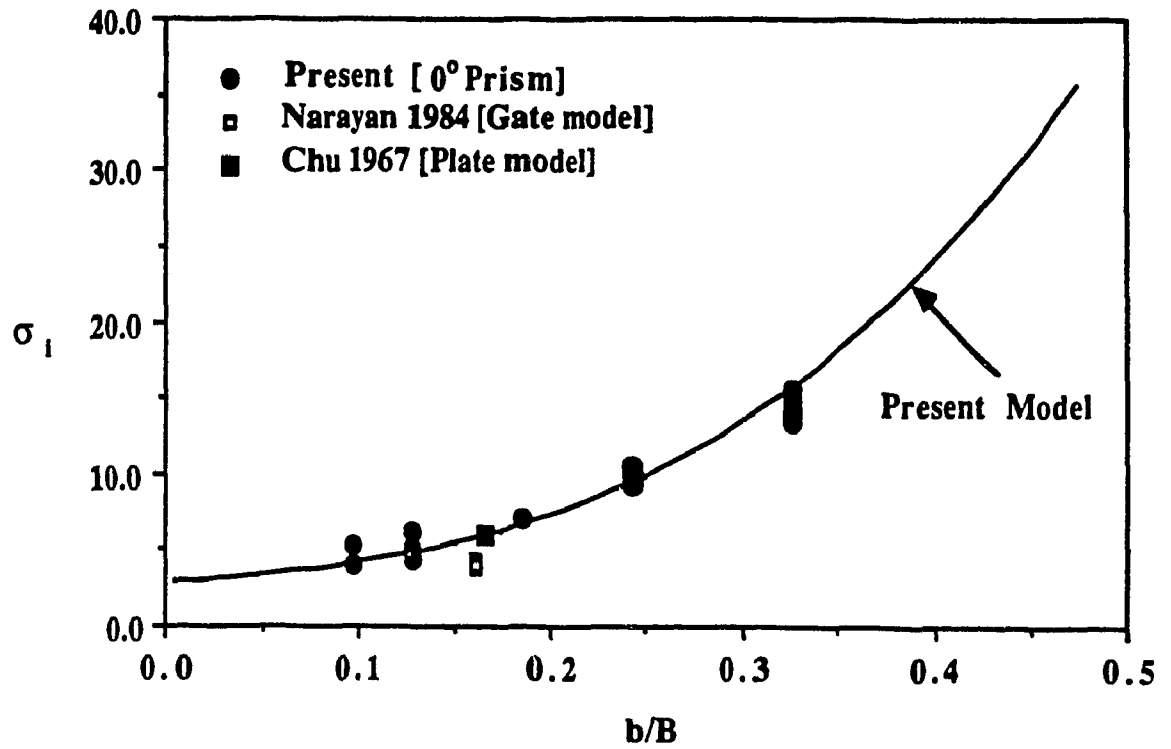


Fig. 4.6: Variation of Inception cavitation number with blockage ($Re = 200,000$)

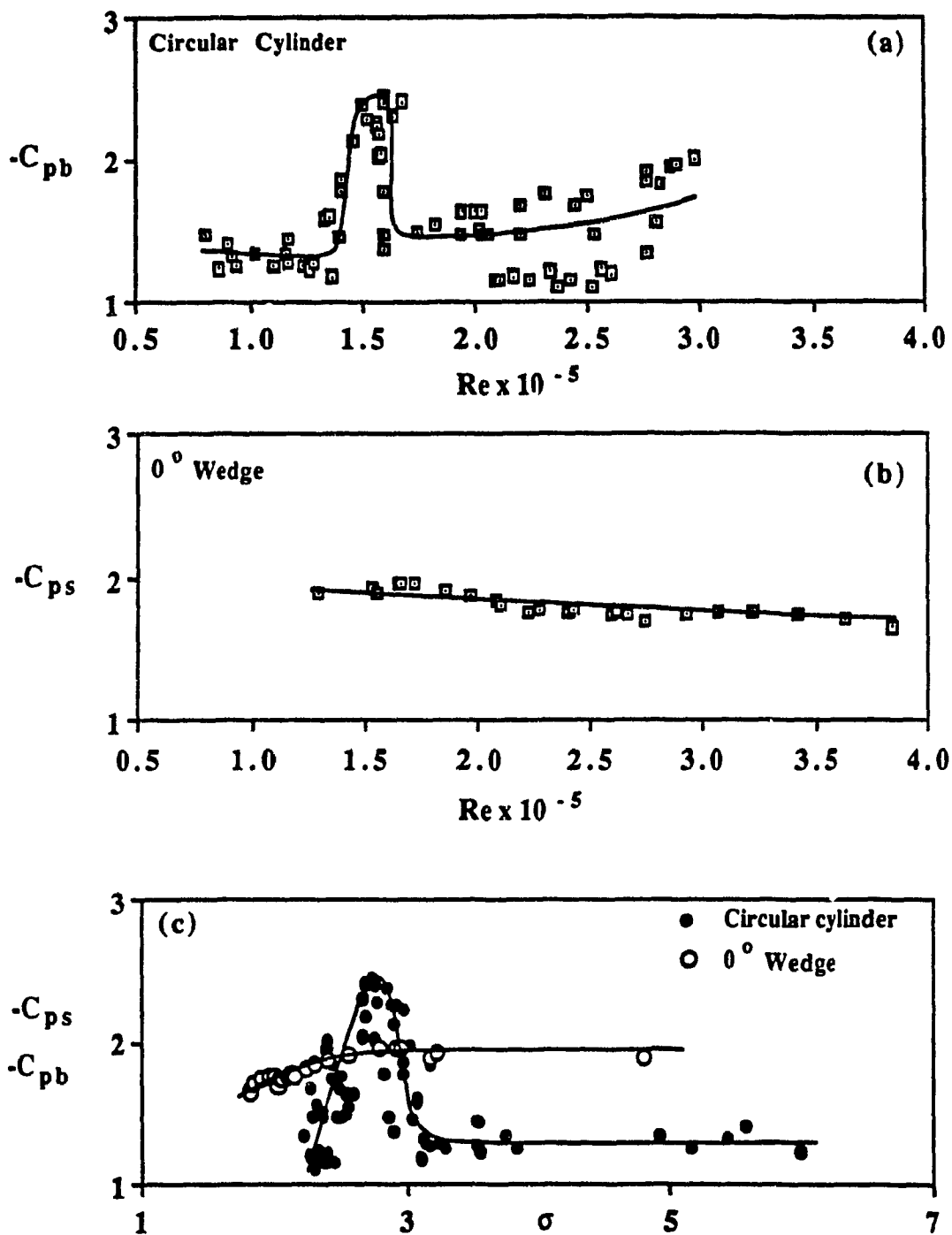


Fig.5.1: Influence of Reynolds number on test results at very small blockages

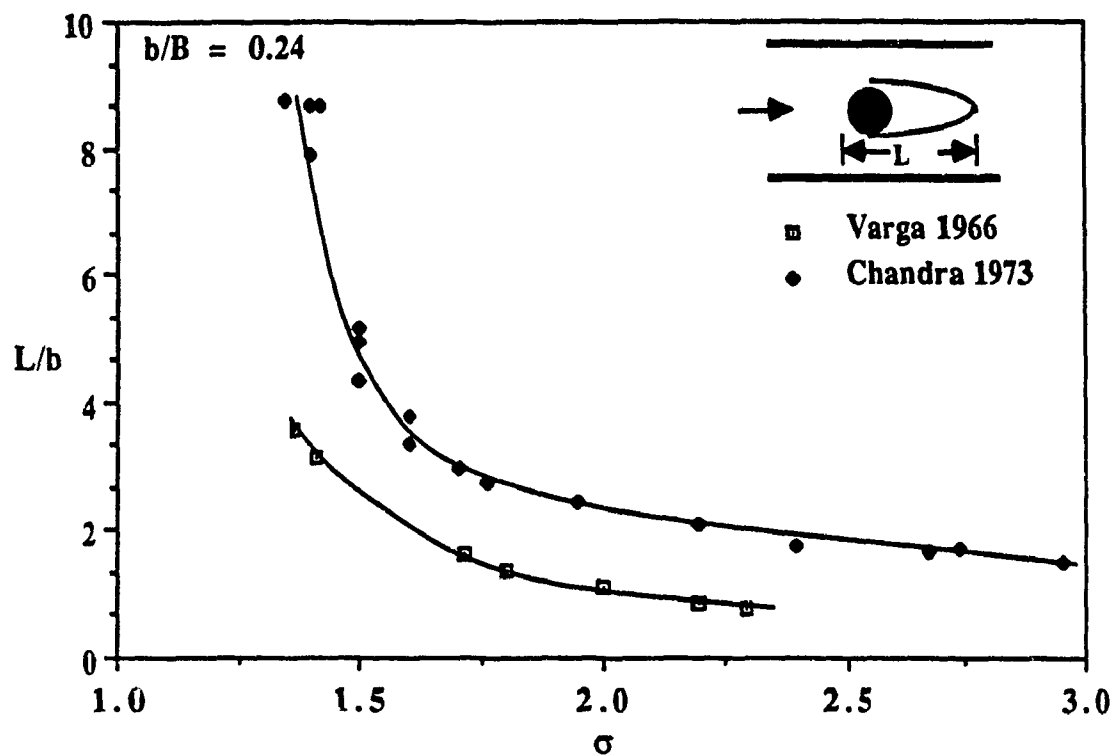


Fig.5.2: Variation of L/b with cavitation number for circular cylinders

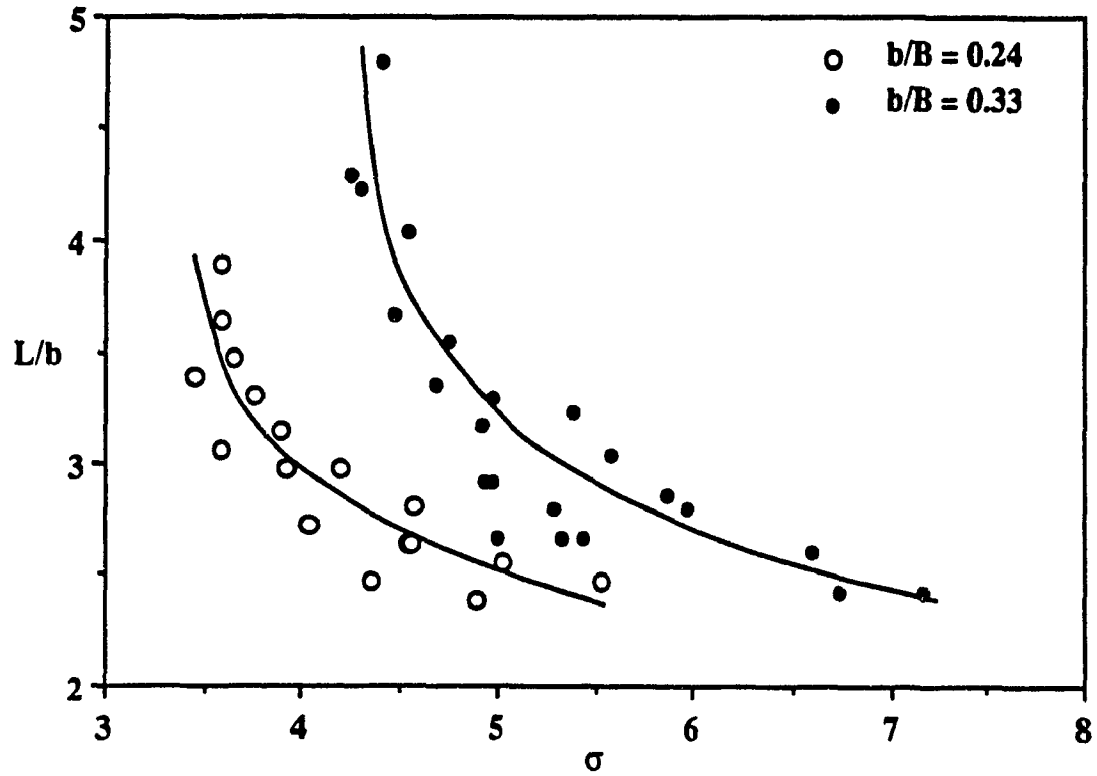


Fig.5.3: Variation of L/b with σ

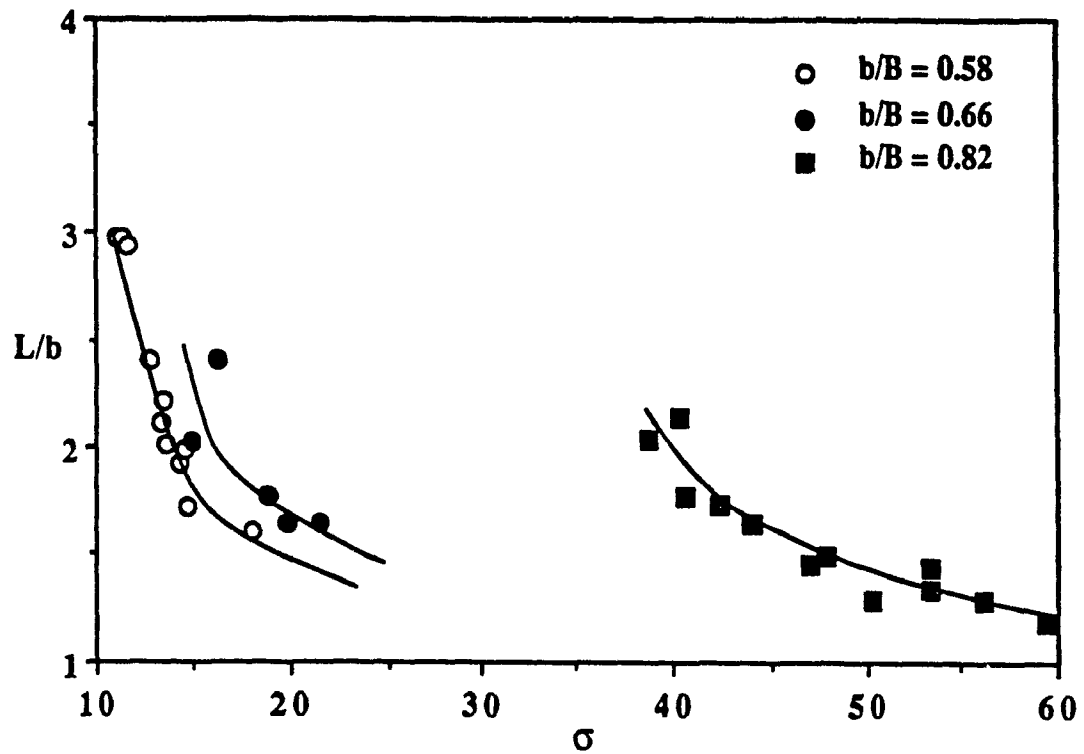
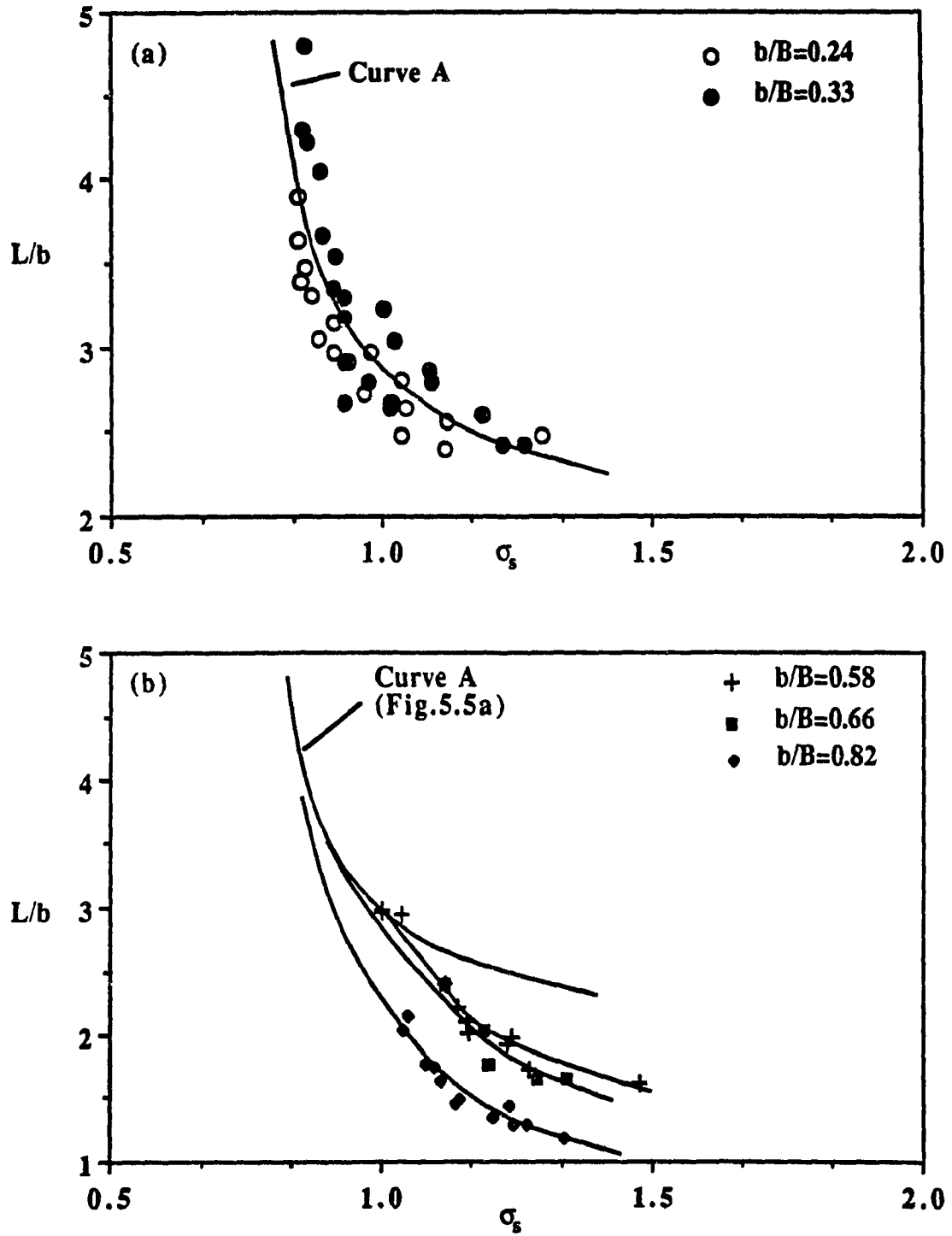


Fig. 5.4: Variation of L/b with cavitation number ($0.58 < b/B < 0.82$)

Fig.5.5: Variation of L/b with σ_s

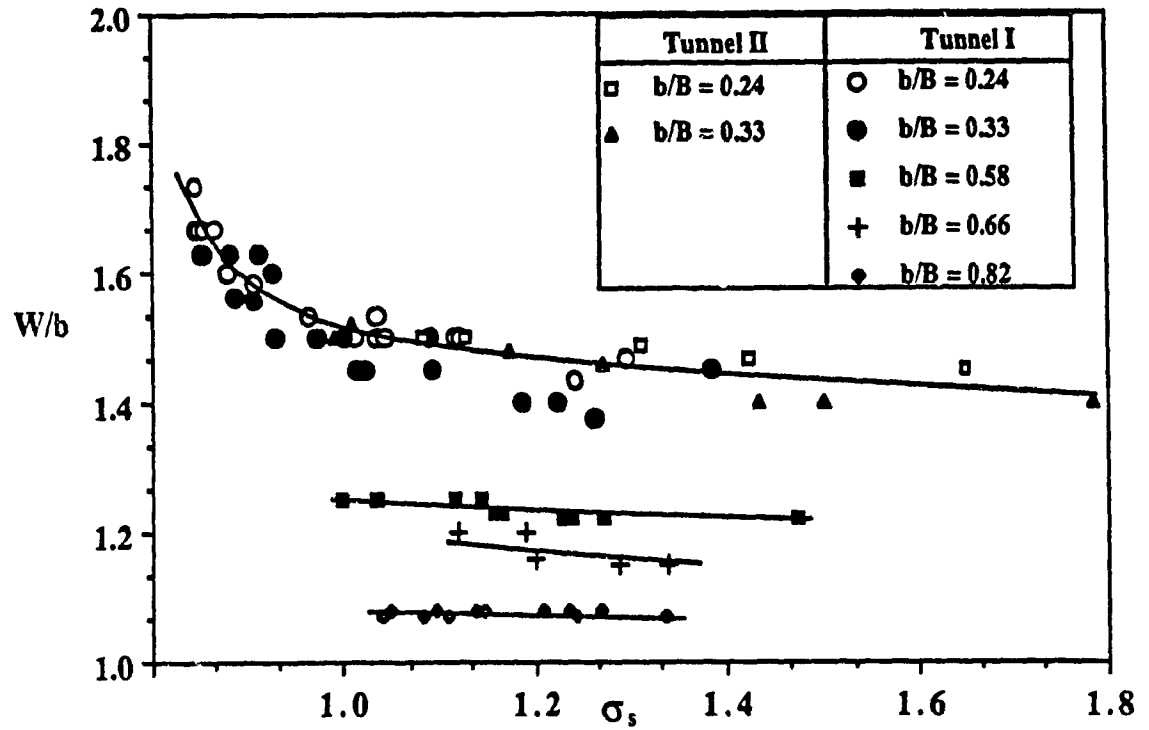


Fig.5.6: Variation of W/b with σ_s

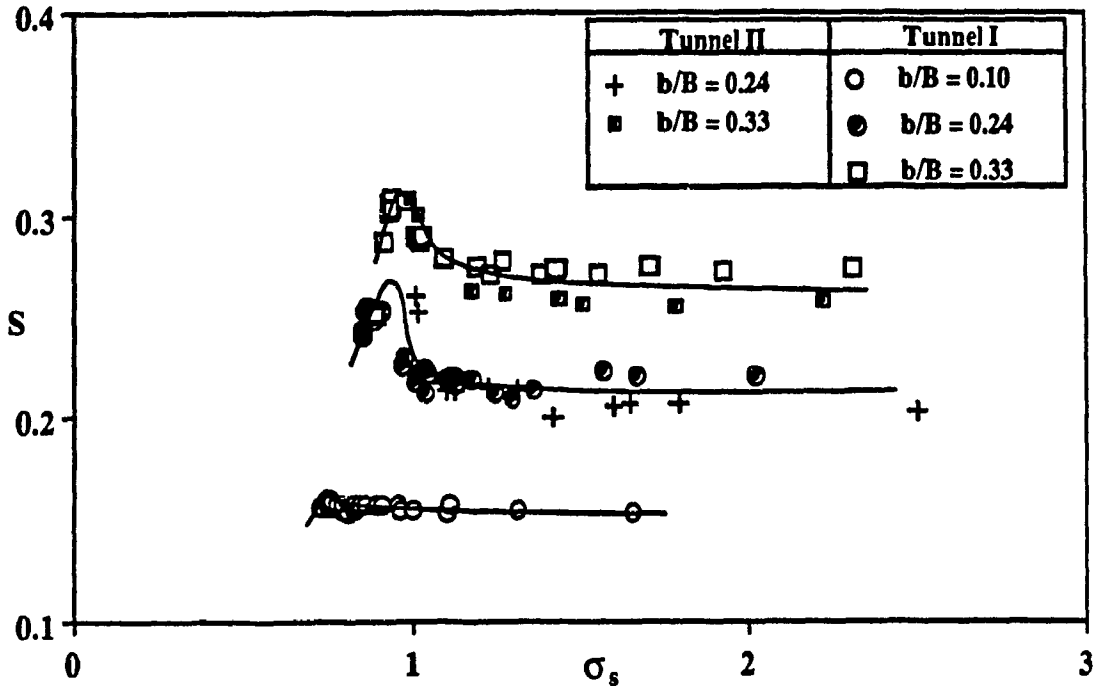


Fig.5.7: Variation of S with σ_s ($0.10 < b/B < 0.33$)

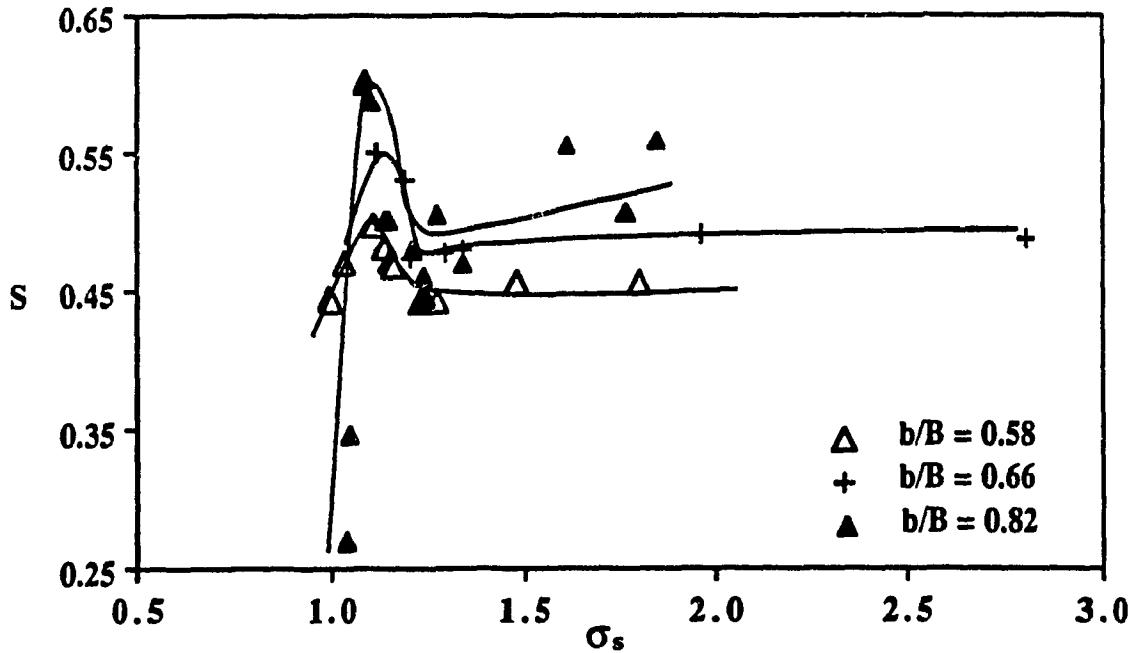


Fig.5.8: Variation of S with σ_s ($0.58 < b/B < 0.82$)

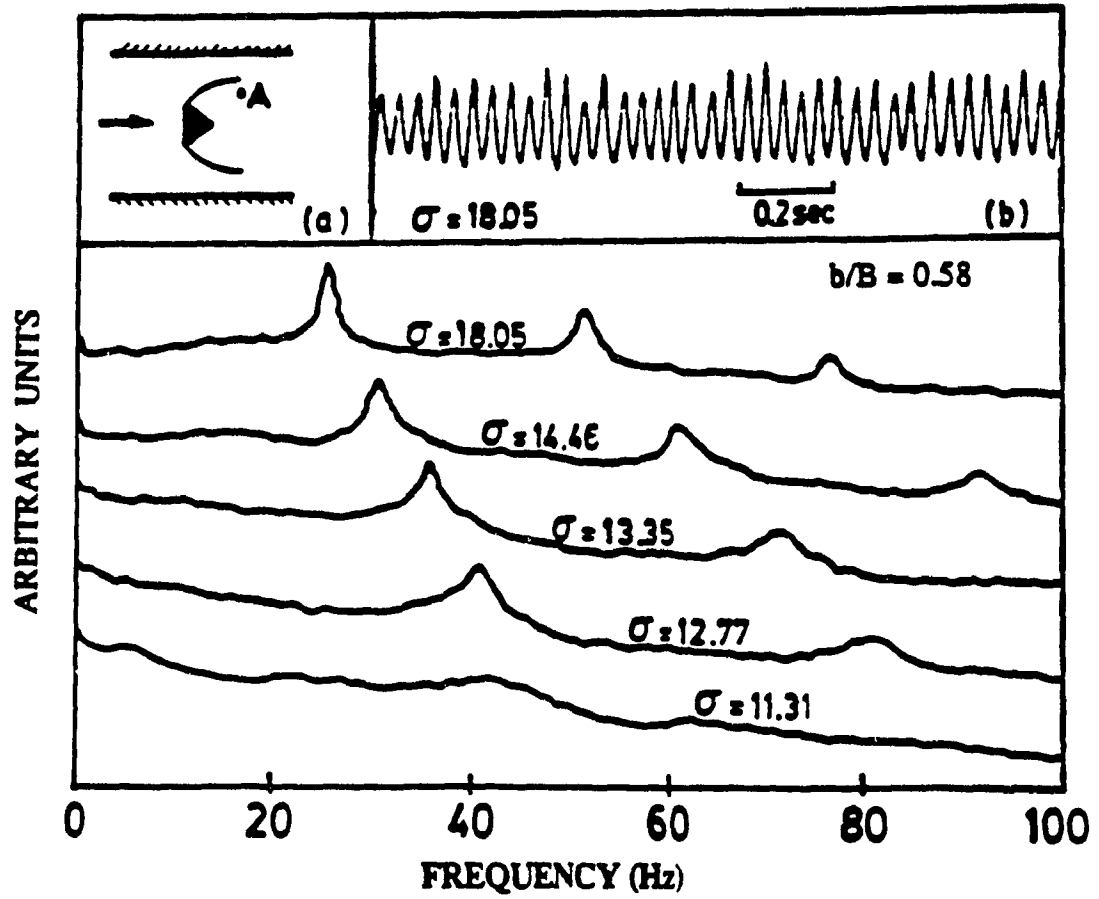


Fig.5.9: Power Spectra at various σ ($b/B = 0.58$)

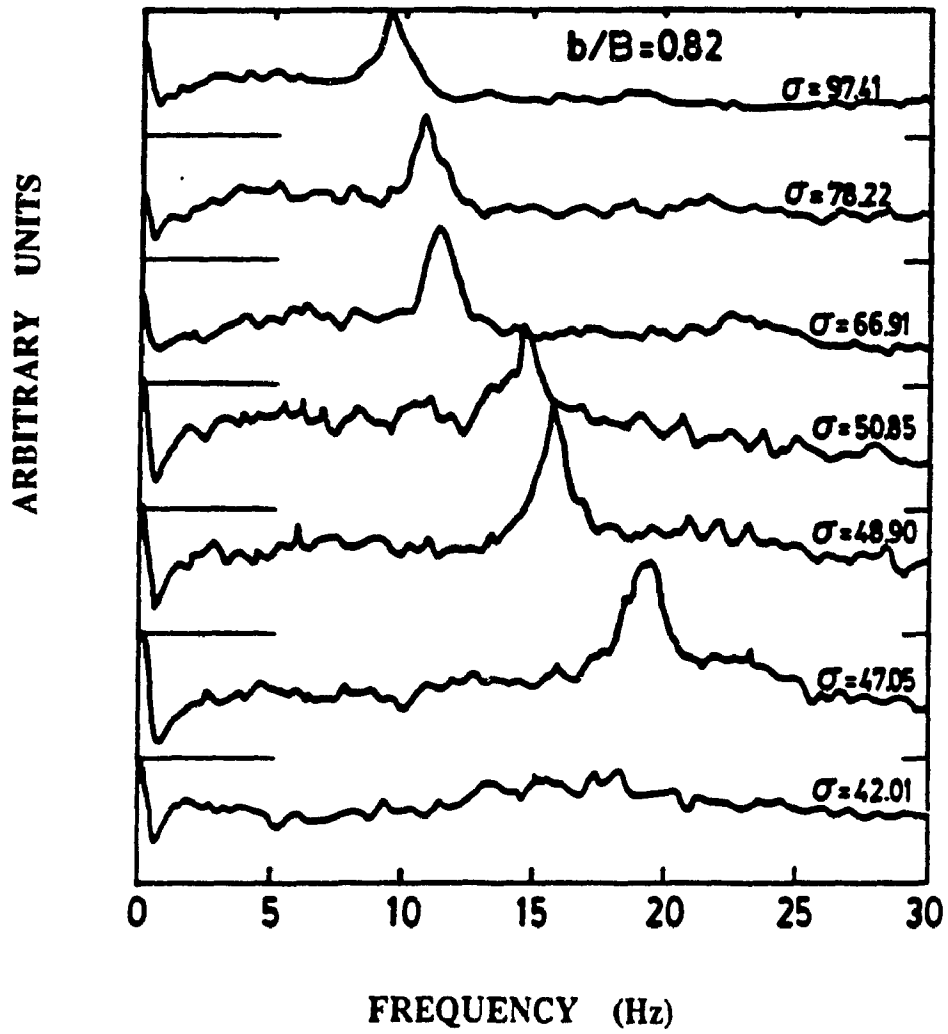


Fig.5.10: Power Spectra at various σ ($b/B = 0.82$)

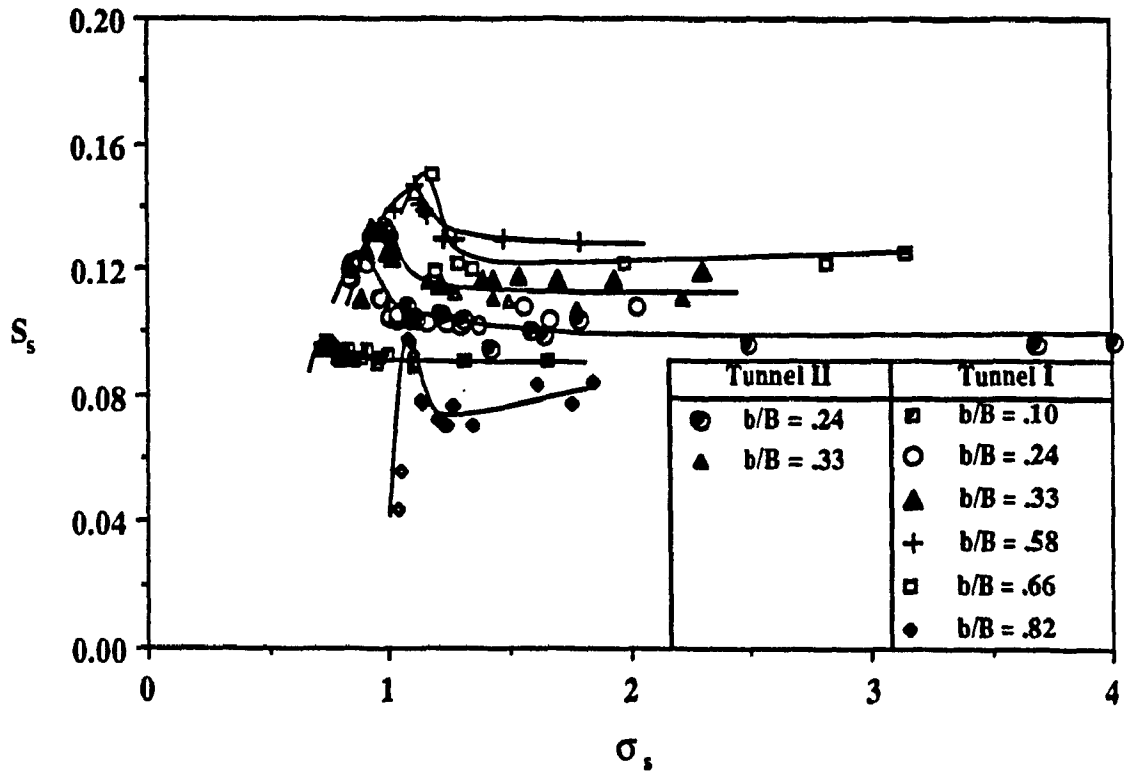


Fig.5.11: Variation of S_s with cavitation number ($0.10 < b/B < 0.82$)

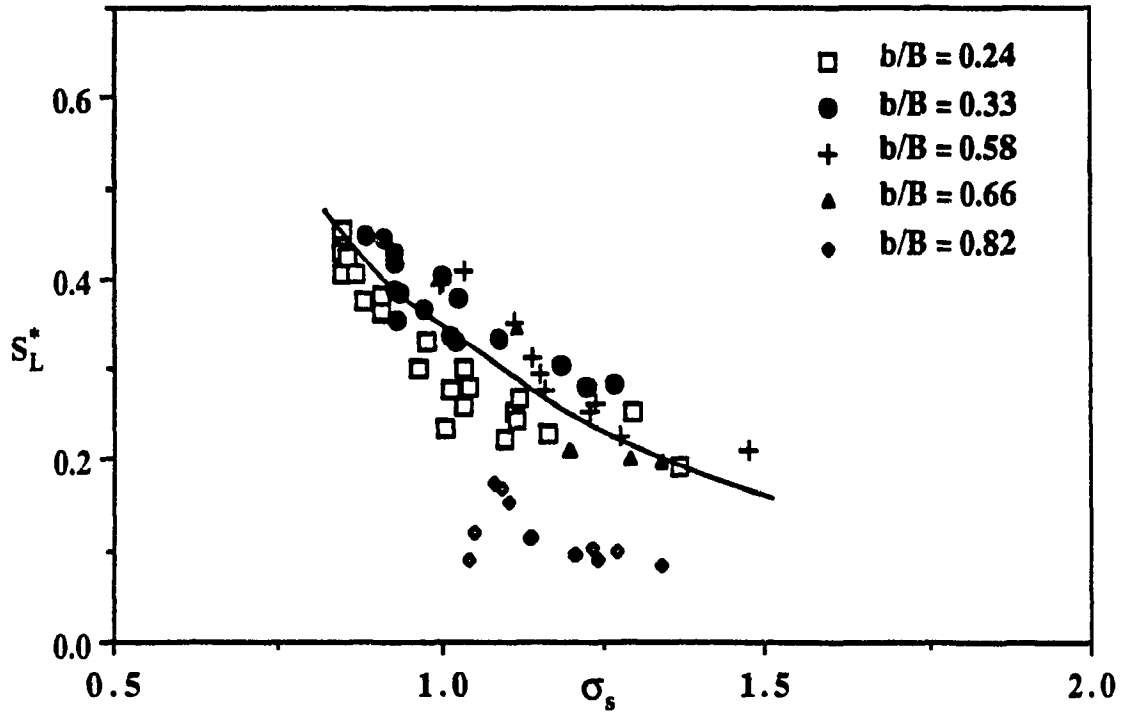


Fig.5.12: Variation of S_L^* with σ_s

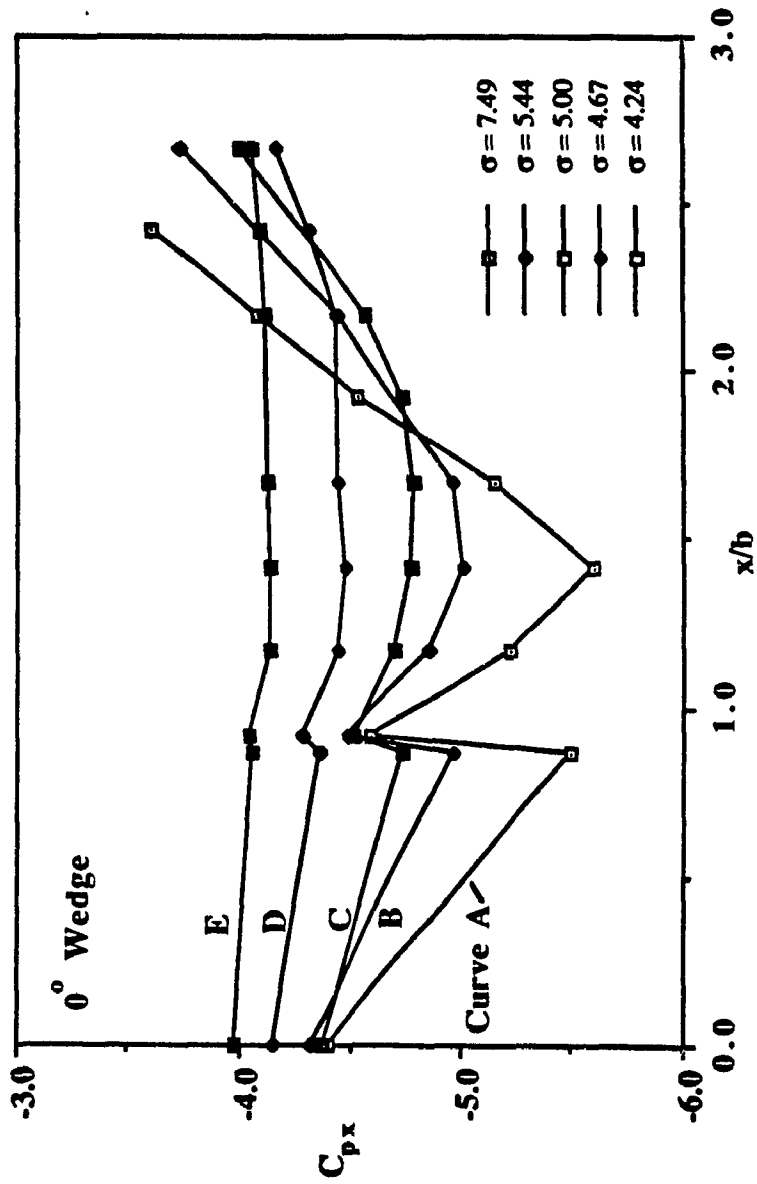


Fig.5.13a: Wake static pressure distribution for $b/B = 0.325$

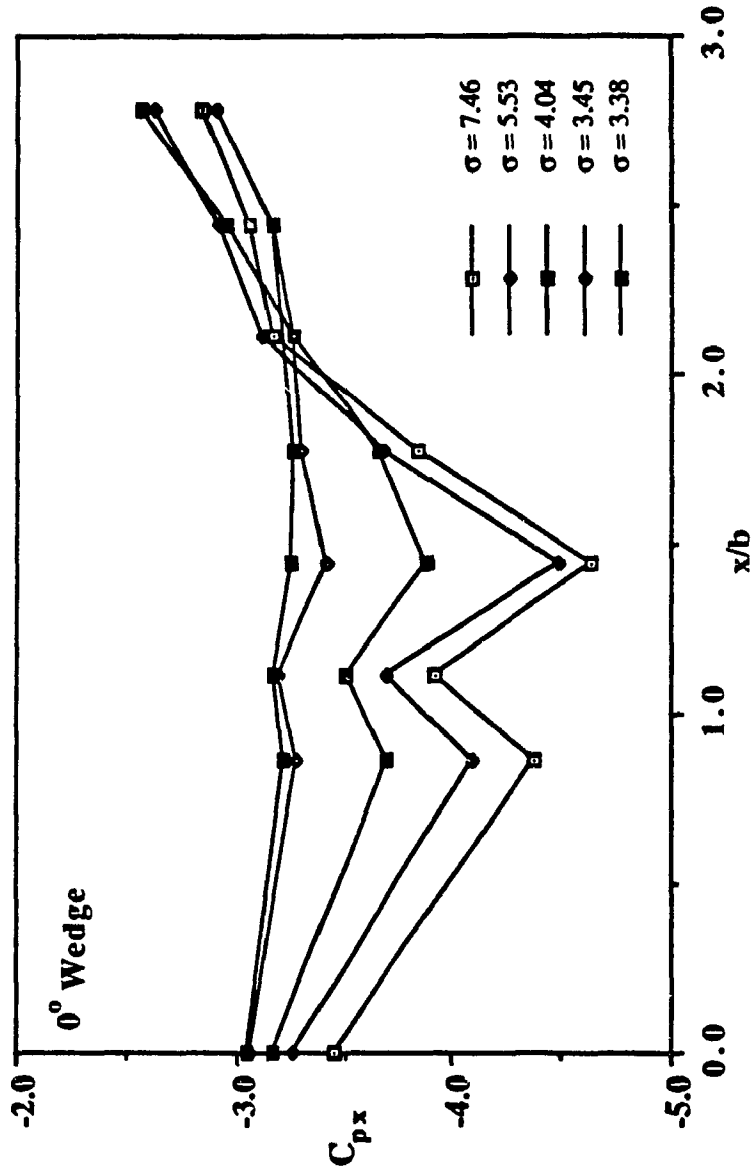


Fig. 5.13b: Wake static pressure distribution for $b/B = 0.243$

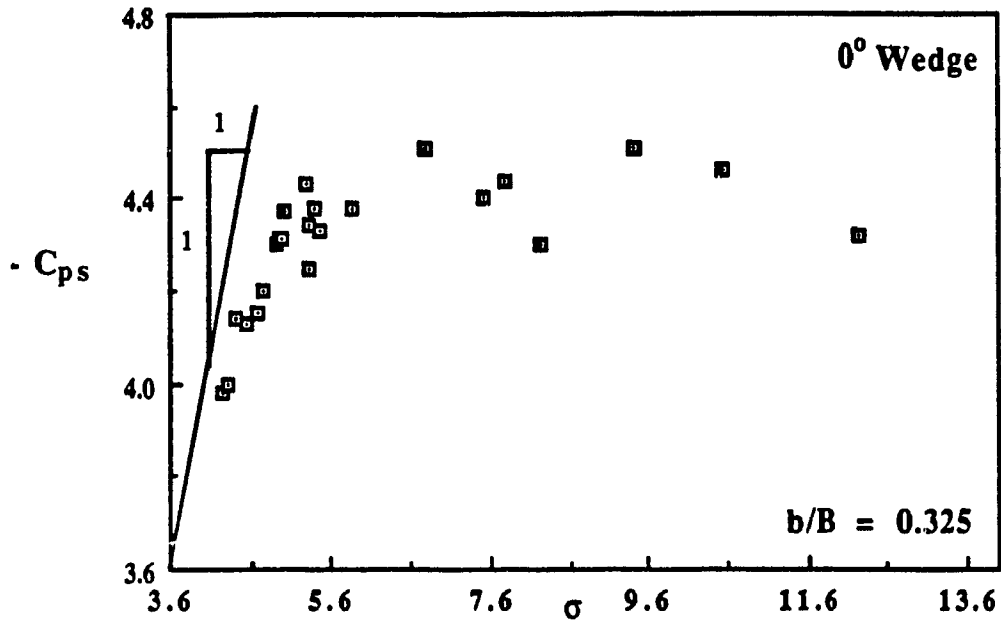
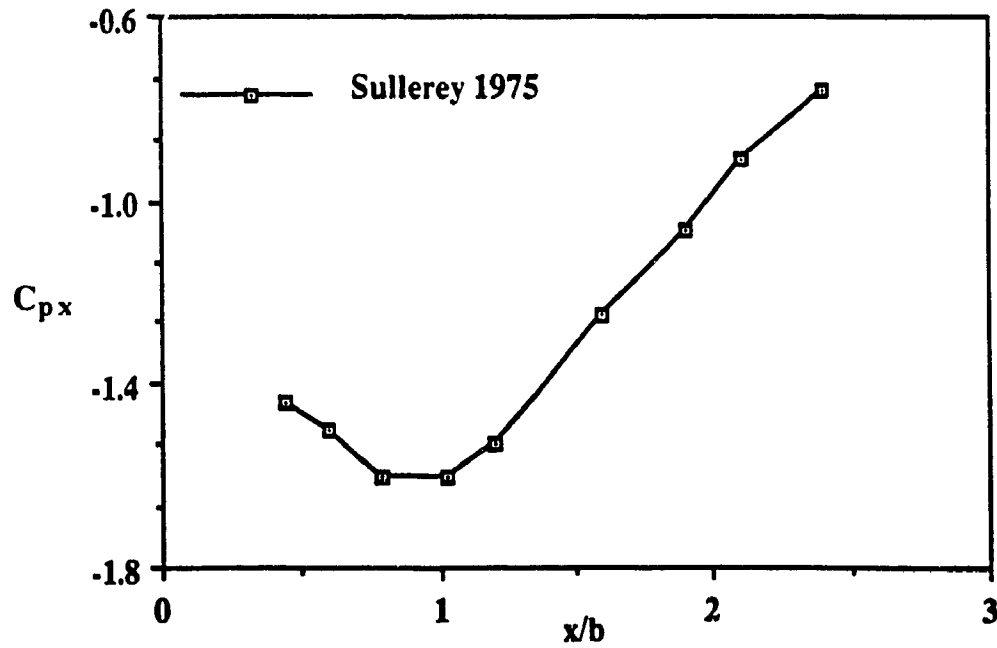
Fig.5.14a: Variation of $-C_{ps}$ with σ 

Fig.5.14b: Wake pressure distribution for no-cavitating normal plates (Sullerey 1975)

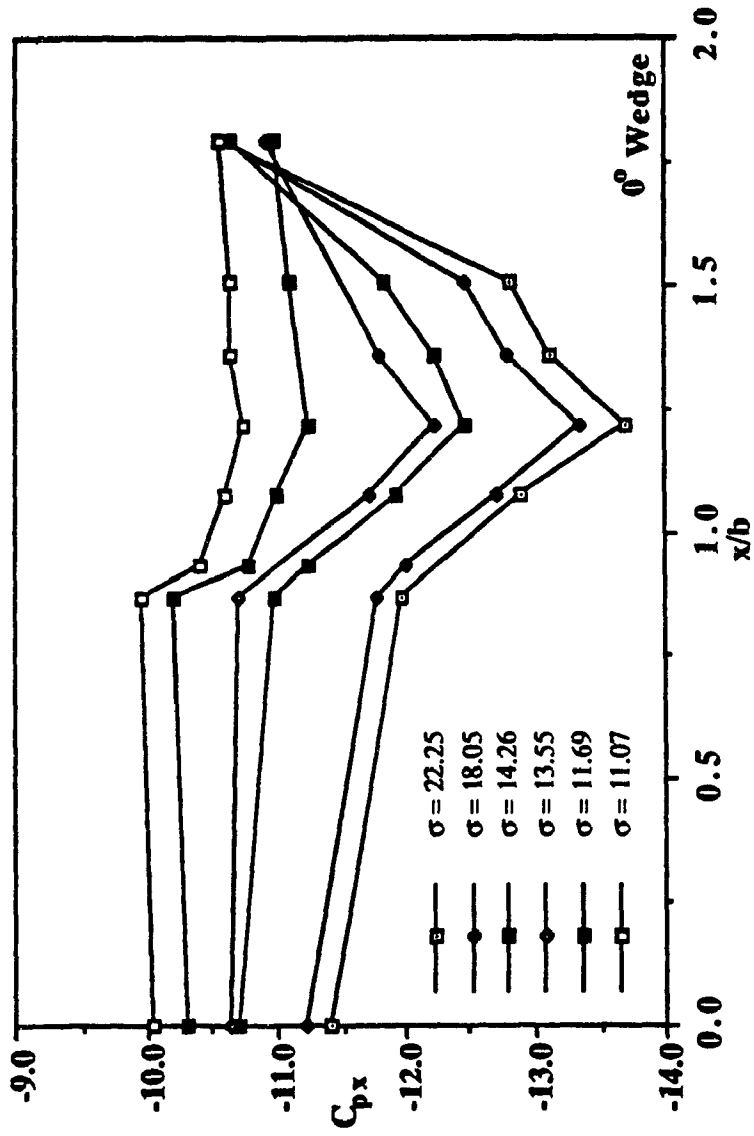


Fig.5.15a: Wake static pressure distribution ($b/B = 0.58$)

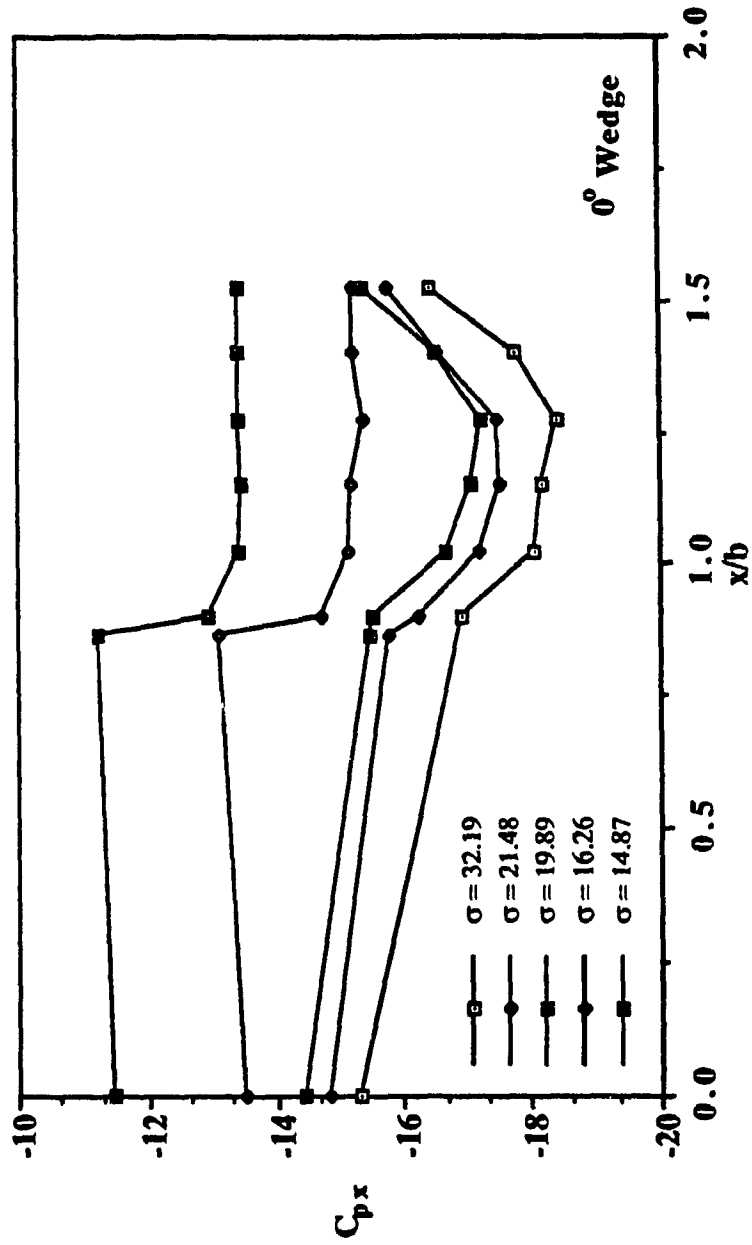


Fig.5.15b: Wake static pressure distribution ($b/B = 0.66$)

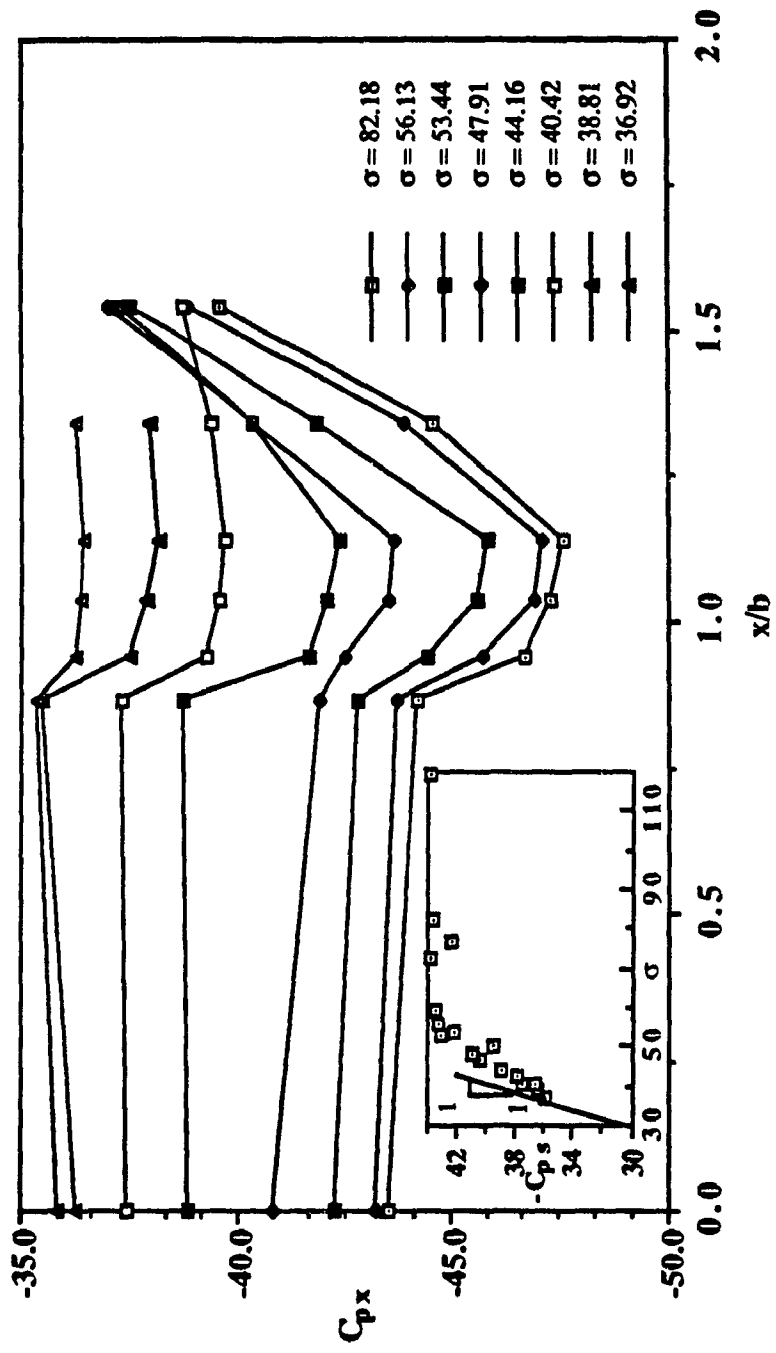


Fig.5.15c: Wake static pressure distribution ($b/B = 0.82$)

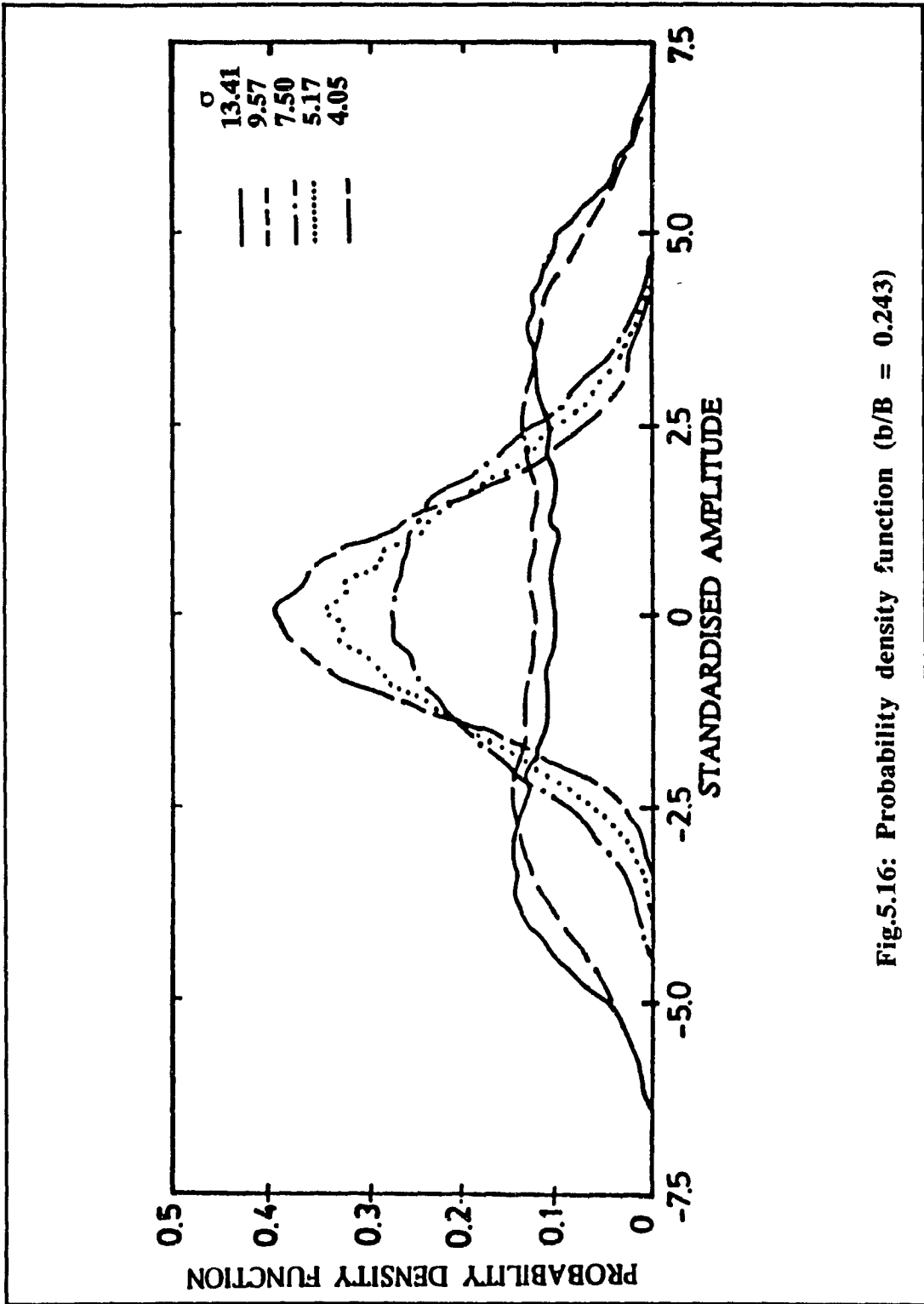


Fig.5.16: Probability density function ($b/B = 0.243$)

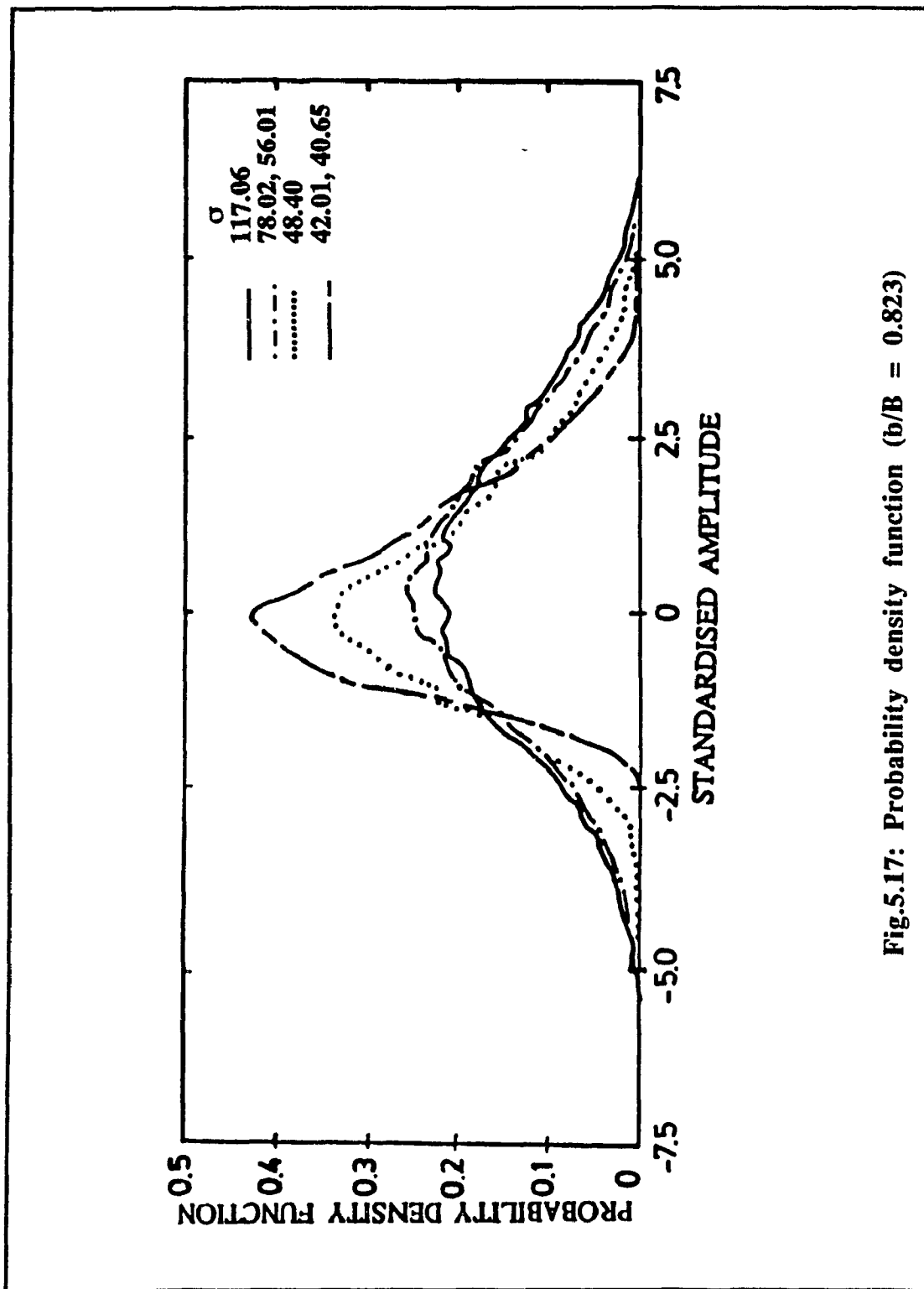


Fig.5.17: Probability density function ($b/B = 0.823$)

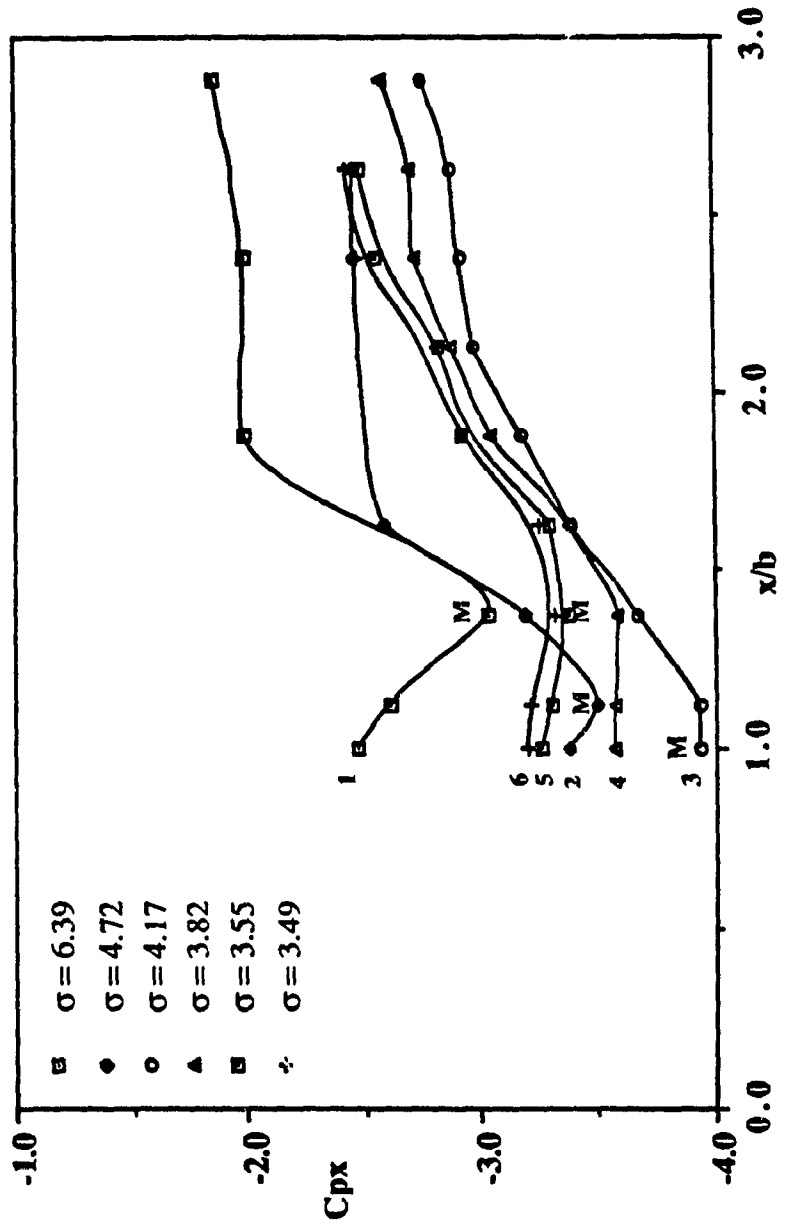


Fig.5.18: Wake static pressure distribution for circular cylinder ($b/B = 0.33$)

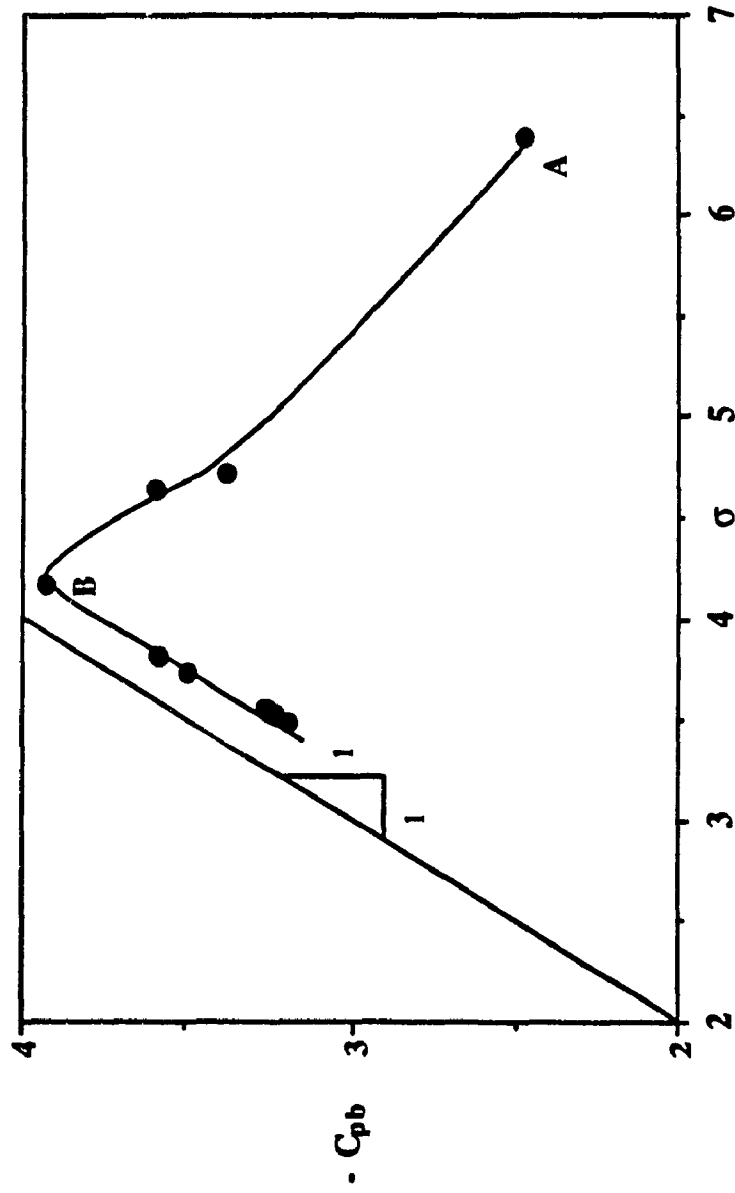


Fig.5.19: Variation of $-C_{pb}$ with σ for circular cylinder ($b/B = 0.33$)

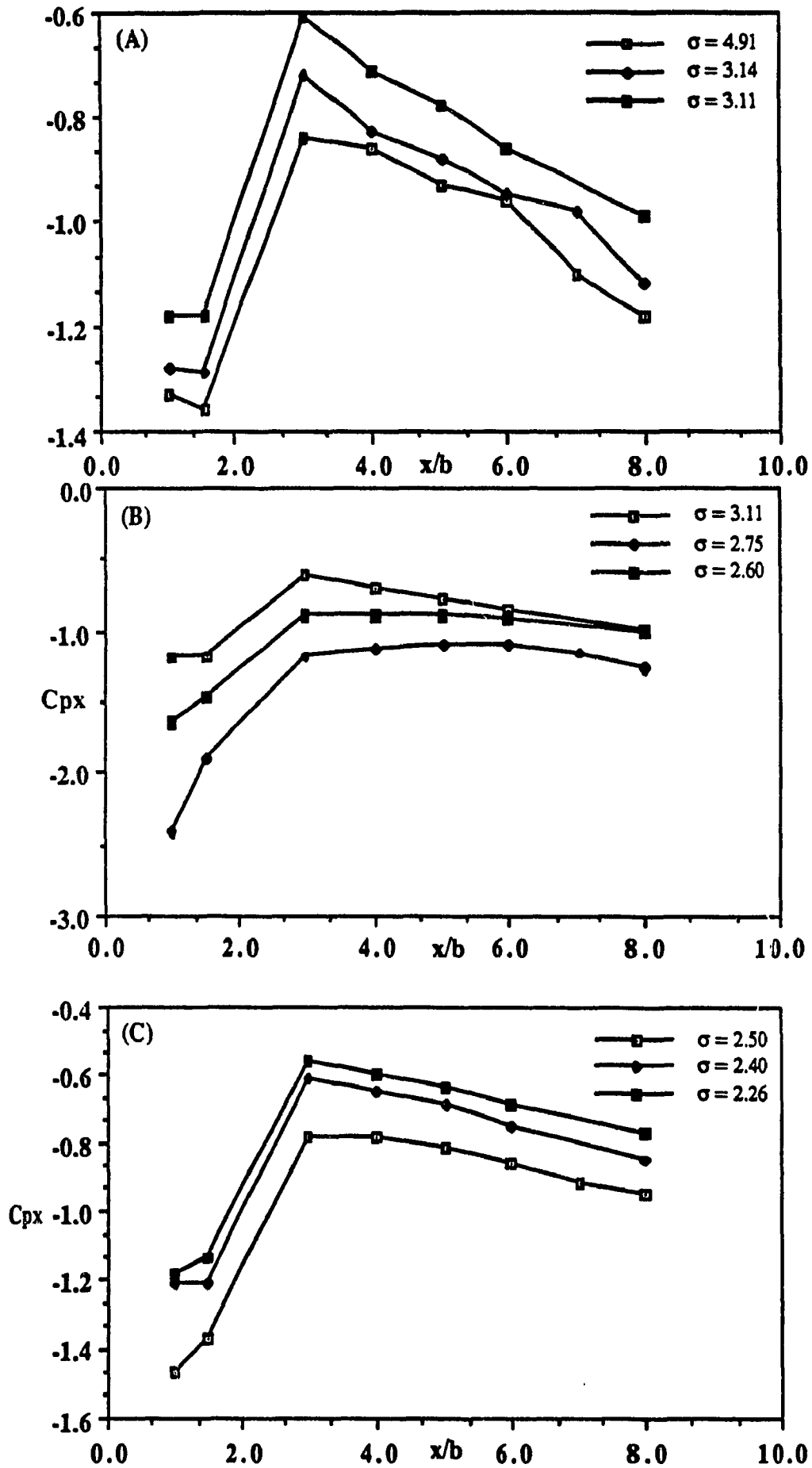


Fig.5.20: Wake static pressure distribution for circular cylinder ($b/B = 0.08$)

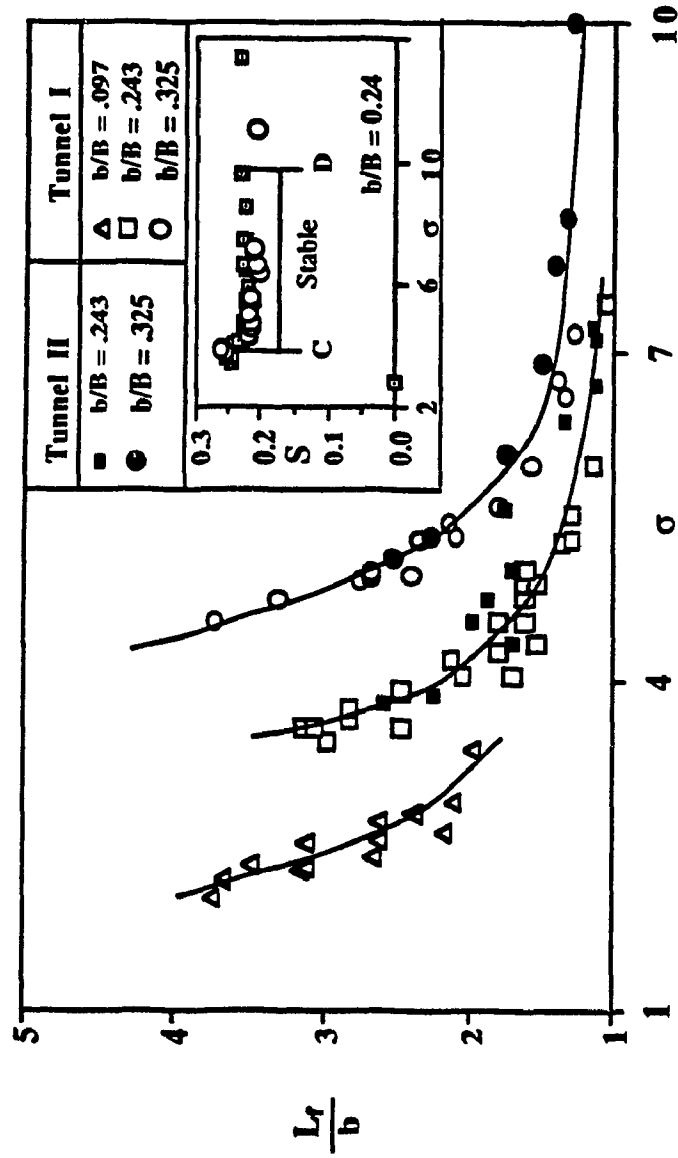


Fig. 5.21: Variation of L_r/b with σ

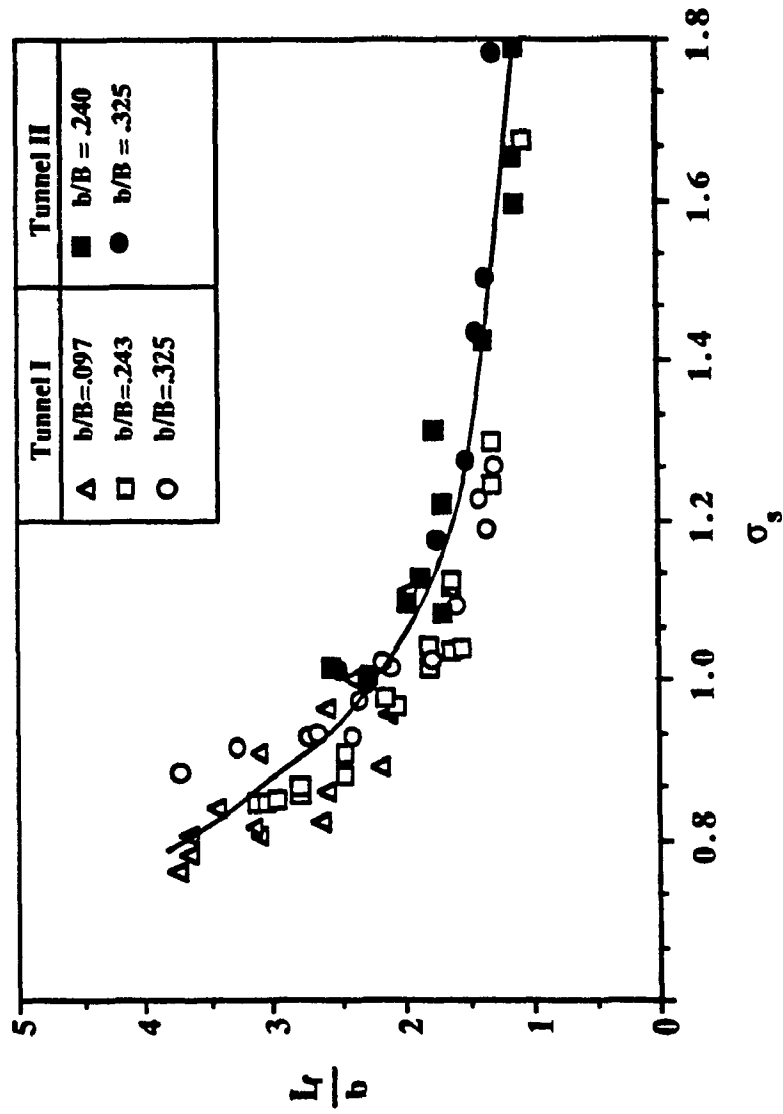
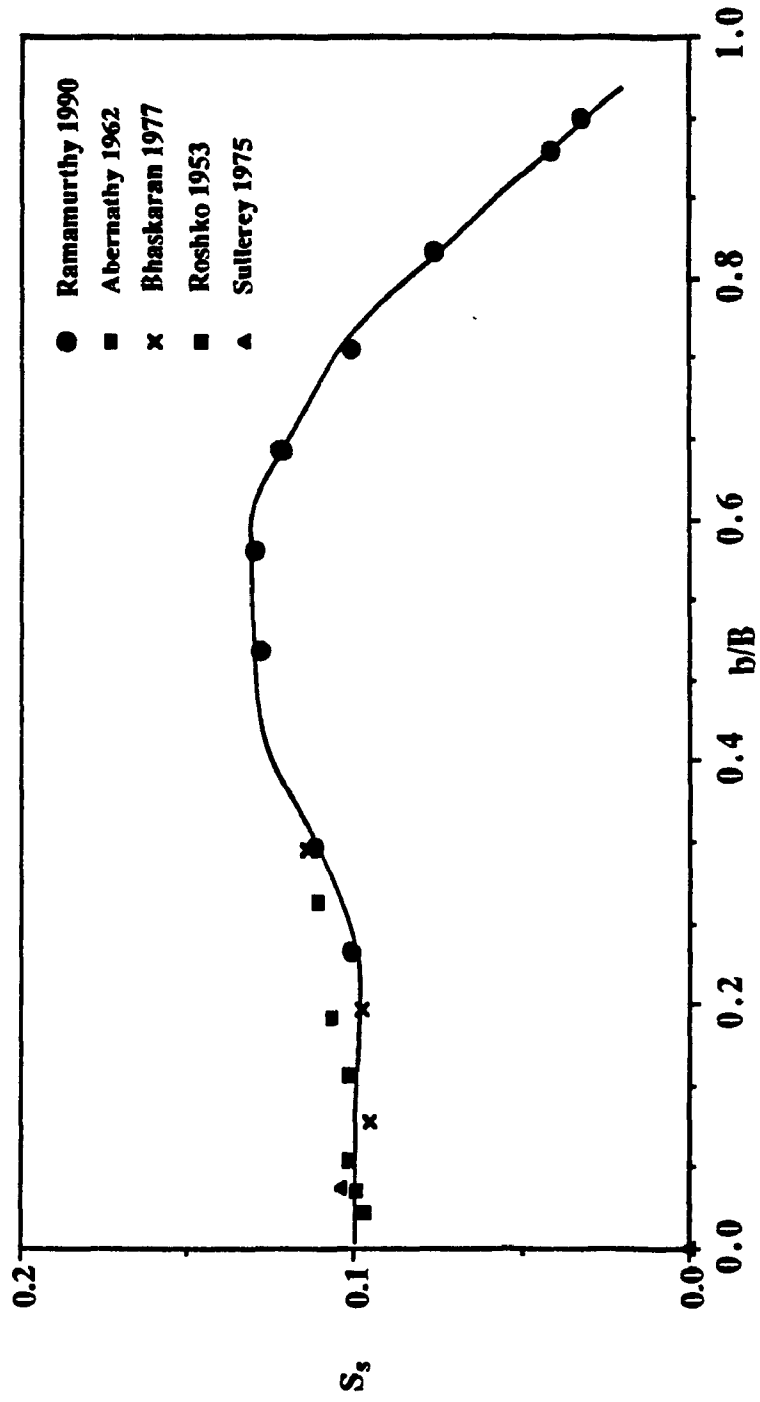


Fig. 5.22: Variation of L_r/b with σ_s

Fig.5.23: Variation of S_s with b/B

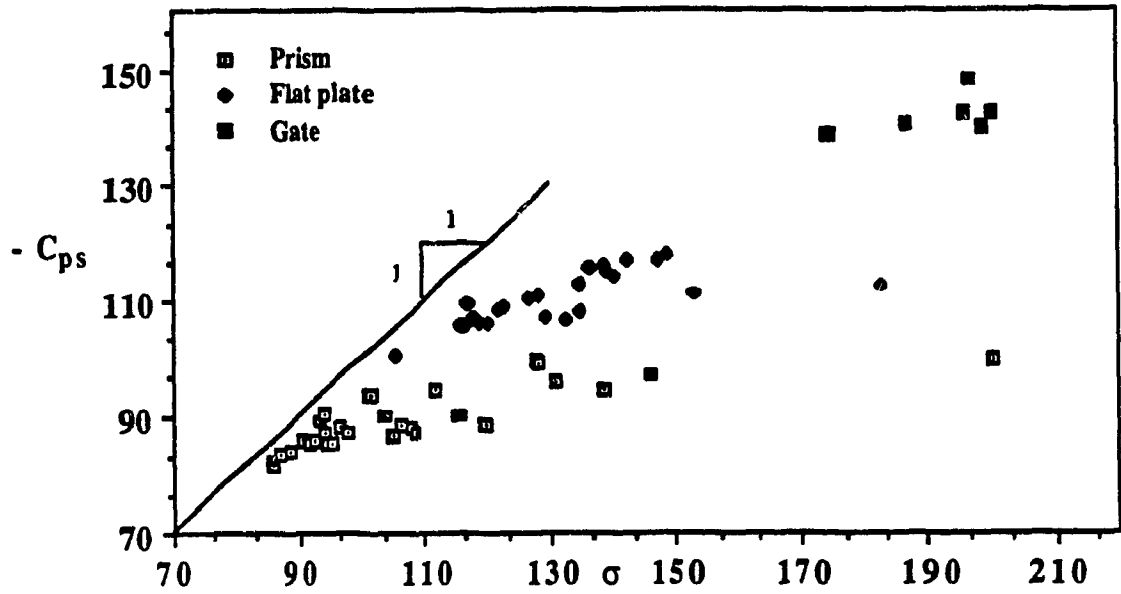


Fig.5.24: Variation of $-C_{ps}$ with σ ($b/B = 0.932$)

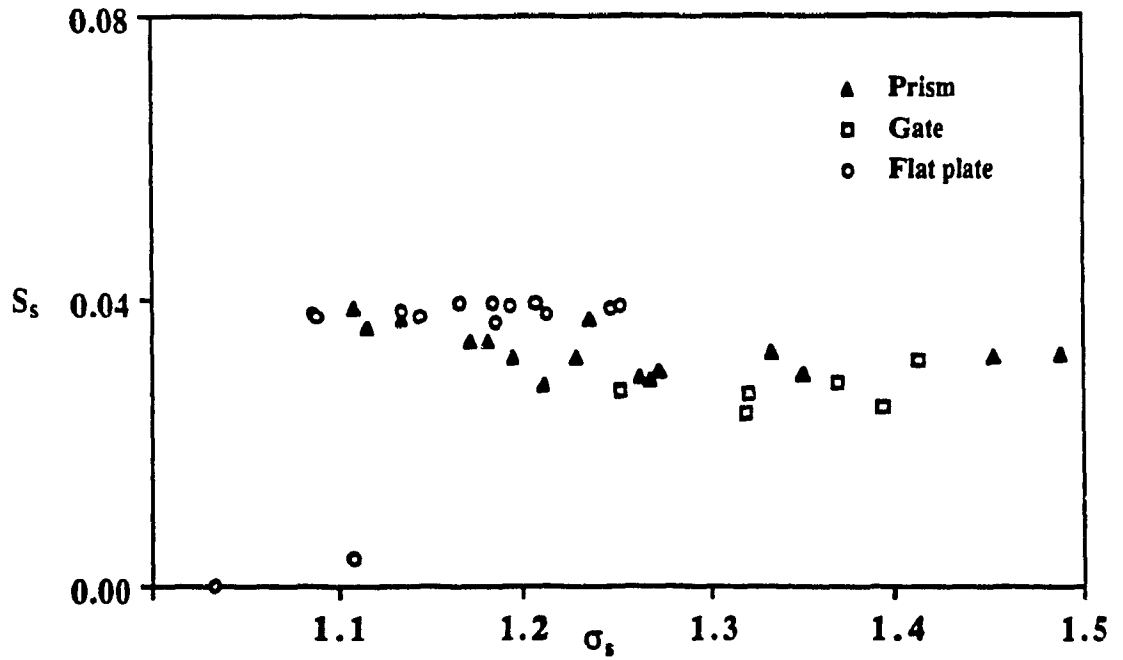
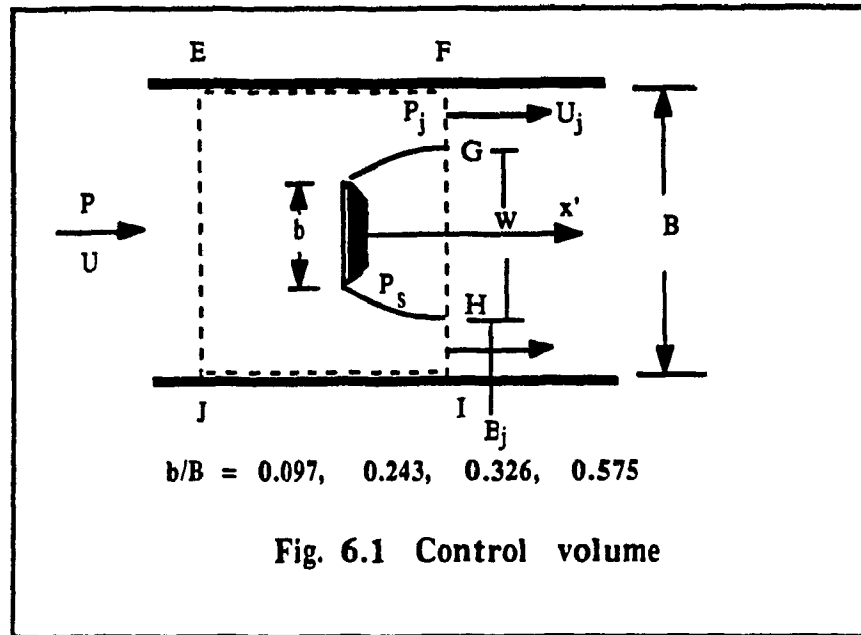


Fig.5.25: Variation of S_s with σ_s ($b/B = 0.932$)



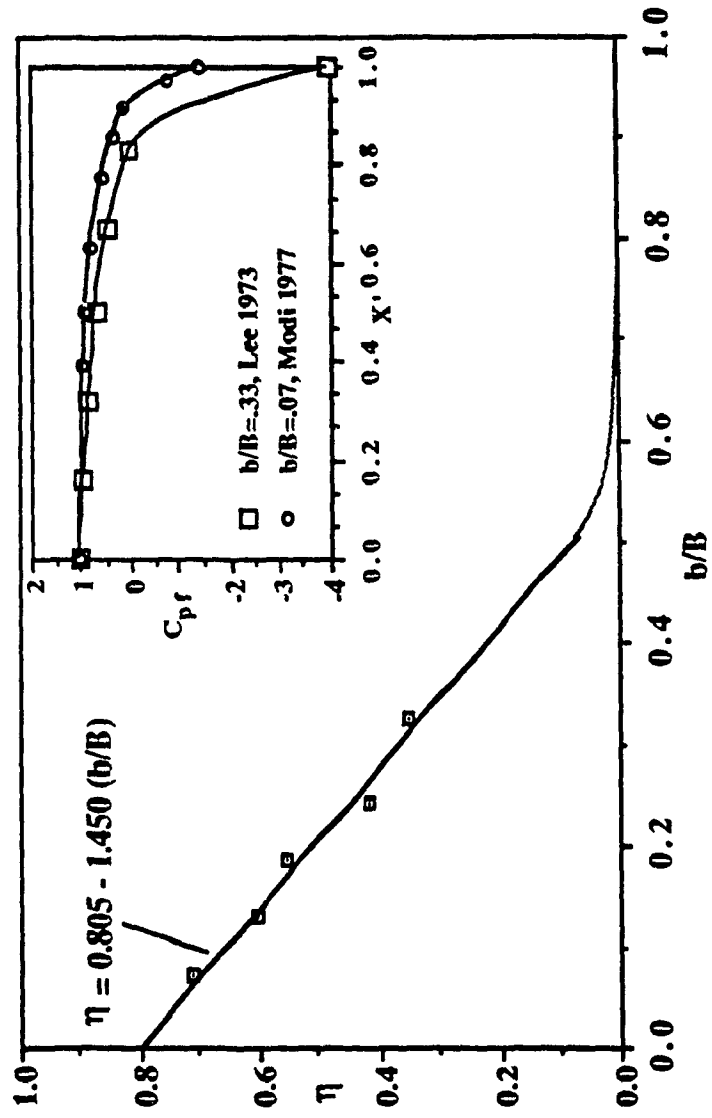


Fig. 6.2: Variation of η with b/B

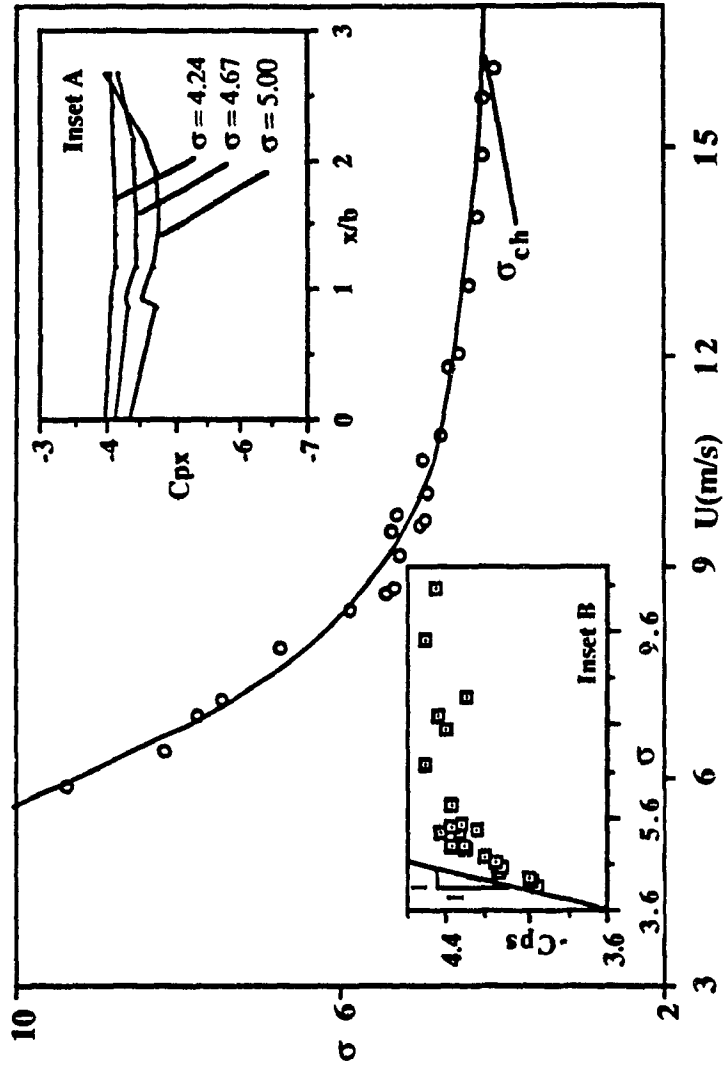


Fig. 6.3: Variation of σ with velocity

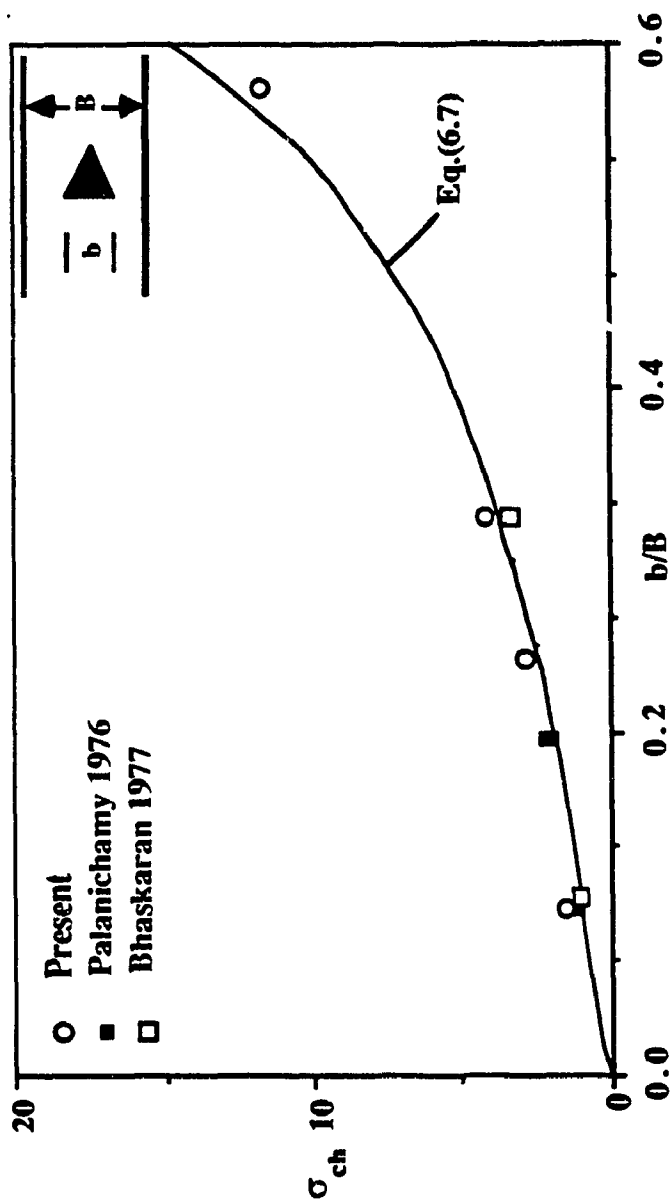


Fig.6.4: Variation of σ_{ch} with b/B

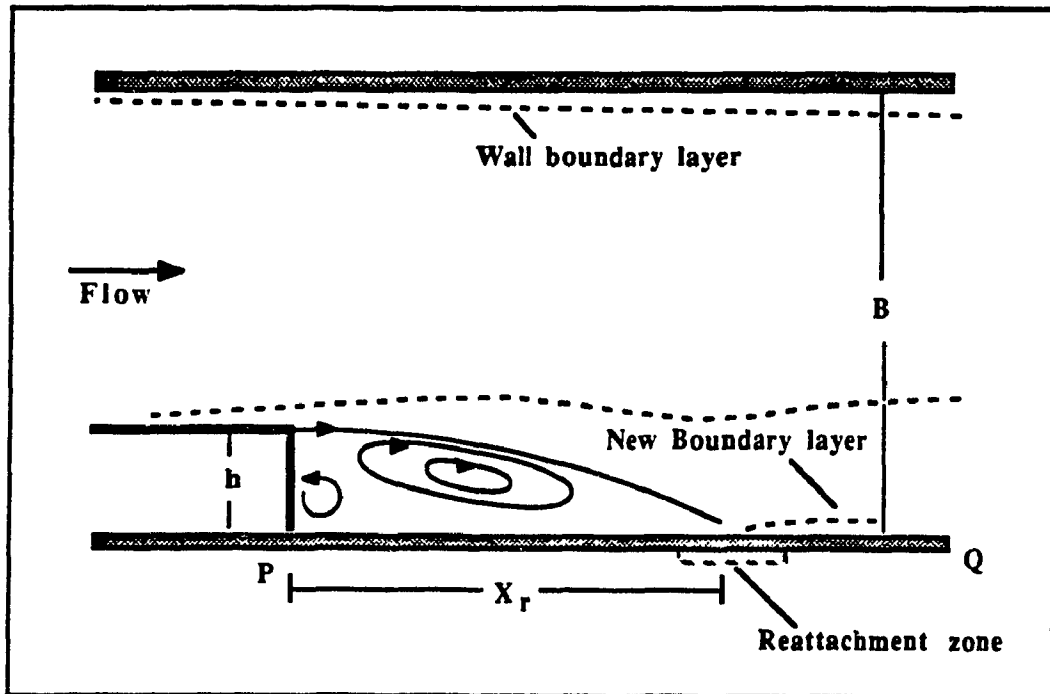


Fig.7.1: Flow past a backward facing step

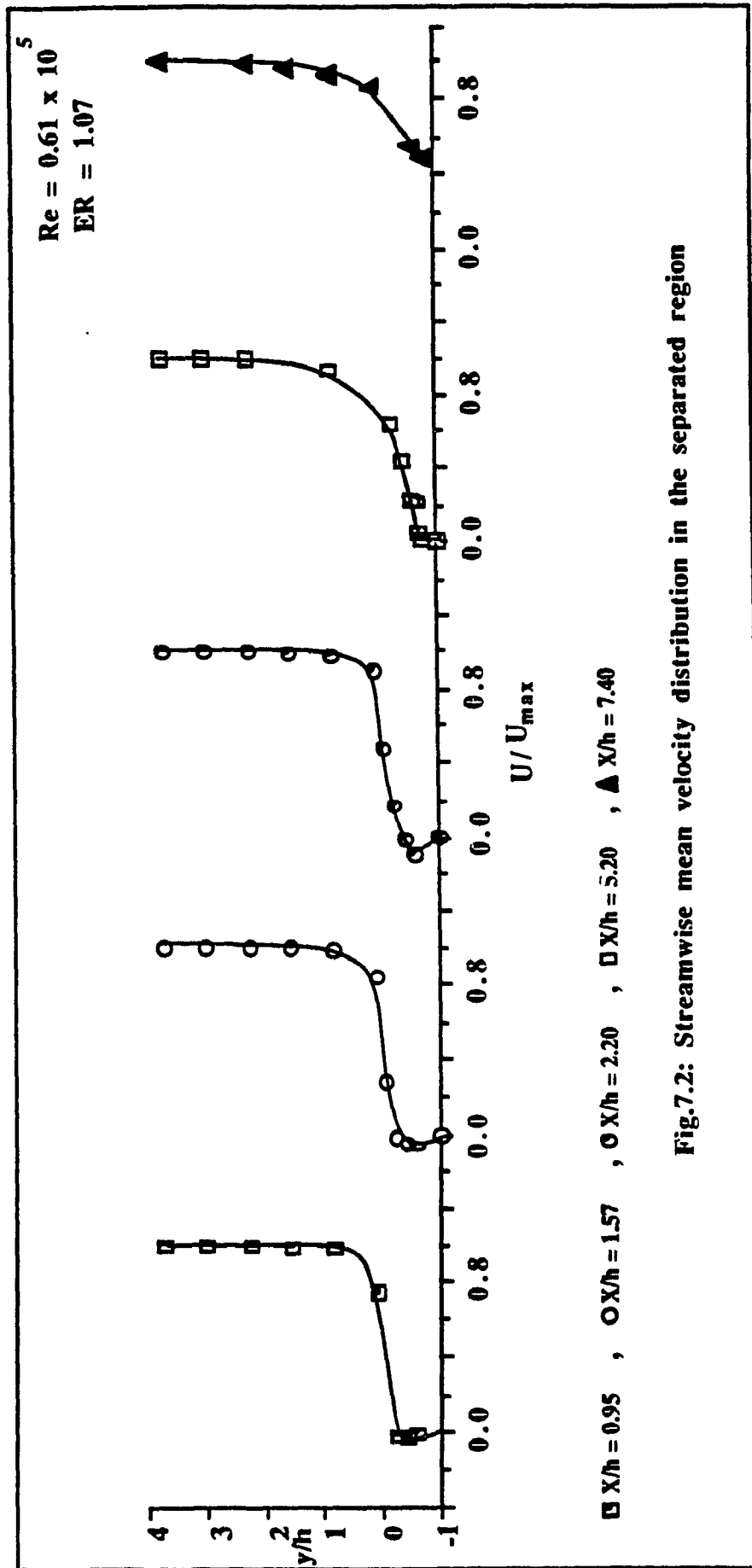


Fig.7.2: Streamwise mean velocity distribution in the separated region

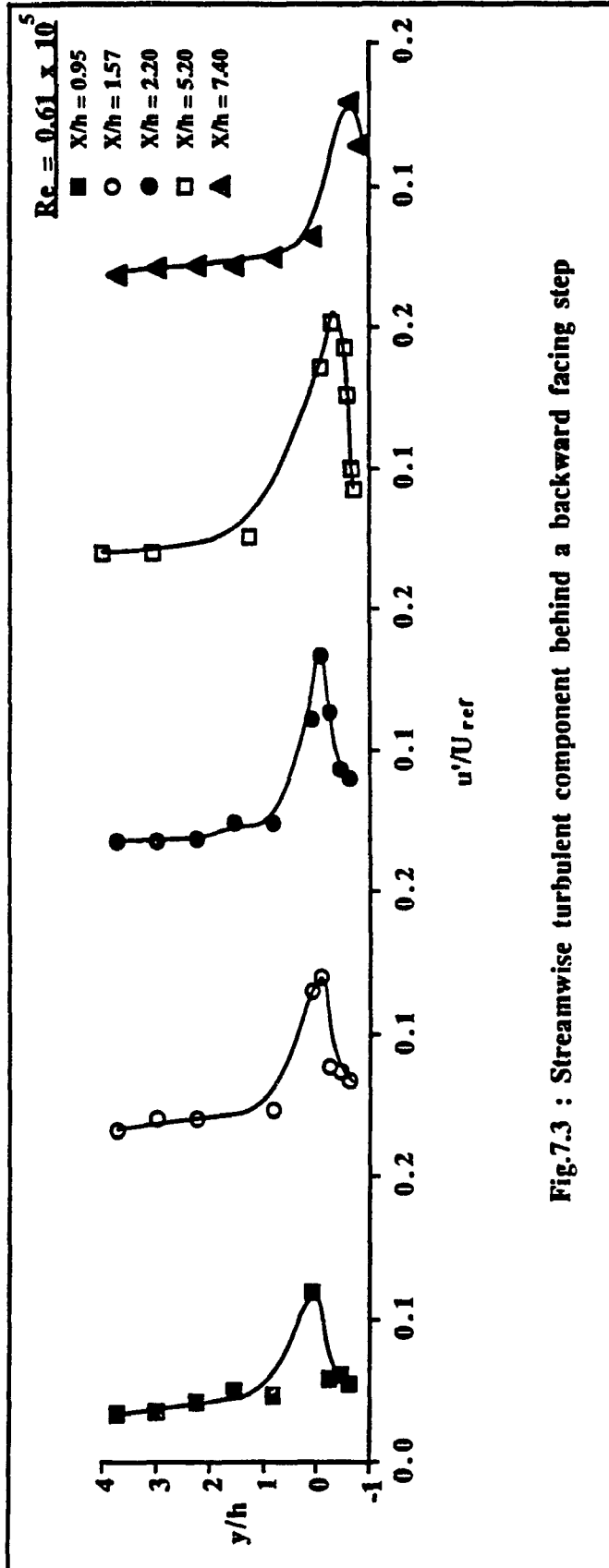
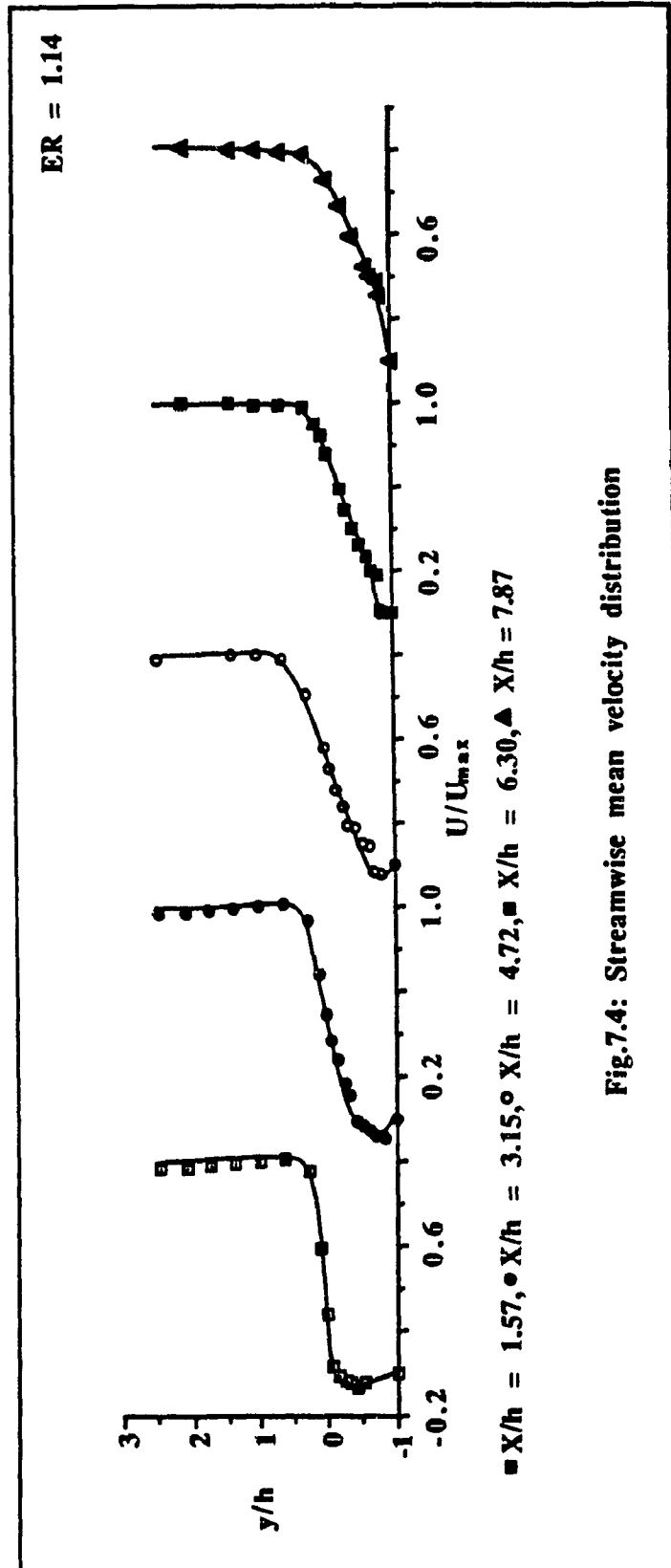
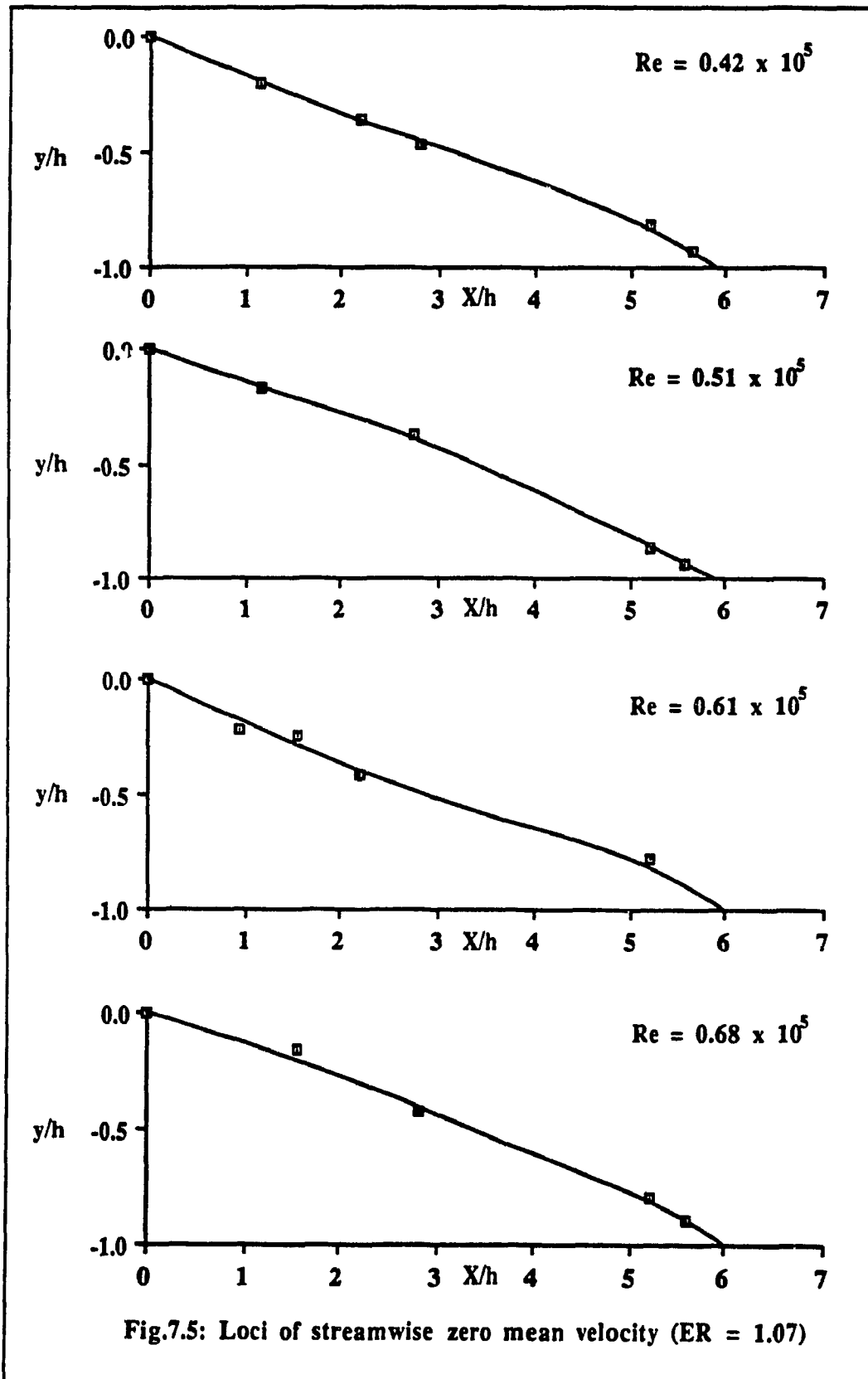
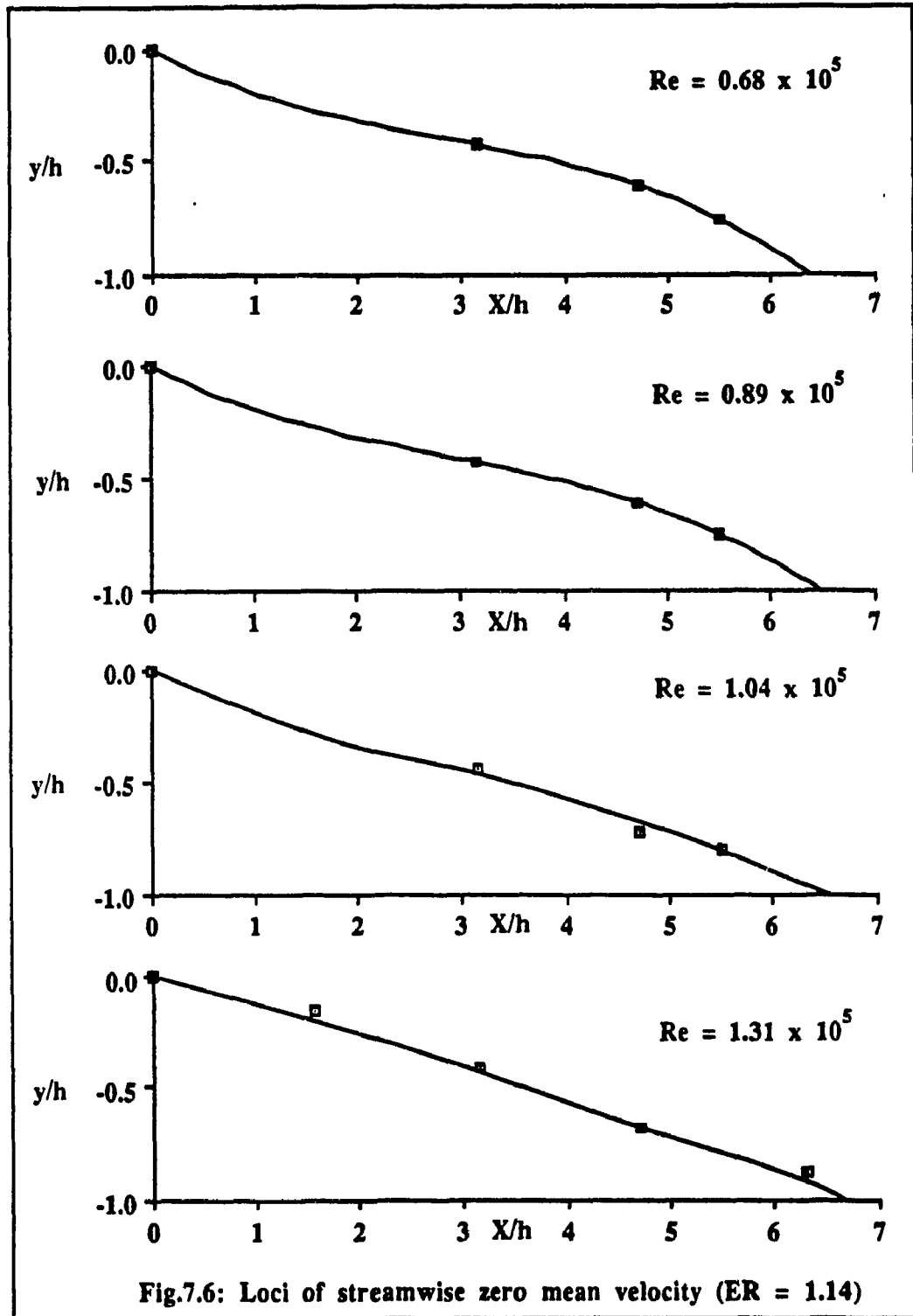


Fig.7.3 : Streamwise turbulent component behind a backward facing step







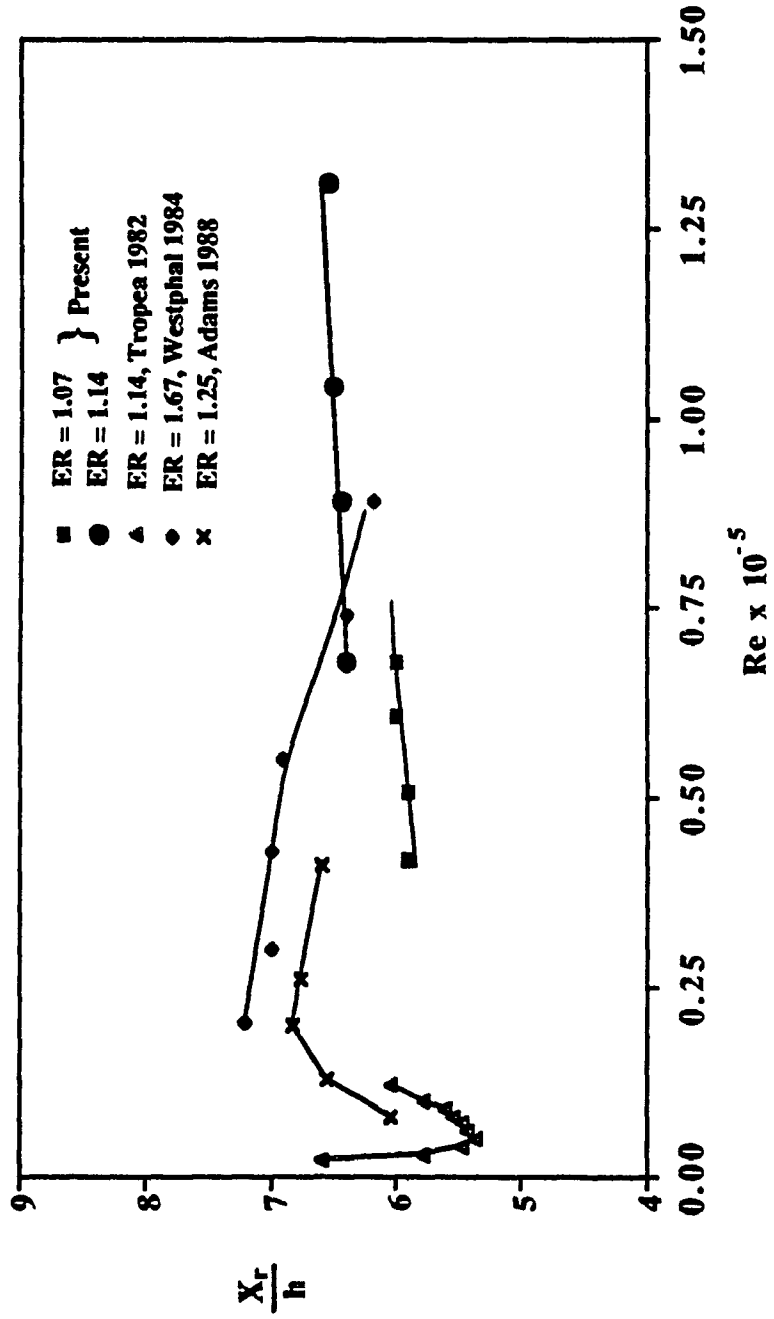


Fig.7.7: Variation of X_r/h with Reynolds number

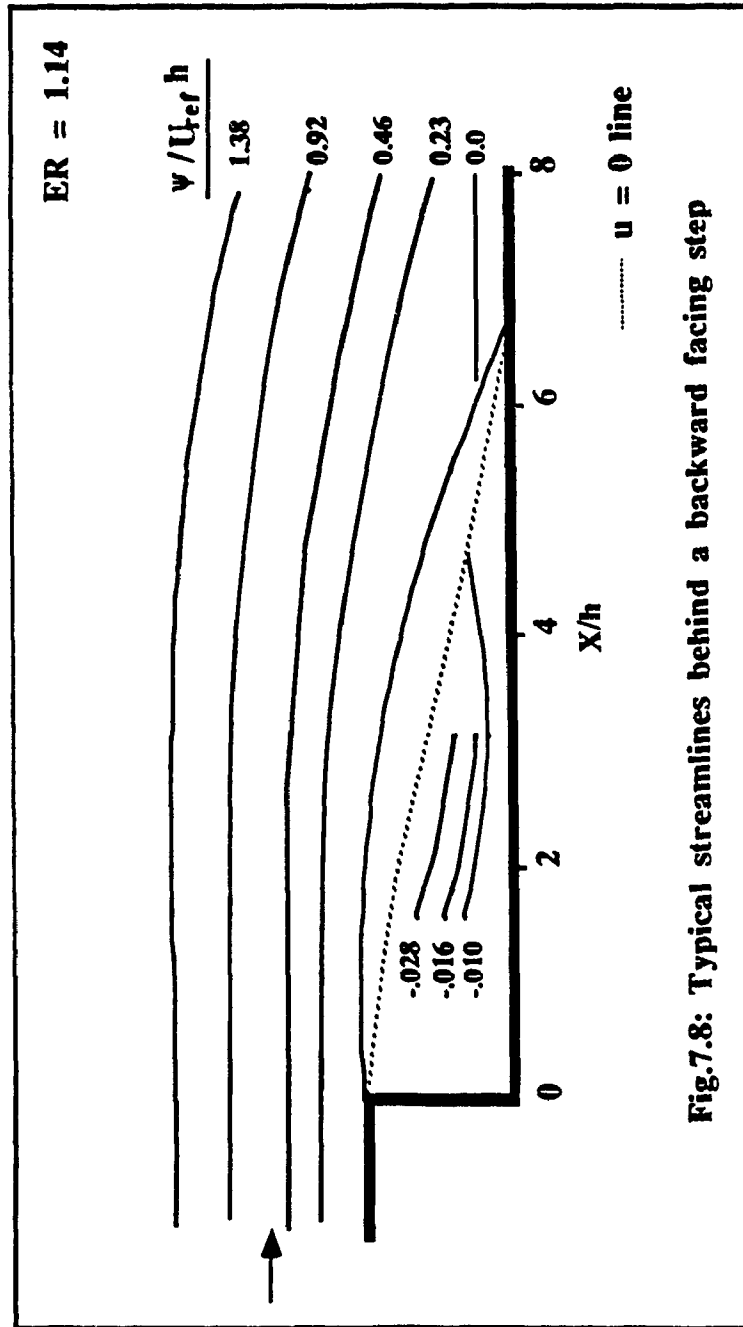


Fig.7.8: Typical streamlines behind a backward facing step

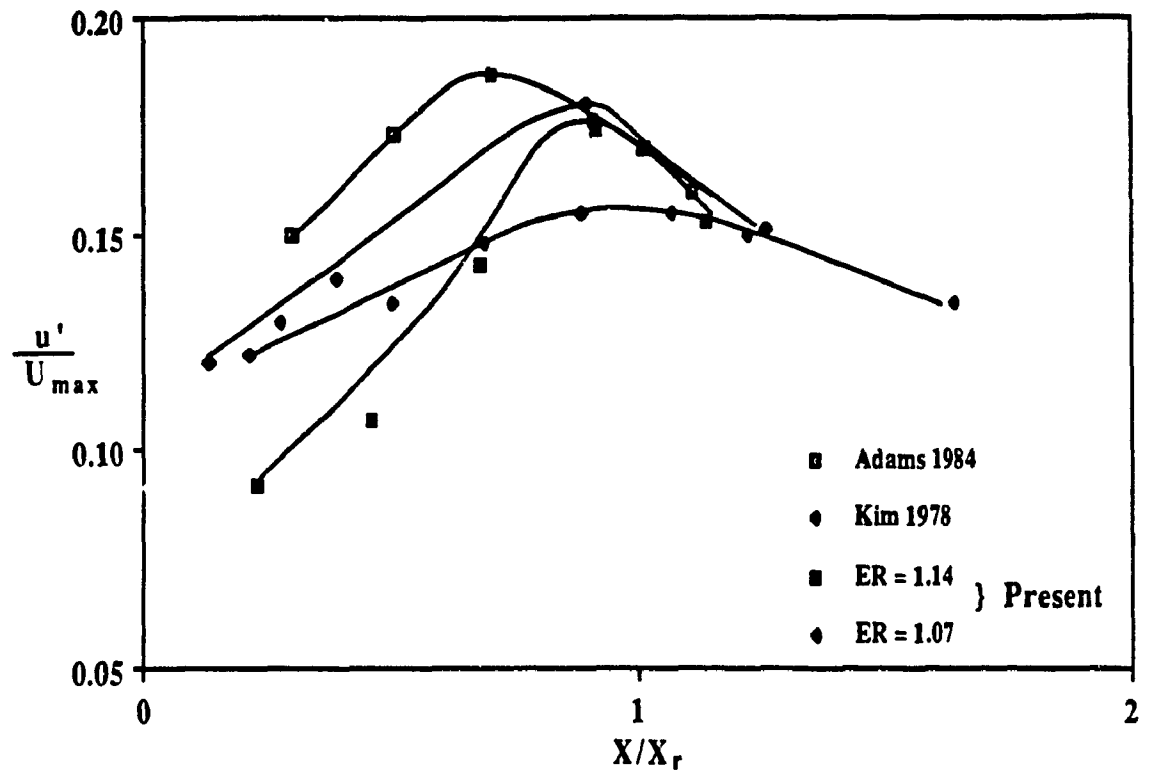


Fig.7.9a: Variation of u'/U_{max} with X/X_r

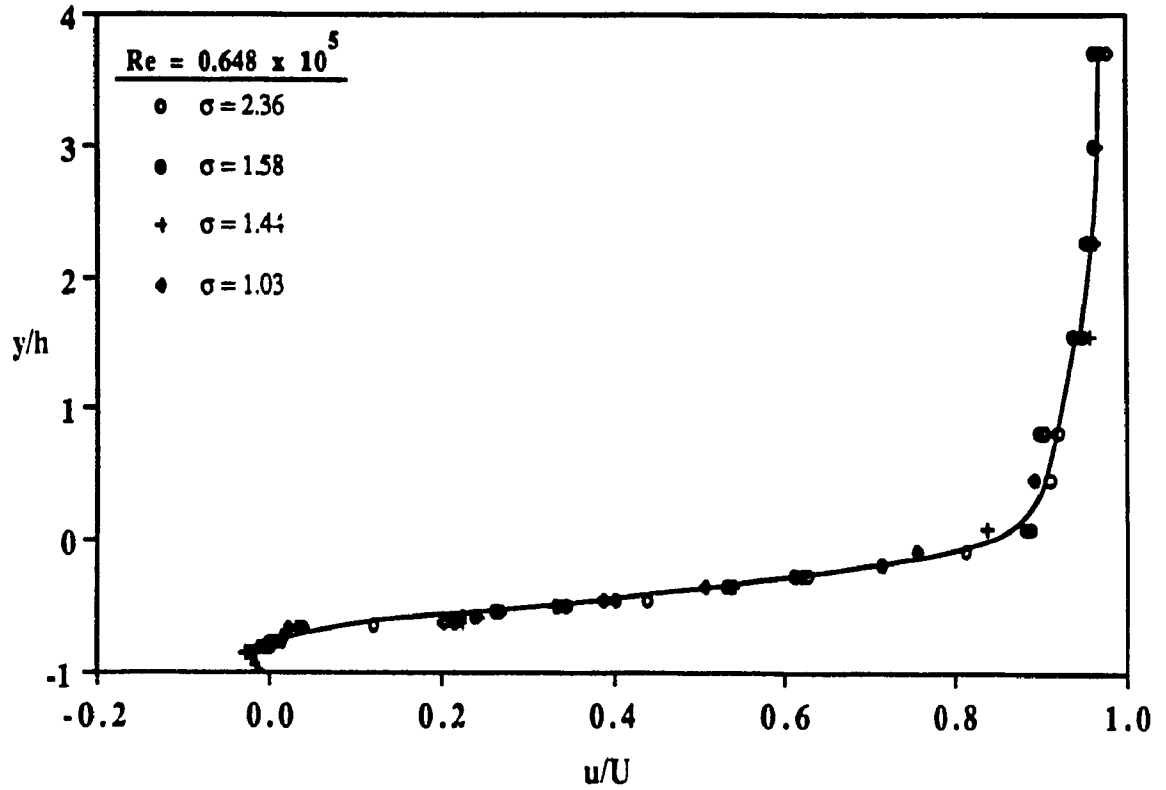


Fig.7.9b: Velocity distribution at X/h =5.2

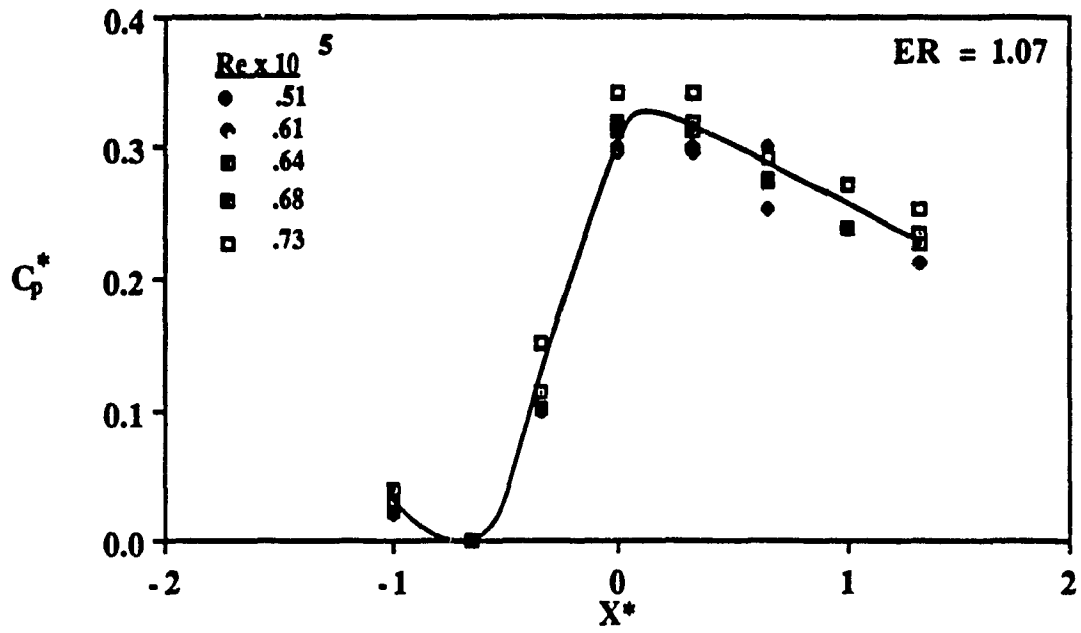


Fig.7.10 : Variation of C_p^* with X^*

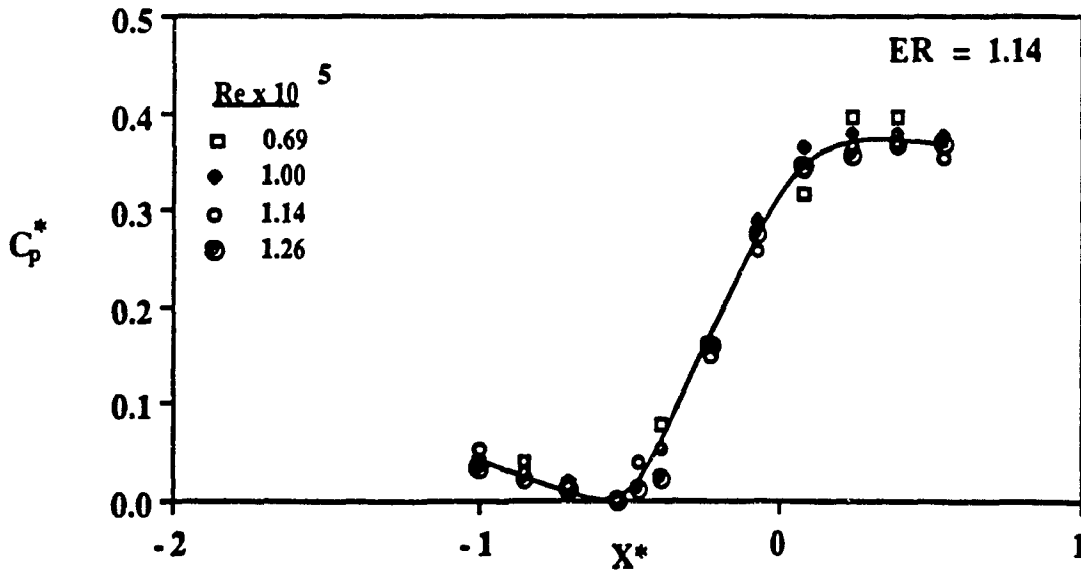
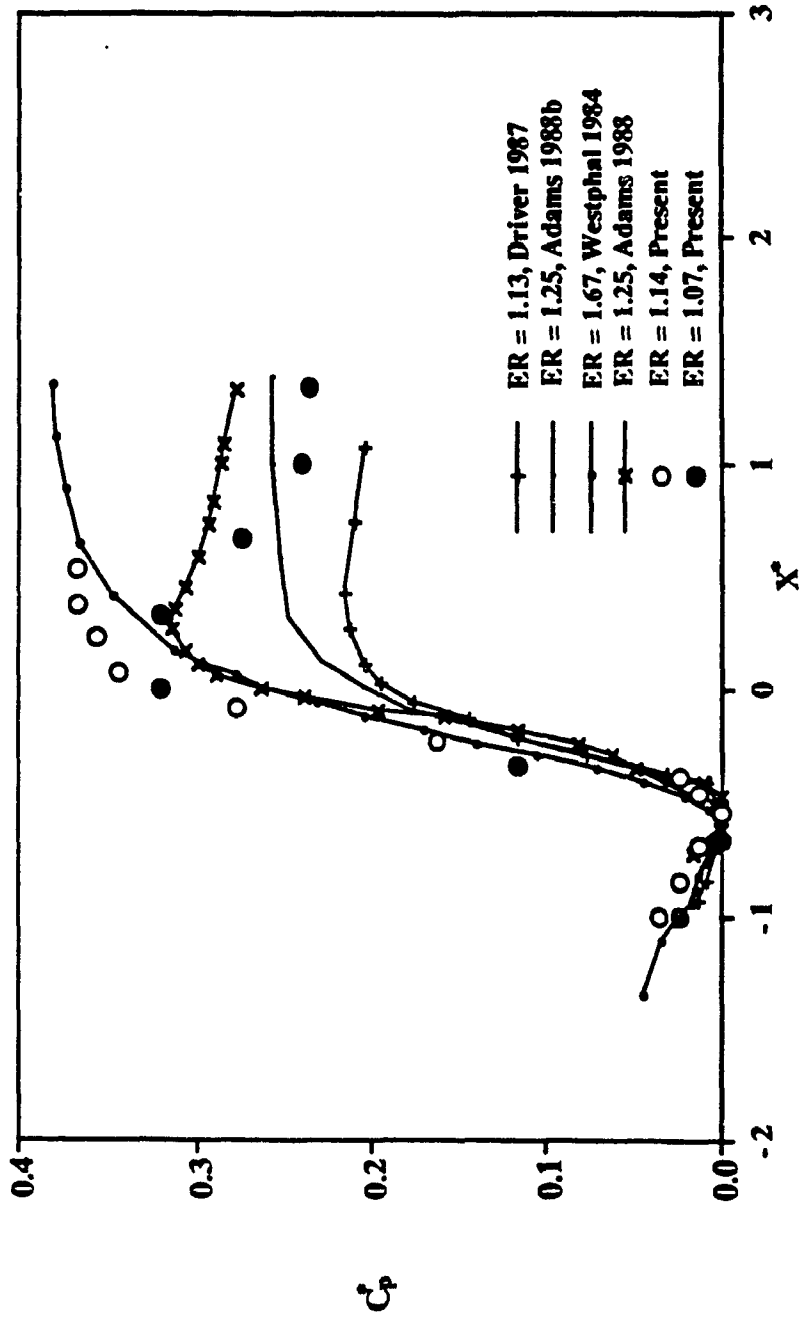


Fig.7.11 : Variation of C_p^* with X^*

Fig.7.12: Variation of C_p with X^*

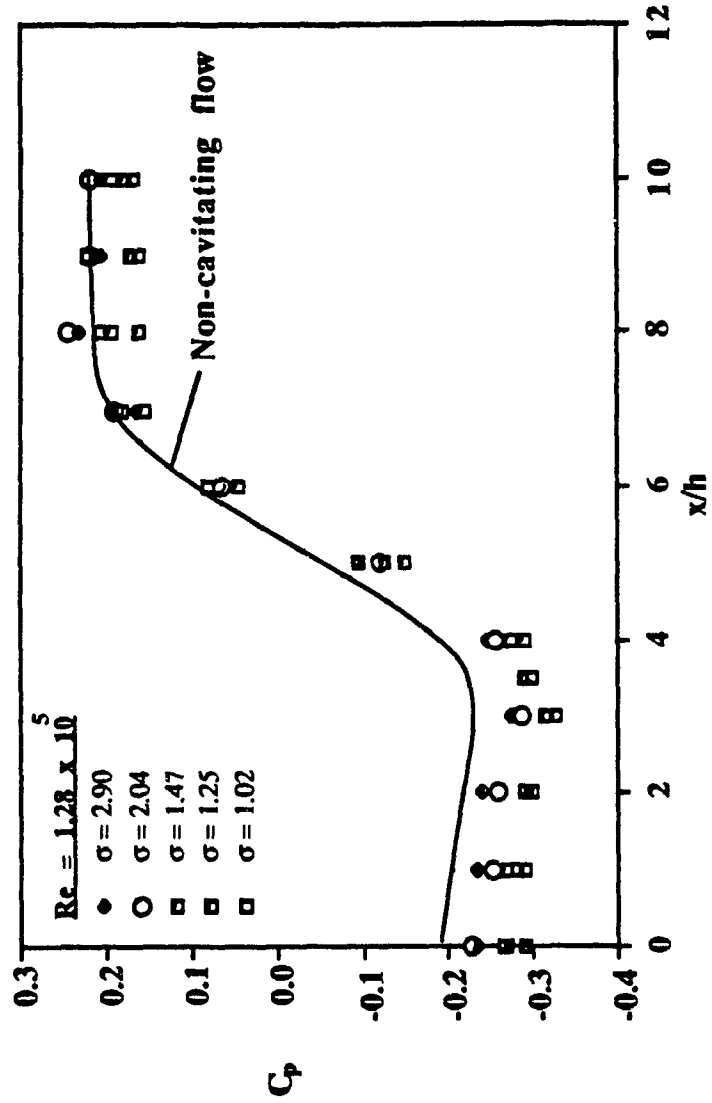


Fig.7.13: Variation of C_p with x/h ($ER = 1.14$)

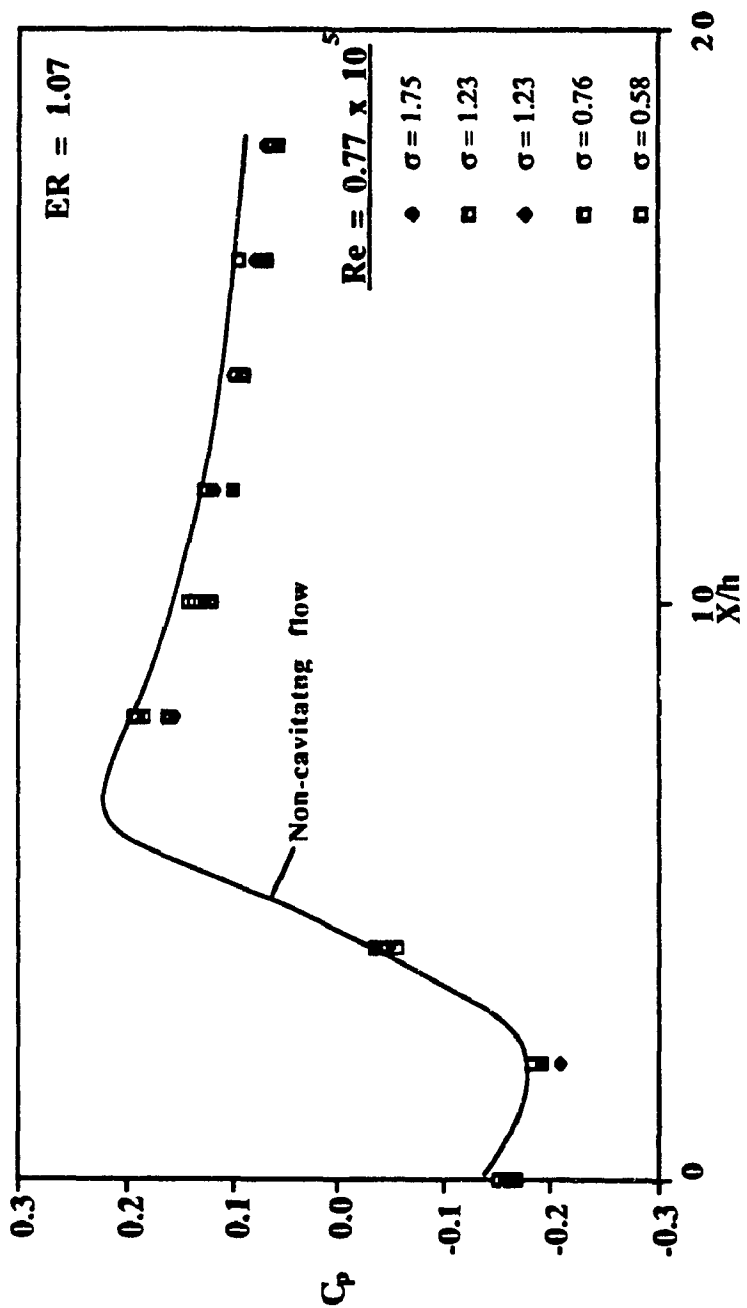


Fig.7.14: Variation of C_p with X/h (ER = 1.07)

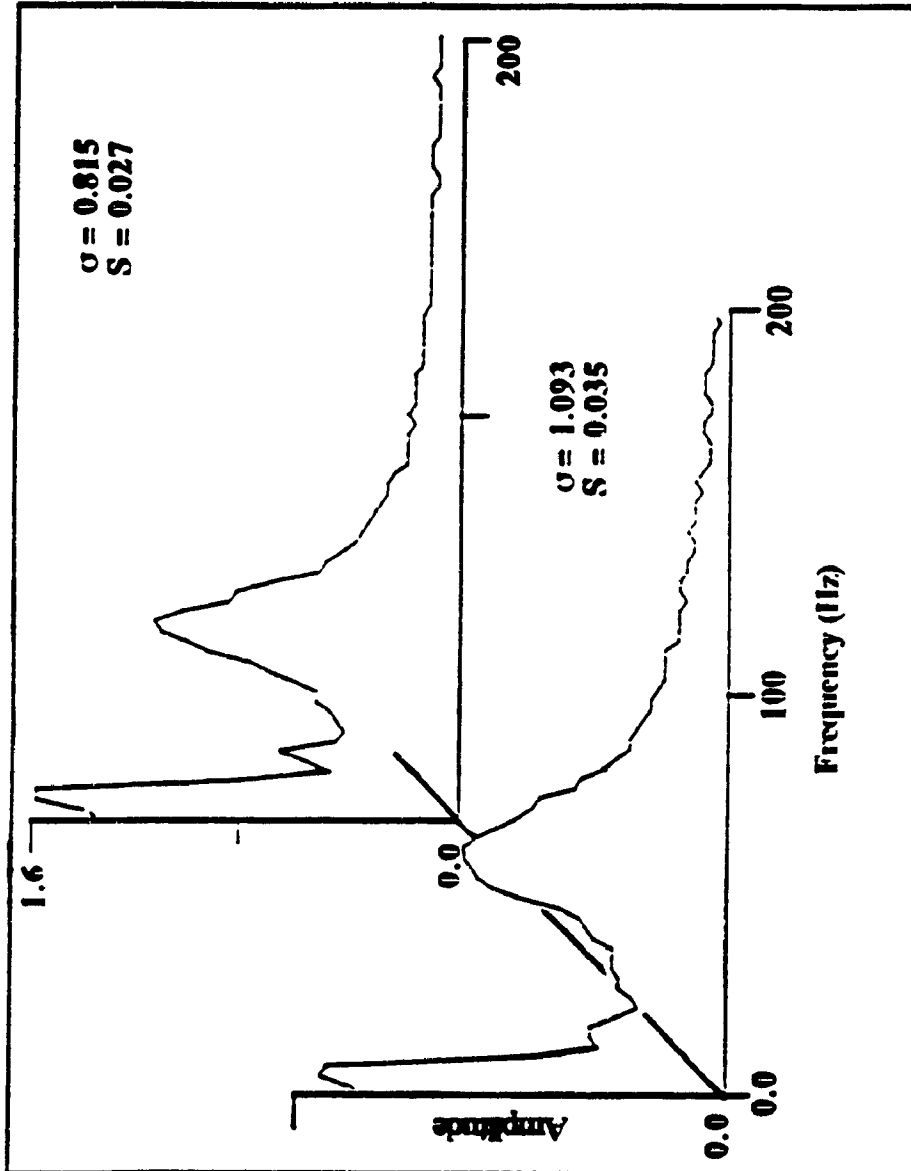
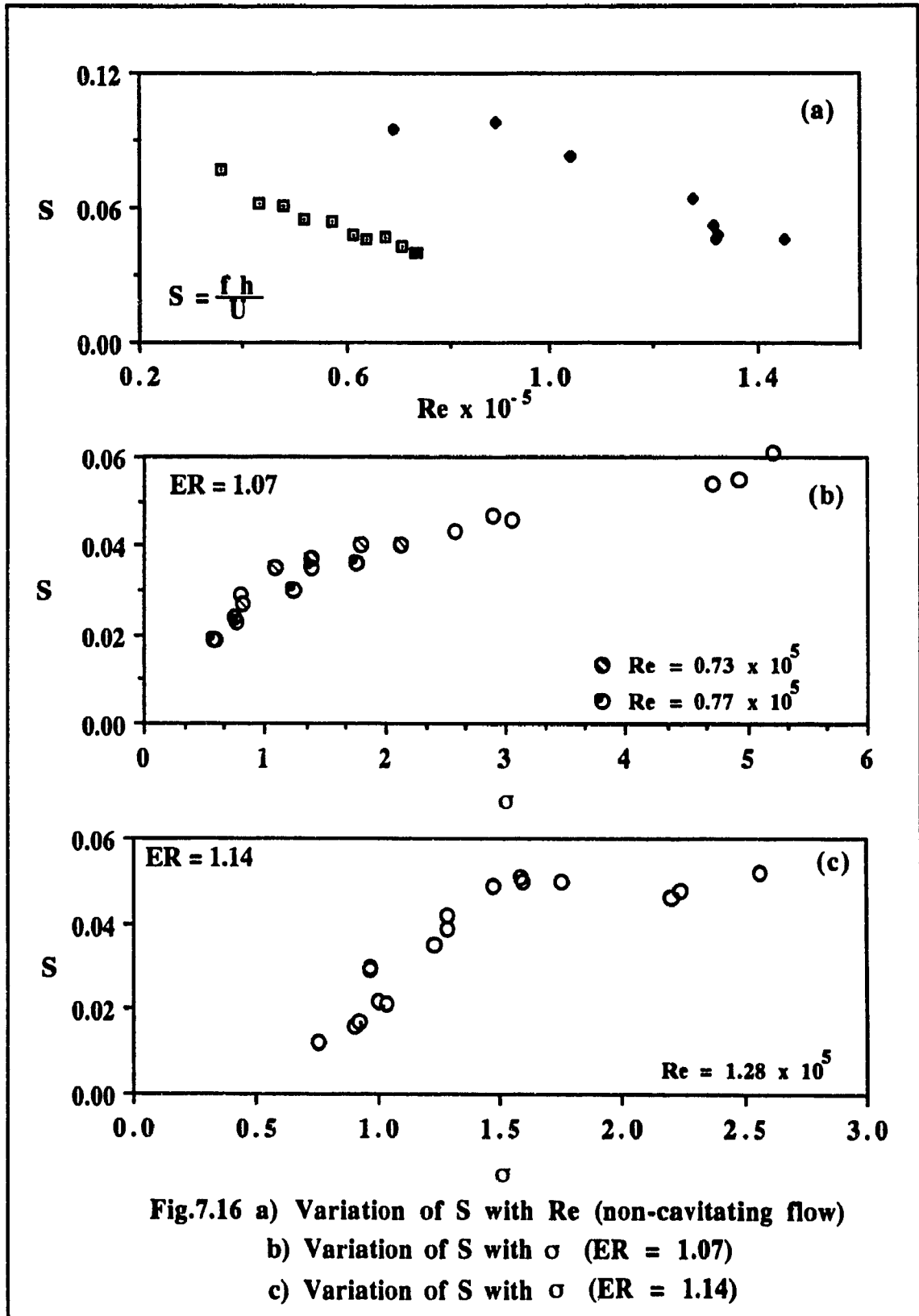


Fig.7.15: Typical spectra of pressure fluctuations downstream of a backward facing step ($ER = 1.07$).



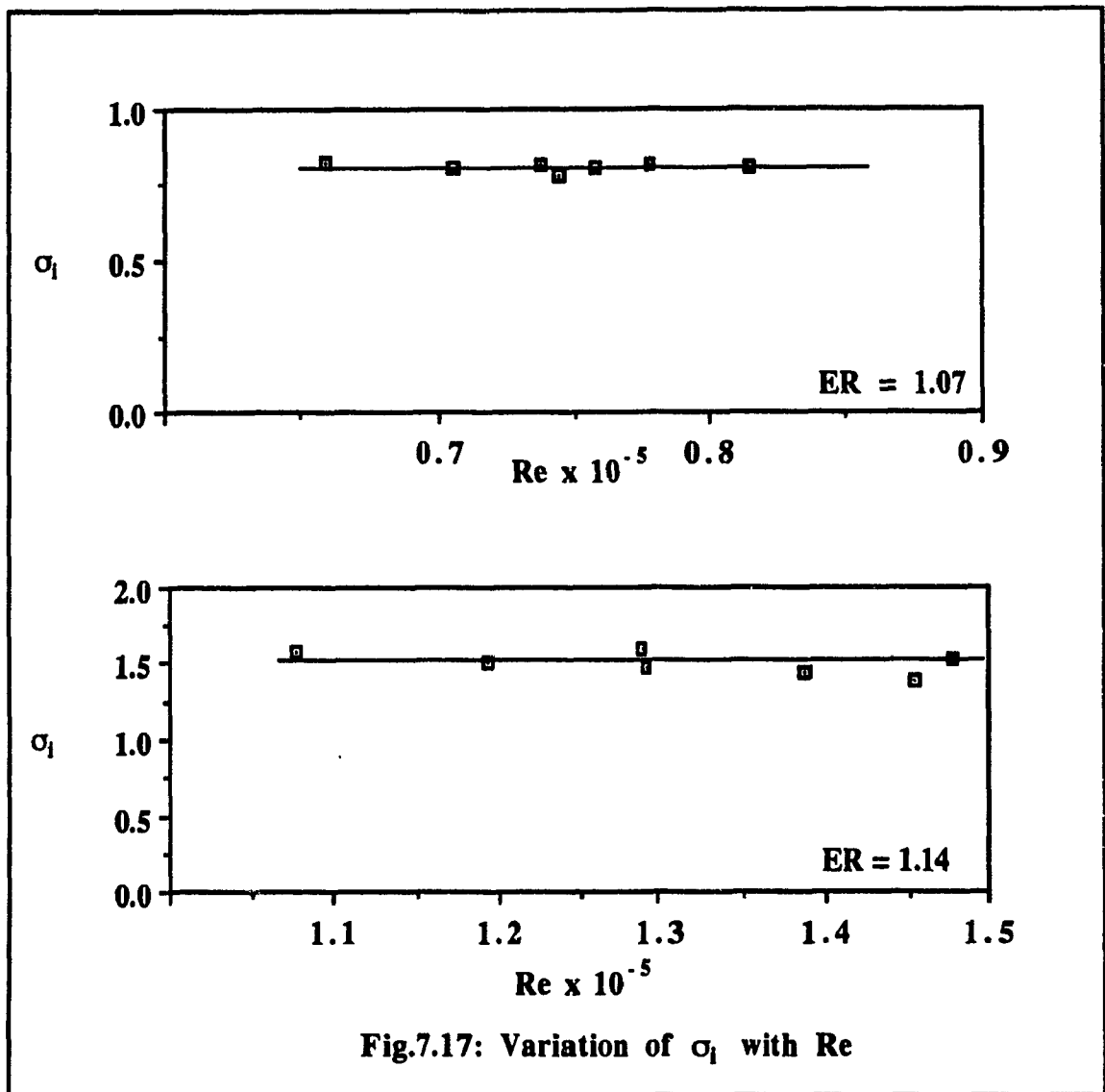


Fig.7.17: Variation of σ_1 with Re

APPENDIX III

TABLES

Reference	Flow type	Remarks
Shalnev 1977 Varga 1966 Syamala Rao 1975 Chandra 1973 Oba 1981 Ramamurthy 1977		Characteristics of cavitating flow past circular cylinders
Ramamurthy 1977		Flow past wedges. Damage and noise characteristics were also obtained. Partially cavitating conditions.
Young et al., 1966 Ramamurthy 1977		Flow past symmetric wedges
Sarkaya 1961		Flow past butterfly valves. Limited studies related to cavitation characteristics.
Kermeen 1957 Arndt 1976		Flow past sharp edged disks - Cavitation inception characteristics.
Narayanan 1984		Flow past a normal wall. Limited studies related to inception.
Reference	Flow type	Remarks
Nurmachi 1960		Flow past an orifice plate. Inception characteristics
Holl 1960		Flow past roughness elements.
Yen-hsi Chu 1967		Flow past a wall.
Katz 1982		Flow past blunt axis-symmetric bluff body
Arakci 1981		Flow past axis-symmetric backward facing step
Vigander 1965		Flow past boundary discontinuities

Table 1: Summary of some related previous studies

b/B = 0.243		b/B = 0.325	
Log (Re)	σ_i	Log (Re)	σ_i
5.330	10.06	5.516	13.47
5.348	9.25	5.562	13.51
5.361	10.03	5.529	14.21
5.390	10.40	5.556	14.19
5.414	9.80	5.583	13.69
5.432	9.80	5.598	14.11
5.439	10.28	5.489	14.84
5.457	10.02	5.507	14.89
5.478	10.36	5.604	13.49
5.521	10.09	5.481	15.57
5.340	9.51	5.501	15.07
5.459	9.40	5.375	14.86
5.523	10.05	5.553	13.61
5.546	10.48	5.550	13.90
		5.634	14.24

Table. 2: Cavitation Inception data for b/B = 0.243 and 0.325

Blockage	σ_i
0.097	4.05 to 5.28
0.128	4.73 to 6.13
0.186	7.08
0.243	9.25 to 10.40
0.325	13.47 to 15.57

Table.3: Inception cavitation index at various blockages

σ	$-C_{ps}$	S	σ_s	Re x 10 ⁻⁵
4.79	1.89	.154	1.657	1.298
3.18	1.89	.153	1.120	1.549
2.94	1.97	---	0.990	1.649
2.79	1.96	---	0.943	1.716
2.29	1.84	.154	0.806	2.088
2.04	1.73	.159	0.747	2.587
2.02	1.68	.156	0.754	2.746
3.23	1.93	.153	1.102	1.532
2.56	1.92	---	0.877	1.865
2.22	1.81	.155	0.790	2.111
2.12	1.77	.159	0.765	2.285
2.00	1.75	.156	0.755	3.073
2.91	1.97	---	0.980	1.654
2.40	1.88	.156	0.833	1.977
2.14	1.76	.158	0.775	2.229
2.08	1.75	.160	0.756	2.408
2.08	1.76	.160	0.754	2.607
2.11	1.78	.159	0.759	2.425
2.06	1.74	.159	0.752	2.661
2.04	1.74	---	---	2.926
1.97	1.75	---	---	3.222
1.90	1.74	---	---	3.412
1.85	1.70	---	---	3.634
1.80	1.65	---	---	3.835

Table 4a: Test results for 0° Wedge, b/B = 0.097

σ	S	S_s	L/b	W/b	S_L	S_L^*	σ_s
8.52	.221	0.108					2.023
6.66	.223	0.108					1.566
4.78	.217	0.105	2.305	1.500	0.500	0.242	1.120
4.90	.221	0.105	2.389	1.500	0.528	0.252	1.116
4.55	.222	0.106	2.639	1.500	0.586	0.280	1.042
4.19	.230	0.111	2.972	1.500	0.684	0.330	0.977
3.90	.253	0.122	3.139	1.583	0.794	0.383	0.907
5.03	.221	0.104	2.555	1.500	0.565	0.267	1.122
4.54	.222	0.105	2.639	1.500	0.586	0.277	1.013
3.93	.254	0.122	2.972	1.583	0.755	0.363	0.907
3.76	.255	0.122	3.305	1.667	0.943	0.405	0.867
3.58	.243	0.118	3.639	1.667	0.884	0.429	0.845
3.66	.253	0.122	3.472	1.667	0.878	0.424	0.855
3.58	.240	0.117	3.889	1.733	0.933	0.453	0.845
4.90	.219	0.104	2.139	1.467	0.468	0.222	1.098
4.27	.218	0.106	2.222	1.500	0.484	0.235	1.007
5.30	.212	0.103		1.433			1.244
3.58	.248	0.123	3.055	1.600	0.758	0.376	0.880
4.04	.226	0.111	2.722	1.533	0.615	0.301	0.966
4.35	.213	0.104	2.472	1.533	0.527	0.257	1.036
3.45	.242	0.120	3.389	1.667	0.820	0.407	0.848
5.28	.219	0.103	2.222	1.433	0.487	0.229	1.170
5.97	.214	0.102	1.889	1.400	0.404	0.193	1.369
7.46	.220	0.104					1.672
5.53	.210	0.102	2.472	1.467	0.519	0.251	1.296
4.56	.224		2.805	1.500	0.628	0.299	1.034

Table 4b: Test data for 0 deg. wedge ($b/B = 0.243$)

σ	S	S_s	L/b	W/b	S_L	S_L^*	σ_s
5.86			2.854	1.500			
5.39	.290	0.125	3.229	1.500	0.936	0.404	1.002
4.97	.304	0.132	2.917		0.887	0.385	0.936
4.67			3.354	1.560			0.907
4.29			4.229	1.630			0.858
4.24			4.291	1.630			0.851
4.24			4.291	1.630			0.851
10.52	.273	0.117					1.927
12.26	.274	0.119					2.305
8.20	.272	0.118					1.547
7.49	.272	0.117		1.450			1.387
5.44	.287	0.124	2.667	1.450	0.765	0.331	1.021
5.33	.289	0.126	2.667	1.450	0.771	0.337	1.015
5.00	.309	0.133	2.667	1.500	0.824	0.356	0.931
10.55	.278						
9.42	.275	0.117					1.710
7.79	.274	0.117					1.432
6.75	.271	0.115	2.417	1.400	0.655	0.279	1.225
5.29	.307	0.132	2.792	1.500	0.857	0.368	0.974
4.94	.306	0.133	2.917	1.500	0.893	0.388	0.930
4.92	.303	0.132	3.167	1.600	0.960	0.417	0.928
4.75	.287	0.126	3.542	1.630	1.017	0.446	0.913
4.54	.252	0.111	4.041	1.630	1.018	0.449	0.885
4.40			4.791	1.630			0.856
7.17	.278		2.417	1.375	0.672	0.282	1.265
6.60	.275		2.604	1.400	0.716	0.304	1.187
5.97	.279		2.792	1.450	0.779	0.333	1.093
5.59	.290		3.042	1.450	0.882	0.378	1.025
4.97	.302		3.292	1.500	0.944	0.430	0.929
4.47			3.667	1.563			0.888

Table 4c: Test data for 0 deg. wedge ($b/B = 0.325$)

σ	S	S_s	S_L	L/b	W/b	S^*_L	σ_s
22.25	.456	0.129	-----	-----	-----	-----	1.793
14.71	.443	0.130	0.762	1.72	1.22	0.224	1.274
14.26	.443	0.130	0.855	1.93	1.22	0.251	1.230
13.55	.467	0.137	0.939	2.01	1.23	0.275	1.164
13.36	.482	0.141	1.070	2.22	1.25	0.313	1.142
11.69	.469	0.139	1.375	2.94	1.25	0.410	1.034
18.05	.455	0.130	0.733	1.61	1.22	0.210	1.476
14.46	.466	0.130	0.888	1.99	1.22	0.260	1.238
13.35	.472	0.139	0.996	2.11	1.23	0.293	1.156
12.77	.497	0.147	1.193	2.40	1.25	0.353	1.116
11.31	.445	0.132	1.322	2.97	1.25	0.393	0.999
11.07	.443	0.133	1.320	2.98	1.25	0.397	1.000

Table 4d: Test data for 0 deg. wedge ($b/B = 0.575$)

σ	S	S_s	σ_s	L/b	W/b	\dot{S}_L
32.19	.490	.122	1.97	1.65	1.15	.198
21.48	.479	.120	1.34	1.65	1.15	.201
19.89	.478	.122	1.29	1.77	1.16	.211
18.87	.473	.119	1.20	2.40	1.20	.346
16.26	.549	.144	1.12	2.03	1.20	.304
14.87	.530	.150	1.19	---	---	---
48.32	.492	.125	3.15	---	---	---
44.48	.486	.122	2.81	---	---	---

Table 4e: Test results for 0 deg. wedge ($b/B = 0.658$)

σ	L/b	W/b	S	S _s	S _L	S _L *	α_s
76.41	---	---	.506	0.077	---	---	1.760
72.23	---	---	.554	0.083	---	---	1.614
59.51	1.19	1.07	.469	0.070	0.558	0.084	1.339
53.36	1.34	1.08	.480	0.072	0.743	0.097	1.209
56.13	1.29	1.08	.505	0.076	0.651	0.098	1.270
82.18	---	---	.558	0.084	---	---	1.845
53.44	1.44	1.08	.460	0.070	0.662	0.101	1.235
47.91	1.49	1.08	.500	0.077	0.745	0.115	1.145
42.42	1.74	1.08	.603	0.097	1.094	0.169	1.095
47.08	1.46	1.08	.500	0.078	0.730	0.114	1.139
44.16	1.64	1.07	.588	0.093	0.964	0.153	1.108
40.42	2.14	1.08	.345	0.056	0.738	0.119	1.049
50.31	1.29	1.07	.440	0.070	0.572	0.090	1.242
40.70	1.77	1.07	.600	0.098	1.060	0.173	1.082
38.81	2.04	1.07	.270	0.044	0.552	0.090	1.041
78.22	---	---	.509	0.077	---	---	---
97.41	---	---	.509	0.076	---	---	---
56.01	---	---	.440	0.067	---	---	---
50.85	---	---	.547	0.084	---	---	---
48.90	---	---	.466	0.072	---	---	---
47.05	---	---	.537	0.084	---	---	---
43.35	---	---	.555	0.088	---	---	---

Table 4f: Test data for 0 deg. wedge (b/B = 0.823)

x/b	$\sigma = 7.46$	$\sigma = 5.53$	$\sigma = 4.04$	$\sigma = 3.45$	$\sigma = 3.38$
0.000	-3.46	-3.27	-3.18	-3.07	-3.05
0.866	-4.38	-4.09	-3.70	-3.28	-3.23
1.111	-3.92	-3.70	-3.50	-3.20	-3.18
1.445	-4.63	-4.48	-3.89	-3.42	-3.26
1.778	-3.85	-3.69	-3.66	-3.31	-3.27
2.111	-3.17	-3.13	-3.27	-3.27	---
2.445	-3.06	-2.92	-2.95	-3.17	-3.17
2.779	-2.84	-2.64	-2.58	-2.90	---

Table 5a: Wake centre-line static pressure distribution $b/B = 0.24$ (Wedge 0°)

x/b	$\sigma = 7.49$	$\sigma = 5.44$	$\sigma = 5.33$	$\sigma = 5.00$	$\sigma = 4.67$	$\sigma = 4.24$
0.000	-4.40	-4.33	-4.25	-4.37	-4.16	-3.98
0.866	-5.49	-4.96	-4.85	-4.75	-4.36	-4.05
0.917	-4.60	-4.49	-4.44	-4.53	-4.29	-4.05
1.167	-5.23	-4.85	-4.80	-4.71	-4.45	-4.13
1.417	-5.60	-5.01	-4.94	-4.78	-4.48	-4.14
1.667	-5.16	-4.96	-4.91	-4.80	-4.45	-4.13
1.917	-4.54	---	-4.86	-4.75	---	---
2.167	-4.09	-4.45	-4.49	-4.58	-4.43	-4.12
2.417	-3.62	---	---	---	-4.31	-4.09
2.667	---	-3.74	-3.76	-4.00	-4.17	-4.07

Table 5b: Wake centre-line static pressure distribution $b/B = 0.33$ (Wedge 0°)

x/b	$\sigma = 22.25$	$\sigma = 18.05$	$\sigma = 14.26$	$\sigma = 13.55$	$\sigma = 11.69$	$\sigma = 11.07$
0.000	-11.41	-11.23	-10.69	-10.64	-10.31	-10.05
0.867	-11.97	-11.78	-10.97	-10.70	-10.20	- 9.96
0.931	---	-12.03	-11.24	---	-10.78	-10.41
1.075	-12.89	-12.72	-11.93	-11.71	-11.00	-10.59
1.218	-13.69	-13.35	-12.46	-12.25	-11.24	-10.74
1.361	-13.12	-12.80	-12.24	-11.79	---	-10.63
1.505	-12.81	-12.47	-11.83	---	-11.10	-10.63
1.791	-10.57	-10.60	-10.63	-10.92	-10.97	-10.55

Table 5c: Wake centre-line static pressure distribution $b/B = 0.58$ (Wedge 0°)

x/b	$\sigma = 32.19$	$\sigma = 19.89$	$\sigma = 14.87$	$\sigma = 21.48$	$\sigma = 16.26$
0.0	-15.33	-14.44	-11.52	-14.83	-13.54
0.866	-----	-15.48	-11.27	-15.77	-13.11
0.898	-16.91	-15.55	-12.94	-16.24	-14.71
1.023	-18.09	-16.69	-13.45	-17.20	-15.18
1.149	-18.20	-17.08	-13.50	-17.54	-15.21
1.274	-18.43	-17.25	-13.43	-17.51	-15.40
1.399	-17.79	-16.50	-13.43	-16.55	-15.23
1.525	-16.44	-15.41	-13.43	-15.79	-15.23

Table.5e: Wake centre-line static pressure data for $b/B = 0.658$ (Wedge 0°)

x/b	$\sigma = 82.18$	$\sigma = 56.13$	$\sigma = 53.44$	$\sigma = 47.91$	$\sigma = 44.16$	$\sigma = 40.42$	$\sigma = 38.81$	$\sigma = 36.92$
0.000	-43.55	-43.21	-42.27	-40.84	-38.86	-37.52	-36.29	-35.88
0.866	-44.21	-43.73	-42.80	-41.89	-38.69	-37.36	-35.49	-35.34
0.938	-46.71	-45.75	-44.47	-42.53	-41.63	-39.27	-37.58	-36.27
1.038	-47.34	-46.94	-45.64	-43.51	-42.08	-39.57	-37.90	-36.41
1.138	-47.60	-47.15	-45.84	-43.68	-42.36	-39.69	-38.17	-36.44
1.338	-44.60	-43.89	-41.83	---	-40.36	-39.37	-38.00	-36.27
1.539	-39.55	-38.83	-37.59	-37.10	-37.30	-38.73	---	---

Table.5e: Wake centre-line static pressure distribution $b/B = 0.82$ (Wedge 0°)

σ	S	C_{ps}	L_f/b	σ_s
2.62	0.158	-1.94	2.188	0.891
2.55	0.157	-1.97	2.611	0.859
2.31	0.157	-1.87	3.121	0.805
2.21	0.158	-1.83	3.669	0.781
2.27	0.157	-1.79	3.161	0.814
2.39	0.157	-1.91	2.653	0.821
2.89	0.157	-2.03	2.125	0.954
3.37	0.157	-2.04	1.976	1.109
2.80	0.155	-1.80	2.399	1.000
2.73	0.155	-1.84	2.611	0.961
2.53	0.157	-1.79	3.121	0.907
2.32	0.157	-1.77	3.458	0.838
2.17	-----	-1.70	3.669	0.804
2.02	0.156	-1.65	3.754	0.762
3.77	0.155	-1.88	-----	1.309

Table 6: Length of formation region data for $b/B = 0.097$

b/B = 0.243			b/B = 0.325		
σ	L_f/b	σ_s	σ	L_f/b	σ_s
4.78	1.639	1.120	5.44	2.167	1.021
4.90	1.639	1.116	5.33	2.104	1.015
4.55	1.805	1.042	5.00	2.667	0.931
4.19	2.139	0.977	6.75	1.417	1.225
3.90	2.472	0.907	5.29	2.354	0.974
5.03	1.639	1.122	4.94	2.667	0.930
4.54	1.805	1.013	4.92	2.729	0.928
3.93	2.472	0.907	4.75	3.292	0.913
3.76	2.805	0.867	4.54	3.729	0.885
3.58	3.139	0.845	7.17	1.292	1.265
3.66	2.805	0.855	6.60	1.354	1.187
3.58	3.055	0.845	5.97	1.604	1.093
4.90	1.555	1.098	5.59	1.792	1.025
4.27	1.805	1.007	4.97	2.417	0.929
5.30	1.305	1.244			
3.58	2.472	0.880			
4.04	2.055	0.966			
4.35	1.555	1.036			
3.45	2.972	0.848			
5.28	1.389	1.170			
5.97	1.139	1.369			
7.46	1.055	1.672			
5.53	1.305	1.296			
4.56	1.639	1.034			
4.05	1.713	0.962			

Table 7: Length of formation region data for
 $b/B = 0.243$ and $b/B = 0.325$

$Re \times 10^{-5}$	σ	$-C_{pb}$
1.59	2.73	2.43
1.59	2.75	2.41
1.55	3.14	1.28
0.90	5.58	1.40
1.15	3.75	1.34
1.27	3.30	1.24
1.40	3.04	1.45
1.50	2.85	2.38
1.68	2.68	2.41
2.12	2.40	1.16
0.86	5.99	1.22
0.92	5.44	1.31
1.10	3.85	1.24
1.17	3.54	1.27
1.24	3.30	1.25
1.29	3.17	1.26
1.36	3.07	1.59
1.41	2.97	1.86
1.46	2.90	2.13
1.52	2.78	2.28
1.64	2.67	2.31
.936	5.16	1.24
1.17	3.55	1.44
1.34	3.07	1.58
1.41	2.97	1.78
1.64	2.66	2.29
2.02	2.37	1.51
2.44	2.27	1.67
2.03	2.37	1.48
2.53	2.28	1.48
2.60	2.26	1.19
2.76	2.21	1.34
2.18	2.34	1.17
2.25	2.37	1.16
2.37	2.29	1.11
2.52	2.29	1.11
2.82	2.27	1.83
1.56	2.88	2.27
1.56	2.91	2.26
1.56	2.96	2.23
1.55	3.01	1.99

Table 8: Test results for Circular body ($b/B = .08$)

$Re \times 10^{-5}$	σ	$-C_{pb}$
1.55	3.17	1.84
1.54	3.13	1.31
1.54	3.24	1.28
1.02	4.91	1.33
2.10	2.46	1.16
2.42	2.40	1.15
0.80	7.90	1.48
2.32	2.50	1.76
2.50	2.43	1.73
2.21	2.49	1.66
2.76	2.40	1.92
2.86	2.38	1.95
2.98	2.40	2.00
2.76	2.44	1.84
2.89	2.41	1.97
1.94	2.60	1.64
2.00	2.55	1.63
2.04	2.56	1.64
2.34	2.40	1.21
2.56	2.33	1.23
2.80	2.32	1.57
1.75	2.54	1.49
1.94	2.50	1.47
2.07	2.49	1.47
2.21	2.47	1.48
1.83	2.57	1.54
1.27	3.57	1.22
1.37	3.11	1.18
1.57	2.69	2.18
1.57	2.75	2.02
1.60	2.83	1.78
1.60	2.86	1.48
1.60	2.89	1.36
1.58	2.67	2.04

Table 8 (Contd.) : Test data for circular body ($b/B = .08$)

x/b	$\sigma = 7.90$	$\sigma = 4.91$	$\sigma = 3.14$	$\sigma = 3.11$	$\sigma = 2.75$	$\sigma = 2.60$	$\sigma = 2.50$	$\sigma = 2.40$	$\sigma = 2.26$
1.000	-1.68	-1.33	-1.28	-1.18	-2.41	-1.64	-1.47	-1.21	-1.19
1.500	-1.68	-1.36	-1.29	-1.18	-1.91	-1.47	-1.37	-1.21	-1.14
3.000	-1.30	-.84	-.72	-.61	-1.19	-.89	-.78	-.61	-.56
4.000	-1.30	-.86	-.83	-.71	-1.12	-.89	-.78	-.65	-.60
5.000	-1.30	-.93	-.88	-.78	-1.10	-.89	-.81	-.69	-.64
6.000	-1.30	-.96	-.95	-.86	-1.10	-.91	-.86	-.75	-.69
7.000		-1.10	-.98	-.99	-1.16	-1.00	-.92		
8.000	-1.30	-1.18	-1.12		-1.26		-.95	-.85	-.77

Table.9: Wake static pressure distribution data for $b/B = .08$ (Circular body)

x/b	$\sigma = 6.39$	$\sigma = 4.72$	$\sigma = 4.17$	$\sigma = 3.82$	$\sigma = 3.55$	$\sigma = 3.49$
1.000	-2.470	-3.370	-3.930	-3.580	-3.250	-3.190
1.125	-2.600	-3.500	-3.930	-3.580	-3.290	-3.200
1.375	-3.040	-3.180	-3.680	-3.590	-3.370	-3.310
1.625	---	-2.580	-3.380	-3.370	-3.280	-3.240
1.875	-1.980	---	-3.170	-3.050	-2.920	-2.930
2.125	---	---	-2.980	-2.880	-2.830	-2.810
2.375	-1.980	-2.460	-2.920	-2.710	-2.550	-2.470
2.625	---	-2.450	-2.880	-2.690	-2.480	-2.420
2.875	-1.860	---	-2.750	-2.570	---	---

Table 10: Wake centre-line static pressure distribution for $b/B = .33$ (Circular body)

E.R = 1.07			E.R = 1.14		
$Re \times 10^{-5}$	σ_i	S	$Re \times 10^{-5}$	σ_i	S
0.659	0.825	0.020	1.453	1.39	0.044
0.704	0.807	0.019	1.478	1.53	0.045
0.744	0.778	0.021	1.387	1.43	0.048
0.779	0.812	0.022	1.299	1.66	0.050
0.815	0.810	0.022	1.193	1.51	0.048
0.757	0.804	0.029	1.077	1.58	0.044
0.738	0.815	0.027	1.292	1.47	0.049
			1.288	1.60	
			1.288	1.64	

Table 11: Inception cavitation data for backward facing steps

E.R = 1.07		E.R = 1.14	
σ	S	σ	S
5.22	0.061	2.24	0.048
4.93	0.055	2.56	0.052
4.72	0.054	2.20	0.046
6.35	0.048	1.23	0.035
3.06	0.046	1.03	0.021
2.9	0.047	1.28	0.042
2.57	0.043	1.28	0.039
2.13	0.040	1.47	0.049
1.78	0.040	0.97	0.029
1.37	0.037	0.96	0.030
1.09	0.035	1.00	0.022
0.80	0.029	0.92	0.017
0.82	0.027	0.90	0.016
0.75	0.024	0.75	0.012
0.58	0.019	1.39	0.044
6.03	0.062	1.53	0.045
10.8	0.077	1.43	0.048
		1.66	0.050
		1.51	0.048
		1.58	0.044

Table 12: Strouhal number data for cavitating flow past backward facing steps

X/h	$\sigma = 1.75$	$\sigma = 1.38$	$\sigma = 1.23$	$\sigma = 0.76$	$\sigma = 0.58$
0	-0.161	-0.160	-0.161	-0.166	-0.151
2	-0.210	-0.176	-0.193	-0.193	-0.183
4	-0.041	-0.056	-0.033	-0.054	-0.044
8	0.155	0.175	0.163	0.184	0.190
10	0.122	0.153	0.120	0.126	0.137
12	0.117	0.126	0.100	0.118	0.126
14	0.100	0.110	0.089	0.089	0.097
16	0.080	0.094	0.070	0.068	0.094
18	0.070	0.092	0.060	0.063	0.063

Table 13: Cavitating flow test results for backward facing steps (ER = 1.07)

X/h	$\sigma = 2.90$	$\sigma = 2.82$	$\sigma = 2.04$	$\sigma = 1.64$	$\sigma = 1.25$	$\sigma = 1.02$
0	-0.235	-0.229	-0.228	-0.275	-0.290	-0.265
1	-0.235	-0.242	-0.254	-0.292	-0.290	-0.281
2	-0.240	-0.269	-0.260	-0.298	-0.300	-0.292
3	-0.276	-0.296	-0.288	-0.331	-0.329	-0.318
4	-0.249	-0.269	-0.258	-0.298	-0.290	-0.275
5	-0.096	-0.135	-0.121	-0.140	-0.152	-0.096
6	0.069	0.054	0.068	0.072	0.048	0.082
7	0.166	0.161	0.190	0.168	0.156	0.181
8	0.230	0.256	0.245	0.201	0.162	0.208
9	0.206	0.242	0.218	0.185	0.172	0.221
10	0.206	0.242	0.218	0.185	0.178	0.194

Table 14: Cavitating flow test results for backward facing steps (ER=1.14)

X/h	δ (cms)	H	R_θ	G	Boundary layer state
0.0	0.191	2.20	2375	---	Laminar
7.4	1.110	1.82	17147	19.64	Turbulent

δ_1 - Displacement thickness

δ_2 - Momentum thickness

$$C_f = 0.123 \times 10^{-0.678H} R_\theta^{-0.268}$$

$$\frac{u_\tau}{u} = C_f^{0.5}$$

$$H = \frac{\delta_1}{\delta_2}$$

(Ludweig - Tillman relation)

$$G = \frac{u}{u_\tau} \frac{(H-1)}{H} \quad (\text{Clauser parameter})$$

Table. 15: Boundary layer parameters for flow past backward facing step (ER = 1.07)

σ	α_s	$-C_{ps}$	S	S_s
8.48	3.02	1.80	0.152	0.091
6.86	2.45	1.81	0.152	0.091
5.46	2.01	1.71	0.153	0.093
4.41	1.62	1.72	0.152	0.092
3.79	1.36	1.78	0.152	0.091
2.86	0.98	1.92	0.157	0.092
2.67	0.98	1.76	0.156	0.094
2.33	0.90	1.61	0.155	0.096

Table 16: Test data for 0 degree wedge ($b/B = 0.097$)

σ	$-C_{ps}$	L_f/b	α_s	S	S_s
11.07	3.43		2.50	0.202	0.096
7.12	2.98	1.12	1.79	0.207	0.104
6.70	3.20	1.12	1.60	0.205	0.100
5.02	3.12	1.70	1.22	0.215	0.106
4.35	3.02	1.70	1.08	0.218	0.109
7.22	3.37	1.15	1.65	0.207	0.099
6.38	3.48	1.36	1.42	0.200	0.095
5.57	3.25	1.76	1.31	0.214	0.104
4.74	3.21	1.87	1.13	0.214	0.104
4.56	3.16	1.97	1.10	0.214	0.105
3.87	2.86	2.27	1.00	0.260	0.132
3.80	2.75	2.58	1.01	0.253	0.131

Table 17: Test data for 0 degree wedge ($b/B = 0.243$)

σ	$-C_{ps}$	L_T/b	σ_s	S	S_s
12.15	4.46		2.23	0.258	0.110
10.01	4.61	1.29	1.78	0.255	0.108
8.23	4.48	1.35	1.50	0.257	0.110
7.79	4.43	1.44	1.44	0.259	0.111
6.90	4.42	1.52	1.27	0.262	0.112
6.08	4.18	1.75	1.17	0.264	0.116
5.32	4.36	2.29	0.99	0.309	0.133
5.12	4.07	2.52	1.01	0.301	0.134

Table 18: Test data for 0 degree wedge ($b/B = 0.325$)

σ_s	S_s
1.235	0.015
1.168	0.010
2.020	0.081
2.514	0.110
2.192	0.092
2.130	0.089
1.897	0.091
1.755	0.104

Table 19: Test data for 0 degree wedge ($b/B = 0.823$)

APPENDIX IV
EXPERIMENTAL UNCERTAINTY

APPENDIX IV
EXPERIMENTAL UNCERTAINTIES

A.4.1 Uncertainty in the measurands:

1. Cavitating bodies	Width = $b \pm 0.02$ mm Height = $h \pm 0.02$ mm
2. Cavitation test section	Linear measurement ± 0.02 mm
3. Pressure measurements	Free stream $\pm .2$ psi Stagnation $\pm .2$ psi Vacuum ± 6.35 mm of Mercury
4. Length of vortex formation region	$L_f \pm 1.6$ mm
5. Cavity geometry	$L \pm 1.6$ mm $W \pm 1.6$ mm
6. Temperature	$T \pm .25^\circ\text{C}$
7. Frequency	$f \pm .25$ Hz
8. LDV measurements: Mean velocity	$U \pm .05$ m/s
Turbulence Intensity	$u' \pm 0.5\%$

A.4.2 Uncertainty in computed results:

The uncertainties in the computed results were obtained by the method described by Kline [1985] at an odds of 20:1. The following are the maximum uncertainties in the computed results:

1. Pressure coefficient	$C_{ps} \pm 5\%$ $C_{px} \pm 5\%$
2. Strouhal number	$S \pm 3\%$

3. Discharge	$Q \pm 3.0\%$
4. Cavitation number	$\sigma \pm 5\%$
	$\sigma_i \pm 5\%$
5. Mean Velocity	$U \pm 3\%$